SUNDSTRAND

SUNDSTRAND TURBO

November 20, 1959

Job No. 7213-07

S/TD No. 1735

STUDY OF TURBINE AND TURBOPUMP DESIGN PARAMETERS

FINAL REPORT - VOLUME IV
LOW SPECIFIC SPEED TURBOPUMP STUDY

Department of the Navy
Office of Naval Research

Contract No. NONR-2292(00)
Task No. NR 094-343

For the period 6 October 1958 through 31 October 1959

Kenneth E. Nichols
Donald G. McPherson

Project Engineers

Dr. O. Eric Balje

Technical Consultant

FOREWORD

This document was prepared by the Denver facility of Sundstrand Turbo, division of Sundstrand Corporation, under USN Contract NONR 2292(00) No. NR 094 343, and is one of four parts comprising the final report. The work described in this volume was accomplished during the period 6 October 1958 through 31 August 1959.

SUNDSTRAND TURBO

A Division of Sundstrand Corporation

S/TD No. 1735
STUDY OF TURBINE AND TURBOPUMP
DESIGN PARAMETERS
FINAL REPORT - VOLUME IV
LOW SPECIFIC SPEED TURBOPUMP STUDY

TABLE OF CONTENTS

TABLE OF CONTENTS (Continued) Page

TABLE OF CONTENTS (Continued)

TABLE OF CONTENTS (Continued)

TABLE OF CONTENTS (Continued)

TABLE OF CONTENTS (Continued)

TABLE OF CONTENTS (Continued)

1. ABSTRACT

An investigation of maximum efficiencies of low specific speed turbopumps obtainable with the present state of the art is covered. Optimum suction specific speed and optimum efficiency are analyzed and a theoretical method of determining the detailed design criteria for each optimum design performed. Experimental evidence was accumulated to substantiate the analysis and the final design parameters are presented as functions of pump specific speed and specific diameter..

2. INTRODUCTION

This report has been prepared in accordance with the requirements of ONR Contract NONR 2292(00), Phase III, Turbopump Study. This report deals with pump performance at the design or best efficiency point and is not concerned with the performance range or the performance characteristics of the pump types investigated.

The investigations have been undertaken by the Turbomachinery Development Group of Sundstrand Turbo in Denver, with Dr. O. E. Balje as Technical Consultant, D. G. McPherson and K. E. Nichols as Project Engineers and R. Anderson as Research Engineer,

and D. K. Crockett, H. Baeverstad and R. H. Ball rendering assistance with computer programming.

The conclusions presented in this report are considered final for optimum efficiencies and the suction specific speed of conventional centrifugal pumps, but are of a preliminary nature, and subject to revisions for some of the design criteria of centrifugal pumps and for Pitot pumps in general due to the limited amount of experimental data for component performance, such as probe drag losses, probe diffusion losses, losses involved in the momentum transfer between fluid streams and the influence of variations in geometric configurations (i.e., blade depth, number and angle, clearances, etc.).

Sundstrand Turbo would like to acknowledge the very valuable test data and information supplied by Austin H Church, Professor of Mechanical Engineering, New York University; Mr. Frederick C. Gilman of the Worthington Corporation; Mr. E. D. Higgins, Aurora Pump Division of the New York Airbrake Co.; Mr. George Wilfley of Wilfley & Sons, Denver, Colorado; and Mr. J. L. Dooley of the McCulloch Corporation. The information supplied by these individuals was essential in verifying the theoretical analysis and in constructing the N_s-D_s diagram from test data.

3. TECHNICAL SUMMARY

Through the technique known as dimensional analysis, the similarity parameters specific speed N_s, specific diameter D_s, pump Reynolds number R_e*, and suction specific speed S, are derived which serve as convenient parameters for presenting the performance criteria of turbomachines. As will be shown later, these four parameters are sufficient to describe completely the performance of geometrically similar pumps. For a given flow and a given head rise through a pump, specific speed is a number indicative of the rotative speed of the pump and specific diameter is a number indicative of the impeller diameter or size of the pump. Reynolds number expresses the ratio of inertia force to viscous force and reflects the properties of the fluid being pumped and the speed of the machine. Suction specific speed will indicate whether or not cavitation exists. If cavitation does not exist, then pump performance will be as expected. Although other groups of similarity parameters may be derived which express the performance criteria of turbopumps with equal accuracy, specific speed and specific diameter possess the obvious advantage of giving an indication of pump speed and size for a given pump requirement -- that is, for a given flow and head rise.

The maximum obtainable efficiency for optimized design geometries is presented for all investigated pump types in a single diagram, Figure 1. The data for centrifugal pumps has been confirmed by a large quantity of test data representing more than three hundred pumps produced by many manufacturers. The data for Pitot pumps is of a preliminary nature because of the lack of experimental data available in literature, and is confirmed principally by a limited number of tests made by Sundstrand Turbo. Only a few test data points were available representing other manufacturers.

The application of the N_S-D_S diagram of Figure 1 follows from the definitions of specific speed and specific diameter as indicated in Figure 1. For a given pumping requirement, the required head rise, the volume flow, and the rotative speed of the driving vehicle can be established, from which the specific speed N_S is calculated. Figure 1, then, indicates the maximum obtainable efficiency and the corresponding specific diameter D_S as a function of N_S. Introducing the head rise, volume flow, and D_S value into the equation for D_S yields the required rotor diameter.

An example of the use of N_S-D_S diagrams follows: For a given pump application the volume flow Q, the head rise H, and the

desired rotative speed N are generally known. The specific speed may be calculated from the equation

$$N_s = \frac{N\sqrt{Q}}{H^{3/4}}$$

Entering the N_S-D_S diagram (Figure 1) with the calculated specific speed, the best possible efficiency and the corresponding values of D_S are shown. The specific diameter may then be used to calculate the diameter of the pump impeller from the defining equation

$$D_s = \frac{DH^{1/4}}{\sqrt{Q}}$$

The geometric configuration of this pump (i.e., blade number, inlet to impeller diameter ratio, etc.) are also specified and shown on the overlays of Figure 1.

The simplicity of the N_S-D_S diagram may easily be demonstrated as follows: Assume that it is desired to drive a pump with an electric motor at 3580 RPM, that the required volume flow is .225 $\frac{ft^3}{sec}$ and that the required head rise is 375 ft. or $\frac{ft\text{-}lb}{lb}$; calculating specific speed

$$N_s = \frac{N\sqrt{Q}}{H^{3/4}} = \frac{3580\sqrt{.225}}{375^{\frac{3}{4}}} = 20$$

Entering the N_s-D_s diagram of Figure 1 at $N_s = 20$, it is seen that an efficiency of 69% is possible with a centrifugal pump. The optimum geometry required to produce this efficiency is shown on the overlays. The blade outlet angle $\beta_2 = 85^{\circ}$, the blade number $Z = 22$, and the impeller diameter ratio $\delta = .25$. These parameters may be read directly from the N_s-D_s diagram. Other geometric parameters may also be read in the same manner but have not been described here for the sake of simplicity.

The impeller diameter may be calculated from the indicated value of $D_s = 6.4$ as follows:

$$D = \frac{D_s\sqrt{Q}}{H^{1/4}} = \frac{6.4 \times .474}{4.4} = .689 \text{ ft.} = 8.26 \text{ in.}$$

The N_s-D_s diagram for centrifugal pumps shown also indicates that a high blade number is required to attain 69% efficiency for this centrifugal pump. High blade numbers increase the manufacturing cost of a pump; therefore, economic considerations might restrict the blade number to standard commercial practice (about ten vanes) with a resulting decrease in efficiency and an increase in the impeller diameter. Nevertheless, the optimum pump performance and configuration are still shown on the N_s-D_s diagram. If ten vanes were to be

used, then the D_s required would be 7.2 and a new impeller diameter would result. The resulting efficiency would be some less than 69%.

Thus, it is seen that the N_s-D_s diagram furnishes a useful tool for preparing preliminary design studies and, furthermore, it greatly reduces the cost of determining optimum geometry parameters in the detailed design phase.

4. DIMENSIONAL ANALYSIS AND SIMILARITY TO TURBOPUMPS

The technique of dimensional analysis may be applied to obtain the form and the number of the dimensionless similarity parameters required to describe the dynamic similarity of turbopumps. The π -Theorem, proposed by Buckingham (Reference 1), serves as the basis for formal dimensional analysis and states that a physical phenomenon may be expressed in the form of a specific number of π -terms, where each π -term is the product of some of the variables affecting the phenomenon raised to exponents such that, in terms of the primary dimensions, each π -term is dimensionless. The number of π -terms required to express the performance of turbopumps is equal to the number of variables minus the number of primary dimensions. The primary dimensions are mass M, length

L and time T. For incompressible flow, the seven variables to be considered are shown in Table 1.

TABLE I

Variable	Definition	Dimension
Q	rate of volume flow	L^3/T
H	head rise	L^2/T^2
N	revolutions per minute	$1/T$
D	impeller diameter	L
ρ	fluid density	M/L^3
μ	absolute viscosity	M/LT
H	net positive suction head	L^2/T^2

With three primary dimensions and seven variables, four π-terms are required to completely describe dynamic similarity among the turbopumps. Selecting Q, H, and ρ as independent variables, four π -terms are formed by successively multiplying these three independent variables, raised to unknown exponents, by each of the four remaining variables, and solving for the unknown exponents as follows:

$$\pi_1 = Q^{a1} H^{b1} \rho^{c1} D = \left(\frac{L^3}{T}\right)^{a1} \left(\frac{L^2}{T^2}\right)^{b1} \left(\frac{M}{L^3}\right)^{c1} L = M^0 L^0 T^0 \qquad \text{Eq. 4.1}$$

To be dimensionally consistent, the sum of the exponents of each primary dimension must be equal on both sides of the equality sign. Hence, for M,

$$c1 = 0$$

Likewise, for L and T,

$$3a1 + 2b1 - 3c1 + 1 = 0$$

$$-a1 - 2b1 = 0$$

Solving these three equations simultaneously,

$$a1 = -1/2$$

$$b1 = 1/4$$

$$c1 = 0$$

Substituting these values of the exponents into Eq. 4.1 gives the equation for specific diameter:

$$\pi_1 = \frac{DH^{1/4}}{\sqrt{Q}} = D_s \qquad \text{Eq. 4.2}$$

Similarly,

$$\pi_2 = Q^{a2} H^{b2} \rho^{c2} N = \left(\frac{L^3}{T}\right)^{a2} \left(\frac{L^2}{T^2}\right)^{b2} \left(\frac{M}{L^3}\right)^{c2} \frac{1}{T} = M^0 L^0 T^0 \qquad \text{Eq. 4.3}$$

$$\pi_3 = Q^{a3} H^{b3} \rho^{c3} \mu = \left(\frac{L^3}{T}\right)^{a3} \left(\frac{L^2}{T^2}\right)^{b3} \left(\frac{M}{L^3}\right)^{c3} \frac{M}{LT} = M^0 L^0 T^0 \qquad \text{Eq. 4.4}$$

and

$$\pi_4 = Q^{a4} H^{b4} \rho^{c4} H_{sv} = \left(\frac{L^3}{T}\right)^{a4} \left(\frac{L^2}{T^2}\right)^{b4} \left(\frac{M}{L^3}\right)^{c4} \left(\frac{L^2}{T^2}\right) = M^0 L^0 T^0 \quad \text{Eq. 4.5}$$

Solving as for π_1,

$$\pi_2 = \frac{N\sqrt{Q}}{H^{3/4}} = N_s \quad \text{Eq. 4.6}$$

which is specific speed, and

$$\pi_3 = \frac{\mu}{\sqrt{Q} H^{1/4} \rho} \quad \text{Eq. 4.7}$$

π_3 is the reciprocal of a form of Reynolds number for pumps, since

$$\sqrt{Q}\ H^{1/4}$$

has the dimensions of length (diameter) times velocity.

The resulting π_4 is

$$\pi_4 = \frac{H_{sv}}{H} = \sigma \quad \text{Eq. 4.8}$$

which is the Thoma cavitation parameter.

Since the π-terms are constant for dynamically similar conditions, products and powers of the π-terms must also remain constant for dynamically similar conditions. Hence, the more conventional form of pump Reynolds number may be obtained

without loss of similitude by dividing the product of π_1^2 and π_2 by π_3:

$$\frac{\pi_1^2 \times \pi_2}{\pi_3} = \frac{D^2 N \rho}{\mu}$$

Since

$$DN \propto U$$

$$Re^* = \frac{DU\rho}{\mu} \qquad \text{Eq. 4.9}$$

which is the conventional form of the pump Reynolds number.

In the same manner, π_4 may be converted to a more convenient parameter by dividing π_2 by $\pi_4^{3/4}$:

$$\frac{\pi_2}{\pi_4^{3/4}} = \frac{N\sqrt{Q}}{H_{sv}^{3/4}} = S \qquad \text{Eq. 4.10}$$

which is the suction specific speed, a convenient parameter developed in Ref. 6. The limiting conditions for cavitation inception are indicated by limiting values of suction specific speed. Below these limiting values, cavitation characteristics are unimportant, since the performance of the pump is unaffected unless cavitation actually occurs.

Thus, specific speed N_S, specific diameter D_S, pump Reynolds number R_e*, and suction specific speed S, as defined by Equations 4.6, 4.2, 4.9 and 4.10 respectively, are sufficient to completely describe similitude among turbopumps handling incompressible fluids.

Reference 2 and its discussion bring out the points that neither Reynolds number nor specific speed is sufficient by itself to describe similarity in turbomachines. Considering non-cavitating conditions only, the application of dimensional analysis shows that three similarity parameters, N_s, D_s, and R_e* are necessary and sufficient criteria for similitude.

By assuming different variables to be independent or by forming various combinations of the π-terms, a number of other π-terms may be derived which describe similitude with the same accuracy as N_s, D_s, R_e* and S, but all of the other similarity parameters which express the relationships between the variables can be presented as functions of these four. Furthermore, their physical significance and common usage make these parameters obviously convenient. For a given flow and a given head rise through a pump, specific speed is indicative of the rotative speed of the pump and specific diameter is indicative of the impeller diameter or size of the pump. The pump Reynolds number reflects the properties of the fluid being pumped, expressing the ratio of inertia force to viscous force. For a given flow and rotative speed, a high suction specific speed indicates that a low suction head is permitted; or, with constant flow and net positive suction head, S is indicative of the permissible rotative speed.

Dynamic similarity presupposes that geometric similarity also exists, and therefore similarity must be maintained in all aspects of the geometry if the conditions of similitude are to be fulfilled. For example, Reynolds number effects, as in pipes, are a function of the relative roughness of the flow passages. Hence, in order to maintain similarity, the relative roughness of the passage, expressed dimensionlessly as the ratio of roughness height to impeller diameter, must remain constant. The power loss due to leakage through the wear ring is a function of wear ring clearance, and the ratio of wear ring clearance to impeller diameter must be constant if similarity is to be maintained. Other geometric parameters which must be constant are the vane angle β_2, ratio of impeller eye diameter to outside diameter, δ ; ratio of hub diameter to eye diameter, r ; the blade number Z ; and the details of the diffuser configuration.

For non-cavitating conditions for each combination of N_s, D_s, and R_e* values, there is an infinite number of geometric configurations that will satisfy the conditions imposed by the three dynamic similarity parameters, but since the condition of geometric similarity is not necessarily satisfied, these pumps are not necessarily similar. Therefore, these pumps of different geometry will not have similar performance characteristics, even though the conditions of constant N_s, D_s, and R_e*

are satisfied. Obviously, it is not possible to graphically represent all of the possible geometric configurations, and some additional restriction is necessary. Of all the configurations possible, a single configuration will yield an optimum value for a given criterion of optimization. Two criteria for optimization are considered in this study; namely, maximum efficiency, η and maximum suction specific speed, S. Hence, for each set of values of N_s, D_s, and R_e*, there is a unique value for optimum efficiency and a unique geometric configuration required to produce this efficiency, the same being true for designs with optimum suction specific speed.

If this information is represented for a fixed value of R_e* in a system of coordinates in which N_s is the abscissa and D_s is the ordinate, each point on the graph represents a family of pumps which are dynamically and geometrically similar in every respect, including their performance characteristics. Assuming that there are no discontinuities in the functional relationships, the various pump parameters may be represented as functions of N_s and D_s by lines of constant parametric value. For instance, lines of constant efficiency, constant blade angle, etc., may be superimposed on each other to form the N_s-D_s

diagram of Figure 1, a very convenient form of presentation for optimum criteria and design parameters for turbopumps.

With proper attention being given to the inclusion of all variables (such as compressibility), this method of presentation has been extended to other classes of turbomachines -- namely, turbines. By superposition of the resulting N_s-D_s diagrams, it becomes possible to select an optimum combination of optimum turbomachinery elements, rendering the N_s-D_s diagrams a very valuable aid in preliminary design and component selection for systems involving multiple turbomachinery elements in direct connection.

Two methods may be employed to obtain the desired N_s-D_s diagrams -- test and design data from actual pumps may be used when available, or equations for calculating the required curves may be derived through theoretical analysis. Actually, pursuit of both methods is desirable. Results compiled from actual test data are required to corroborate the results of a theoretical analysis, but the theoretical analysis is needed to extrapolate test data and to better understand the effects of parametric variations.

It must be recognized that the design of turbopumps generally constitutes a series of compromises dictated by the application,

by manufacturing limitations and by economic considerations, so that for a given application, it may not be practical to attain the optimum configuration. However, a representation of the best configuration possible according to the present state of the art is of considerable value, and the detailed analysis of this pump type should serve as an indication of the effects imposed by necessary compromises.

It must therefore be expected that only a part of the calculated values are actually confirmed by test evidence. This does not necessarily void the unconfirmed values but rather indicates possible avenues of performance improvements, or more specifically, outlines the pump geometries, which could lead to more efficient pump designs in certain performance regimes.

5. ANALYSIS OF CENTRIFUGAL PUMPS

The relationships among the several variables affecting centrifugal pump performance may be established through dimensional analysis as shown in Section 4. The resulting similarity parameters indicate the qualitative effects of the variables and the quantitative effects must be determined empirically through experimental programs and/or generally from kinematic

and dynamic analysis. The compilation of experimental data and a theoretical analysis for centrifugal pumps have both been undertaken as a part of this study. Only single entry pumps will be considered in this theoretical analysis.

5.1 Analysis of Experimental Data for Centrifugal Pumps

Test data for more than three hundred pump configurations manufactured by a number of leading companies were obtained and analyzed. To obtain values of N_S, D_S and R_e* and the corresponding value of efficiency, a data reduction procedure was programmed for a high speed digital computer. Specific speed and specific diameter were calculated accurately from actual values of rotative speed N, volume flow Q, developed head H, and impeller diameter D. Since the density and absolute viscosity of the fluids were not known, the Reynolds number calculations are approximate and subject to error. The calculations were based on the properties of water at $70^{o}F$.

The data points were segregated into three ranges of Reynolds number, and each Reynolds number range was further subdivided by specific speed value, forming groups of data points with a Reynolds number range varying by a factor of ten and a specific speed range with a range of ten in the units position. Each group of data points was plotted separately in Figures 2a-w, with efficiency as the ordinate and specific diameter as the

abscissa, using the units digit of the specific speed value to mark each point. Thus, Figures 2a-w show for each data point the values of efficiency and specific diameter to the accuracy permitted by the scales of the figures and the specific speed value to the nearest digit in the units position.

The data points for each specific speed value form a cluster of points, and an attempt was made to draw an envelope around all points of equal specific speed. At many specific speeds, there were not sufficient points to obtain a reasonable envelope. Furthermore, it was obvious that the peak efficiencies shown for many N_s values were not optimum because they were substantially lower than for adjacent values.

With some minor extrapolations to obtain similarity in the shapes of the envelopes, the upper portions of the higher envelopes were then compiled on a composite chart for Reynolds numbers between $5x10^6$ and $5x10^7$. Three of these envelopes extended far above the envelopes adjacent to them, and it was found that this resulted from four data points. Excluding these four points and revising the corresponding envelopes, the maxima of the envelopes formed a fairly consistent curve. This is shown in Figure 3. The exclusion of four points out of more than three hundred seems justifiable, since these introduce obvious discontinuities, the cause of which is not

discernible from the test information. Furthermore, these data points fall outside all the envelopes of best efficiency versus specific speed, which are shown in Figure 4, as reported by other investigators. Therefore, since it was not possible to determine whether these four points represented erratic data or pump configurations uncommon to the present state of the art, they were excluded in order to eliminate the discontinuities.

Values of specific speed and specific diameter may be read at the points where the envelopes intersect lines of constant efficiency. Plotting these points on the N_s-D_s coordinates results in isoefficiency lines, which are shown in Figure 5. The lack of uniformity in the shapes of the isoefficiency lines is undoubtedly due to insufficient test data in the area affected. There is no reason to believe that the curves should not be smooth and continuous.

Figure 6 shows pump geometry values from other test data (Reference 4) by presenting lines of constant blade angle β_2 and constant diameter ratio δ as functions of N_s-D_s.

Complete optimization of a pump with respect to a single criterion, such as efficiency, may adversely affect some other characteristic or design criterion of the pump and, therefore, this practice is not necessarily employed in actual pump design. For example, sizable variations in blade angle from those indicated in Fig. 6

should not greatly affect the efficiency of the pump, providing adjustments can be made in the blade number to attain the necessary output head coefficient q_{out}, which is the ratio of the output head times the gravitational constant divided by the square of the impeller peripheral velocity (see Equation 5.6). Therefore, efficiency is not necessarily the governing factor in the selection of blade angle, but the blade angle is frequently determined by other performance characteristics. Of particular importance in this regard is the influence of blade angle on the head characteristic with respect to flow. Sufficiently backward swept vanes produce a constantly increasing head characteristic as flow is reduced toward shut-off, thereby eliminating the tendency toward the instability which can cause surging in a system. Values of vane angle, impeller diameter ratio and vane number can also be restricted by stress limitations which confine the impeller tip speed below certain values. The vane number may also be restricted by manufacturing economy, since many small impeller passages would be more costly to manufacture than a few large ones. Consequently, the selection of the various pump design parameters frequently involves a series of compromises to obtain the best overall configuration rather than a configuration that is optimized with respect to a single criterion.

Values of the various pump parameters for the optimum pumps indicated by the above analysis of experimental data were not

available and, hence, could not be determined. Typical values of blade angle β_2 and diameter ratio δ have been extracted and calculated from Figure 9.15 of Reference 4 and presented in modified form in Figure 6.

The data from Reference 4 was actually reduced from pump data and from a number of blowers in which surging is a very important characteristic because of the compressibility of the fluid being pumped. Hence, backward curvature of the vanes is indicated over most of the centrifugal pump regime.

Reference 13 states that the impeller vane number should be

$$Z = k\left(\frac{D_2 + d}{D_2 - d}\right) \sin \frac{\beta_1 + \beta_2}{2}$$

where

$$k = 10 \sin\left(\frac{\beta_1 + \beta_2}{2}\right)$$

Reference 4 suggests that a common rule in centrifugal blower design is to set the vane number equal to one-third the vane angle expressed in degrees. This rule is included here, since it represents an empirical rather than a theoretical approach.

The number of data points at lower Reynolds numbers was insufficient for establishing envelopes, as was done for Figure 3, but the peak points available did provide some interesting information in support of conclusions reached by other investigators regarding Reynolds number effects. Figure 7 shows the envelope of the peak efficiency points at different specific diameters for the three different Reynolds numbers represented. The general

tendencies indicated are in accord with the findings of other investigators and dynamic similarity is fully accounted for. Reference 2 and 3 both report that, in otherwise similar pumps, efficiency is reduced as Reynolds number is reduced. Reference 3 also states that the effect of Reynolds number on efficiency is dependent upon specific speed, the effect of Reynolds number being greater for low specific speed pumps. This tendency is self-evident from the fact that low specific speed designs have lower efficiencies (i.e., larger losses) than high specific speed designs. These same tendencies are apparent from Figure 7, although the volume of test data at the lower specific speeds is insufficient to permit a quantitative evaluation of the effect. In spite of the inaccuracies possible in the Reynolds number calculations, Figure 7 presents a substantial body of test data from several hundred different pumps to support the findings of earlier investigators. It must be cautioned, however, not to accept the numerical values, presented in Figure 7, without qualification. This becomes evident when the data of Figure 7 are compared with some recent investigations, reported in Reference 3. It is customary to express the Reynolds Number influence by the relation

$$\frac{(1-\eta)}{(1-\eta)_{ref}} = \left(\frac{Re_{ref}}{Re}\right)^{\alpha}$$

by arguing that the losses increase exponentially with decreasing Reynolds Numbers. The exponent α was then assumed to have values between .1 and .2. The test data reported in Reference 3 indicate very strongly that the exponent α is a definite function of the Reynolds Number as indicated by the solid line in Figure 7a, whereby $R_e = 10^7$ is used as reference Reynolds number. Evaluating the data of Figure 7 on the same basis, the values represented by a dot in Figure 7a result for $R_{e_{ref}} = 10^7$, and the values represented by a cross in Figure 7a for $R_{e_{ref}} = 10^8$. It is apparent that these exponents are considerably higher than the exponents quoted in Reference 3. Since the tests reported in Reference 3 were specifically designed to investigate the Reynolds Number influence, it may be assumed that the valid line in Figure 7a represents the Reynolds Number influence more realistically than the dots and crosses in Figure 7a, since these data do not necessarily represent optimized designs, and since possible errors in the numerical evaluation of the Reynolds Number exist, as discussed previously.

The suction specific speeds of a number of actual pumps is presented in a modified form from Reference 5, in Figure 8. In the specific speed regime from 60 to 100, where the bulk of the test data points lie, the upper limit of suction specific

speed appears to be fairly flat, which is to be expected from analytical reasoning. The few data points in the low specific speed regime are insufficient to establish an upper limit, but there is no obvious reason why the suction specific speed should be smaller at low specific speeds. A more detailed discussion of this aspect is presented in Section 5.4

5.2 Theoretical Analysis of Centrifugal Pumps

Two criteria of optimization are considered in this study: (1) maximum efficiency, and (2) maximum suction specific speed. In order to perform a theoretical analysis of centrifugal pumps, expressions are needed for efficiency and for suction specific speed as functions of the dynamic similarity and geometric parameters. Following are the derivations of the required equations:

5.2.1 Efficiency as the Criterion of Optimization for Centrifugal Pumps

The efficiency of a pump may be defined as the ratio of output energy to input energy. Expressed in terms of specific energy, in foot-pounds per pound of fluid flow, or more conveniently in equivalent terms of head in feet, efficiency may be defined as,

$$\eta = \frac{H_{out}}{H_{in}} \qquad \text{Eq. 5.1}$$

In the case of a theoretical pump without losses,

$$\eta = 1.00$$

Therefore,

$$H_{out} = H_{in} = H_{th}$$

where H_{th} is called the theoretical head, and represents the actual energy transfer occurring between the impeller and the fluid.

In real pumps, flow losses occur which reduce output head in the same manner that there is a loss of head due to friction in the flow through a length of pipe or past a restriction. The losses which reduce the output head, H_{out} below the theoretical head, H_{th} are: (see Fig 7b) (1) flow losses in the intake section; (2) incidence losses at the leading edges of the impeller vanes; (3) flow losses in the impeller; (4) flow losses in an annual diffuser; (5) flow losses in the scroll; (6) flow losses in the straight diffuser; (7) a mixing loss at the exit of the impeller. Because of its short length and the possibility of good flow conditions, the flow losses in the intake section are generally small compared with other losses, and are dictated primarily by the application of the pump; therefore, this loss is not considered in this analysis. It is assumed that the impeller will be designed for incidence free entry at the design, or best efficiency point and, therefore, the incidence loss is assumed negligible. Considering the remaining

head losses in order, the output head is reduced below the theoretical head as follows:

$$H_{out} = H_{th} - H_{il} - H_{od} - H_{sc} - H_{sd} - H_m \qquad \text{Eq. 5.2}$$

Other losses occur in real pumps which will not affect the output head but do increase the energy input at the shaft necessary to maintain steady state conditions. The losses which increase the required input specific energy or head are: (1) disc friction; (2) wear ring friction; (3) wear ring leakage; and (4) bearing and seal friction. For all but extremely low power pumps, the bearing and seal friction are negligible compared with other losses and are, therefore, excluded. The remaining losses, which may also be expressed in terms of head, are added to the theoretical energy transfer, H_{th} to obtain the input head,

$$H_{in} = H_{th} + H_{df} + H_{rf} + H_{rl} \qquad \text{Eq. 5.3}$$

Substituting Equations 5.2 and 5.3 into 5.1,

$$\eta = \frac{H_{th} - H_{il} - H_{od} - H_{sc} - H_{sd} - H_m}{H_{th} + H_{df} + H_{rf} + H_{rl}} \qquad \text{Eq. 5.4}$$

It is desirable to express efficiency in terms of dimensionless coefficients. This may be accomplished by dividing each head term by a reference head, H_{ref}, defined by,

$$H_{ref} = \frac{U_2^2}{g} \qquad \text{Eq. 5.5}$$

resulting in dimensionless terms called head coefficients, q, defined generally by,

$$q = \frac{H}{H_{ref}} = \frac{Hg}{U_2^2} \qquad \text{Eq. 5.6}$$

Efficiency then becomes,

$$\eta = \frac{q_{out}}{q_{in}} \quad \frac{q_{th} - q_{il} - q_{ad} - q_{sc} - q_{sd} - q_m}{q_{th} + q_{df} + q_{rf} + q_{rl}} \qquad \text{Eq. 5.7}$$

Each of the head coefficients of Equation 5.7 may be expressed in terms of dimensionless pump parameters. The detailed derivations of these expressions are presented in Section 6, and for the sake of clarity and continuity, only the final forms are given here.

The theoretical head coefficient, representing the actual energy transfer between the rotor and the fluid, may be

analyzed for idealized conditions by the application of Newton's laws of motion and empirical factors which correct from ideal to real conditions. This results in the expression

$$q_{th} = \frac{.95(1-K_1\phi\cot\beta_2)}{1+\frac{1+.6\sin\beta_2}{.5Z(1-.28338)}}$$

Eq. 5.8

where K_1 is the ratio of the meridional velocity at impeller outlet, C_{m2} to the meridional velocity at impeller inlet, C_{m1}

$$K_1 = \frac{C_{m2}}{C_{m1}}$$

Eq. 5.9

The quantity

$$1+\frac{1+.6\sin\beta_2}{.5Z(1-.28338)}$$

is known as the slip factor and is referred to as the quantity, m. Several investigators have determined empirical expressions for the value of m, the one shown here being a form of Pfleiderer's expression. A more complete explanation of m and the justification for selecting Pfleiderer's expression is contained in Section 6.

ϕ is the ratio of the meridional velocity at impeller inlet, C_{m1} to the peripheral velocity of the impeller, U_2

$$\phi = \frac{C_{m1}}{U_2} \qquad \text{Eq. 5.10}$$

δ is the ratio of the eye diameter, d to the impeller diameter, D_2

$$\delta = \frac{d}{D_2} \qquad \text{Eq. 5.11}$$

Z is the number of impeller vanes and β_2 is the vane angle at the discharge of the impeller (see Figure 9).

The flow losses through the various passages of the pump have been expressed by an equation of the same form as the Darcy equation for straight pipes. From this and other assumptions, discussed in detail in Section 6, the loss coefficients which represent reductions in the output head are as follows: The head loss coefficient in the impeller may be evaluated by

$$q_{11} = \frac{.0264\phi^{1.75}\left[1-\delta\left(\frac{1+\tau^2}{2}\right)^{\frac{1}{2}}\right]\left(\frac{K_1^2+K_1+1}{3}\right)^{1.5}}{\sin^4\beta_2 R_e^{*\frac{1}{4}}(1-\tau^2)^{1.25}} \qquad \text{(cont.)}$$

$$\left\{ Z \left[\frac{2(\pi J - Z\frac{t}{D})\sin\beta}{Z\delta^2} + \frac{\pi(1-\tau^2)}{2\left(\frac{K_1^2+K_1+1}{3}\right)^{\frac{1}{2}}(\pi J - Z\frac{t}{D})} \right] \right\}^{.625}$$

Eq. 5.12

$$+ \frac{N_{id}}{2} \left[\phi^2 \left(1 - \frac{K_1^2}{\sin^2\beta_2}\right) + \delta^2 \right]$$

where τ is the ratio of the hub diameter to the eye diameter, and N_{id} is a coefficient explained in Section 6.1.2,

$$\tau = \frac{d_h}{d}$$

Eq. 5.13

$\frac{t}{D}$ is the ratio of the vane thickness to the impeller diameter and J is a grouping of terms defined by,

$$J = \frac{1-\delta\left(\frac{1+\tau^2}{2}\right)^{\frac{1}{2}}}{K_1 - 1} \left[\left(\frac{K_1^2+K_1+1}{3}\right)^{\frac{1}{2}} - 1 \right] + \delta\left(\frac{1+\tau^2}{2}\right)^{\frac{1}{2}}$$

Eq. 5.14

The head loss coefficient in the annular diffuser may be evaluated by

$$q_{ad} = \frac{.0854\phi^{1.75}(\lambda-1)}{R_e^{.25}\,\delta^{2.5}} \left[1 + \frac{1}{m^2}\left(\frac{1}{\phi K_1} - \frac{1}{\tan\beta_2}\right)^2 \right]^{1.375}$$

$$\left(\frac{1}{\lambda^2} + \frac{1}{\lambda} + 1\right)^{.375} K_1^3 \left[1 - \frac{q_{ri}}{q_{th}} \right]^{1.75}$$

Eq. 5.15

where λ is the ratio of the outer diameter to the inner diameter of the annular diffuser and the slip factor, m, is defined by,

$$m = 1 + \frac{1 + .6 \sin\beta_2}{.5Z(1 - .2833\delta)} \qquad \text{Eq. 5.16}$$

The head loss coefficient for the scroll may be represented by,

$$q_{sc} = \frac{.155\phi^{1.75}\left(1 - \frac{q_{rl}}{q_{th}}\right)^{1.75} K_1^{2.375}}{\delta^{1.25} R_e^{*.25} (1-\tau^2)\lambda^{1.4375}} \left[1 + \frac{1}{m^2}\left(\frac{1}{\phi K_1} - \cot\beta_2\right)^2\right]^{1.188} \qquad \text{Eq. 5.17}$$

and the head loss coefficient in the straight diffuser may be evaluated by,

$$q_{sd} = \frac{\phi^2(1-\eta_{sd})}{2}\left(1 - \frac{qrl}{qth}\right)^2 \left\{\frac{K_1^2\left[1 + \frac{1}{m^2}\left(\frac{1}{\phi K_1} - \cot\beta_2\right)^2\right]}{\left\{\lambda + 2\left[\frac{m(1-\tau^2)\delta^2}{4K_1\left(\frac{1}{\phi K_1} - \cot\beta_2\right)} + \left[\frac{m\lambda(1-\tau^2)\delta^2}{4K_1\left(\frac{1}{\phi K_1} - \cot\beta_2\right)}\right]^{1/2}\right]\right\}^2} - 1\right\} \qquad \text{Eq. 5.18}$$

and

$$q_m = .125(1-\tfrac{1}{m})^2 \qquad \text{Eq. 5.19}$$

The loss coefficients which represent increases in shaft power may be represented by the following equations:

$$q_{rl} = \frac{2K_l q_{th}}{\phi(1-\tau^2)\left(\frac{k_2}{k_1} f + 15\right)^{1/2}} \qquad \text{Eq. 5.20}$$

$$\left\{ 2\left[q_{th} - q_{ll} - \frac{1}{2m^2}\left(1 + \frac{K_l^2\phi^2}{\sin^2\beta_2} - \frac{2K_l\phi}{\tan\beta_2}\right) - \frac{1-\delta^2}{8} \right] \right\}^{1/2}$$

where k_1, k_2, and f are empirical factors whose values are discussed in Section 6,

$$q_{df} = \frac{2.2\,(1-\delta^5)}{\phi\,\delta^2\,(1-\tau^2)} \qquad \text{Eq. 5.21}$$

and

$$q_{rf} = \frac{8k_2}{\ln\left(\frac{1}{1+k_1}\right) Re^{.2}\phi\delta(1-\tau^2)} \qquad \text{Eq. 5.22}$$

Substitution of Equations 5.8 through 5.21 into Equation 5.7 results in an equation of the efficiency of any centrifugal pump. Because of its complexity and size, the equation will not be shown in its fully expanded form.

5.2.2 Discussion of Component Losses

Only few test data on the losses in the individual components of centrifugal pumps are published in the literature. Usually, these investigations deal with specialized cases; i.e., certain geometries, and usually cover only comparatively limited flow ranges. Some of these data are obtained in stationary experiments instead of rotating experiments; hence, these data might not be applicable in all cases, although the exact magnitude of the difference in flow mechanism between stationary and rotary experiments is not known. Attempts have been made to calculate the losses in the components of pumps of the basis of theoretical considerations (notably Reference 1) whereby usually the pipe friction concept and conventional hydraulic arguments are used. It appears that these considerations yield reasonable results which, in most cases, explain the actually obtained data comparatively well. Hence, in the present investigations, similar arguments are used for expressing the component losses as a function of channel geometry and flow conditions.

The loss relations quoted in 5.2.1 may now be discussed in order to recognize the main trends.

Equation 5.8 states that the theoretical head coefficient q_{th} is mainly a function of the flow factor ϕ and the blade angle β_2. This is graphically shown in Figure 10 which indicates that q_{th} decreases with increasing flow factors and decreasing blade angles β_2 (i.e., with increasing flow rates and increasing "backward sweep" of the blades). It is also evident from Equation 5.8 that q_{th} increases with increasing blade numbers, Z. These tendencies result from the fact that the exit moment of momentum and consequently the change of moment of momentum decreases with increasing flow rates and decreasing blade angles β_2.

The basic trends for the impeller head loss coefficient q_{il} (Equation 5.12) are presented in Figure 11, revealing that the impeller losses increase with increasing flow factors, ϕ, increasing blade numbers Z, decreasing diameter ratios δ, and decreasing blade angles β_2. These trends result since the losses are proportional to the square of the through flow velocity and proportional to the frictional area which increases with increasing blade numbers, increasing blade angles, and decreasing diameter ratios.

In discussing the losses of the annular diffuser (Equation 5.15) it must be realized that the flow path is a logarithmic

spiral. Hence, the flow path length and consequently the losses, increase with decreasing flow angles α_2 (i.e., decreasing flow factors for constant values of λ). These tendencies are graphically presented in Figure 12. This diagram also indicates that the losses increase with increasing blade angles β_2 for constant ϕ values. This tendency is explained by the fact that the flow angle α_2 is a function of ϕ and β_2, decreasing with increasing β_2 values, so that for constant flow factors the flow path length is larger for large β_2 values than for small β_2 values.

It is to be noted that Equation 5.15 deals only with the losses occurring in vaneless annular diffusers. In cases where guide vanes are provided in annular diffusers, the natural flow path of a logarithmic scroll is changed to a shorter and steeper path for the same diameter ratio, meaning that the diffusion rate is larger than the diameter ratio and that the diffuser leaving angle is larger than the entrance angle to diffuser. The frictional area is somewhat increased due to the addition of the vanes. This detrimental effect, however, is overcompensated for by the larger diffusion rate in well designed vane type diffusers so that usually somewhat higher efficiencies occur in vane type annular diffusers than in the

vaneless annular diffusers. It is to be noted that due to the change in absolute flow angles, the approach vector to the scroll is different for vane type diffusers as compared to vaneless annular diffusers, meaning that the scroll areas become somewhat larger if vanes are incorporated in the annular diffuser; thus, Equation 5.15 is not valid for computing the straight diffuser losses. No exact relations have been found for the difference in losses between vane type and vaneless annular diffusers. It appears reasonable to assume that in the high specific speed regime, pumps equipped with vane type annular diffusers have an efficiency which is about 1% to 3% higher than the pump efficiency for designs with a vaneless annular diffuser. It is evident that the smaller difference pertains to pump designs with large degrees of reaction (i.e., blade angles smaller than 90^{o}) since, in this case, the energy conversion taking place in the diffuser is comparatively small, whereas the larger figure pertains to pump designs with smaller degrees of reaction (i.e., with impeller blade angles of 90^{o} and higher). In order to avoid mathematical complications, a comparatively small diameter ratio (i.e., diffusion rate) of the vaneless annular diffuser is assumed in the calculations. A straight diffuser section is then assumed to be provided downstream of the collector scroll, which reduces the velocity to c_{m-1}.

The scroll friction losses are expressed algebraically in Equation 5.17, and graphically in Figure 13. This diagram indicates that the scroll friction losses have a similar tendency as the annular diffuser losses but are in general somewhat smaller than the annular diffuser losses. This difference in magnitude results because the scroll, as defined in this report, is merely a collector and not primarily a diffuser, in contrast to the annular diffuser. (Actually, a slight flow deceleration may occur in many scroll designs due to the decrease in peripheral component from scroll inlet to scroll outlet.) The tendency of the scroll losses to increase with decreasing flow factors results from the comparatively small hydraulic diameter required for small flow rates.

Usually the flow velocity at the scroll exhaust is comparatively large in most designs. Additional deceleration is therefore desired which may be obtained by a straight conical diffuser, mounted at the scroll exhaust. For convenience, it may be assumed that the desired exhaust velocity of the pump is equal to the impeller inlet velocity, c_{m-1}. It is apparent that comparatively large deceleration rates are required in the conical diffuser for cases where the annular diffuser provides only a small diffusion rate. Since the flow

deceleration in the annular diffuser is proportional to λ, it becomes apparent that large conical diffuser losses, q_{sd}, occur for small λ values and the q_{sd} decreases with increasing λ values. This tendency is expressed in Equation 5.15 and graphically presented in Figure 14. This diagram also indicates that q_{sd} decreases with increasing flow factors. This tendency is caused by the assumption that the diffuser exit velocity is equal to the impeller inlet velocity (i.e., proportional to ϕ). Hence, smaller deceleration rates and, consequently smaller losses, occur at large flow factors than at low flow factors.

The disc friction and wear ring friction losses expressed by Equation 5.21 and 5.22 are graphically presented in Figure 14, indicating a significant increase of these losses with decreasing flow factors, and decreasing diameter ratios. This trend exists since the power absorption of the disc and wear ring is mainly a function of the surface velocity and surface area (i.e., tip speed) but independent of the flow rate through the impeller. The power absorption of the impeller, however, is proportional to the flow rate (i.e., flow factor). The loss coefficients q_{df} and q_{rf} express the power loss as percentage of the impeller power absorption which then increases with decreasing flow rates. Since the impeller

flow rate decreases with increasing diameter ratios δ, it follows that the loss coefficients q_{df} and q_{rf} also increase with decreasing diameter ratios.

The wear ring leakage, expressed as head loss coefficient, is graphically presented in Figure 16. It is evident that this loss increases with decreasing flow factors. This tendency results from the fact that the leakage flow is almost constant, due to the constant leakage area, whereas the impeller flow rate decreases with decreasing flow factors. Hence, percentagewise, the leakage increases with decreasing flow factors. Another parameter which influences the leakage flow is the effective pressure difference at the gap. This pressure difference is created by the difference in pumping action inside and outside of the impeller. The liquid at the outside of the impeller is usually assumed to rotate with half the impeller speed due to the shear forces, thus providing a pressure rise which is independent of flow rate. The pressure rise experienced by the flow inside of the impeller is influenced by the blade angle β_2 in such a manner that an almost constant pressure rise (i.e., independent of flow rate) occurs for $\beta_2 = 90^o$ but a pressure rise which decreases with increasing flow rates for $\beta_2 < 90^o$. Hence, the effective

pressure difference at the gap is almost constant for $\beta_2 = 90^\circ$, but decreasing with increasing ϕ values for $\beta_2 < 90^\circ$. This difference is responsible for the tendency that q_{r1} for $\beta_2 < 90^\circ$ decreases more rapidly with increasing ϕ values than q_{r1} for $\beta_2 = 90^\circ$, as shown in Figure 15, and expressed algebraically in Equation 5.20.

5.3 Calculation of N_s-D_s Diagram for Optimum Efficiency:

As pointed out in Section 4, in order to obtain a unique solution for each point on the N_s-D_s diagram, it is necessary to introduce some restriction to the geometric similarity conditions, and this may be accomplished by introducing a criterion of optimization. The criterion of optimization for this part of the study is the restriction to the configuration at each N_s-D_s combination which will produce the maximum possible design point efficiency.

In order to effect a solution for a given N_s-D_s combination, it is therefore necessary to relate the relationships used to express efficiency as functions of N_s and D_s. For mathematical convenience, the equations have actually been expressed in terms of two other parameters which, since they are themselves explicit functions of N_s and D_s, accomplishes the same end. These parameters are q_{out}, which is defined by Equation 5.2 and Ψ, which is defined as,

$$\Psi = \delta \left[\phi(1-\tau^2)\right]^{\frac{1}{2}} \qquad \text{Eq. 5.23}$$

These parameters are expressed explicitly in terms of N_s and D_s by the following equations:

$$q_{out} = \frac{11,750}{N_s^2 D_s^2} \qquad \text{Eq. 5.24}$$

$$\Psi = \frac{4.85}{N_s^{1/2} D_s^{3/2}} \qquad \text{Eq. 5.25}$$

Conversely, for convenience, N_s and D_s are expressed as functions of Ψ and q_{out} by,

$$N_s = 228.5 \frac{\Psi}{q_{out}^{3/4}} \qquad \text{Eq. 5.26}$$

$$D_s = .473 \frac{q_{out}^{1/4}}{\Psi} \qquad \text{Eq. 5.27}$$

Rearranging Equation 5.22 permits solving for δ as an explicit function of ϕ, τ, and ψ.

$$\delta = \frac{\psi}{\left[\phi(1-\tau^2)\right]^{1/2}} \qquad \text{Eq. 5.28}$$

Substituting this expression for δ in each of the head coefficients derived in Section 5.2 and substituting these expressions into Equation 5.7 results in an expression for efficiency in terms of β_2, τ, Z, ϕ, λ, ψ, and q_{out}. Because of the length and complexity of this expression, it is not shown in its fully expanded form. However, a solution for this total expanded expression has been effected through an iterative program written for IBM 650 high speed digital computer.

Preliminary runs on the program indicated that variations in τ and in λ within limits of standard practice had a negligible effect on efficiency and, therefore, constant values of 0 and 1.001 were used, thus reducing the variables to β_2, Z, ϕ, ψ, and q_{out}. In the iterative solution, numerical values of β_2, Z, and ϕ were tried to determine the combination which would result in the maximum efficiency for a given ψ and q_{out} (congruently N_s and D_s) combination. By partially differentiating the component terms of Equation 5.7, a method of convergence was introduced to obtain a reasonable program running time.

The resulting N_s-D_s diagram is shown in the composite diagram of Figure 1.

5.3.1 Discussion of N_s-D_s Diagrams for Maximum Efficiency Designs

The calculated N_s-D_s diagram presented in Figure 1 indicates that optimum efficiencies are obtained at specific speeds of about N_s = 80 and at a specific diameter of about D_s = 1.8. The maximum obtainable efficiency decreases with decreasing specific speeds whereby increasing specific diameters are required with decreasing specific speeds in order to obtain maximum efficiencies. It is evident that the peak efficiency regime centers around head coefficients of q_{out} =.7. At smaller q_{out} values, lower efficiencies than peak efficiencies are obtained. A particularly drastic reduction in efficiency is observed in cases where the q_{out} value exceeds a value of .8. The overlay A to Figure 1 reveals that the optimum diameter ratio δ, decreases with decreasing specific speeds (i.e., increasing specific diameters) and that the optimum blade angle follows almost a line of constant head coefficient. It is evident that a blade angle of 90° does not yield optimum efficiencies but blade angles of about 60° at large specific speed and somewhat higher blade angles in the lower specific speed regime. Overlay B to Figure 1 indicates that a blade number of 20 is optimum for almost all specific speeds and that the lengths of the straight portion

of the diffuser becomes a multiple of the impeller diameter in order to obtain the efficiencies shown in the low specific speed regime; whereas, at larger specific speeds, the lengths of the straight portion of the diffuser can be as small as .4 to .3 times the impeller diameter. Overlay C to Figure 1 indicates that the optimum flow factor ϕ, increases with increasing specific speeds, meaning that a flow factor of $\phi = .1$, is optimum in the low specific speed regime and a flow factor of $\phi = .3$ to .35 for the high specific speed regime. The lines of constant suction specific speed S, indicate that the suction specific speed inherent in the designs presented in these diagrams increases with decreasing specific speeds, exhibiting suction specific speeds of 300 at high speed and suction specific speeds of 500 in the low specific speed regime.

The tendencies exhibited in Figure 1 can be explained by the following considerations: The most influential values are the conditions at impeller inlet and diffuser inlet. The criterion at the diffuser inlet is the angle α_2 of the absolute velocity entering the annular diffuser. In cases where this angle is comparatively small (for example,

below 5^{o}) the frictional path becomes large, meaning that the diffuser losses are comparatively large (since the deceleration ratio depends only on the diffuser diameter ratio and not on the flow angle). Small flow angles α_2 are identical with small flow factors ϕ. Hence, small flow factors cause comparatively large diffuser losses. This holds also for the collector scroll.

For designs with large flow factors ϕ, the through flow losses in the impeller, for example, become comparatively large.

If, now, comparatively small flow rates are passed through the pump (low specific speed designs) then the desirable flow angle α_2 can only be obtained if the impeller width is comparatively narrow. This causes an unfavorable geometry of the impeller as well as diffuser since, then, the frictional area (i.e., the hydraulic diameter) becomes unfavorable. Additionally, the leakage losses tend to increase with this type of impeller geometry so that the optimum diffuser flow angle cannot be realized. The optimum efficiency of low specific speed pumps, therefore, has to be expected at a compromise between diffuser angle and impeller width. This compromise favors lower flow factors with decreasing specific speeds.

Since one of the assumptions of this analysis is that the pump exit velocity is equal to the impeller inlet velocity, it becomes also apparent that a comparatively large diffusion rate is required in cases where the flow factor is comparatively small. This necessitates a comparatively long straight diffuser portion behind the scroll, thus explaining the increase of the X value with decreasing specific speeds. The decrease in optimum flow factor with decreasing specific speeds also explains that the suction specific speed increases with decreasing specific speed since this value is greatly affected by the meridional component.

The tendency that the optimum diameter ratio decreases with decreasing specific speed can be traced back to the impeller inlet conditions. If, for example, at low flow rates (i.e., low specific speeds) a large diameter ratio would be used, then the relative velocity in the inducer w_1 would be comparatively large and would occur at a fairly small angle β_1. This large velocity then will have to be diffused to the value of the relative leaving component at impeller exit and will have to be deflected from the small angle β_1 to the comparatively large angle β_2. This process causes diffusion and deflection losses

which decrease the impeller efficiency. By selecting a smaller diameter ratio, the angle β_1 is increased and the relative velocity in the inducer decreases so that smaller diffusion losses will occur in the impeller. This tendency, however, will increase the wheel disc friction losses. These losses increase with decreasing impeller diameter ratios. Hence, the optimum condition is found at the proper compromise between wheel disc friction losses and impeller losses. This compromise is reflected in Figure 1 by the optimum flow factor and optimum diameter ratio values.

The fact that the optimum blade angle and optimum blade number are almost proportional to the head coefficient q_{out} evolves from the following considerations: The head coefficient q_{out} is, for the ideal machine, proportional to the theoretical head coefficient q_{th}. This coefficient increases with increasing values of the blade angle β_2 and decreasing slip value m (i.e., increasing blade number z). The losses disturb this tendency somewhat as indicated by the divergence of the optimum blade number and blade angle lines. They do not, however, appear to change the main tendencies. It is to be noted that the

divergence of the optimum blade number and optimum blade angle lines can also partly be attributed to the fact that the theoretical head coefficient is also a function of the flow factor for $\beta_2 < 90^o$. This influence increases with increasing flow factors, as evidenced by the divergence between the q_{out} and β_2 lines at large flow factor (i.e., large specific speeds).

The fact that an optimum blade number exists is explained by the consideration that a large number of blade gives a large frictional area, consequently, comparatively large friction losses in the impeller passages. Hence, in spite of the increase in output obtained by the increasing blade number, this tendency is somewhat compensated for by the decrease in frictional area due to the increase in blade number, thus rendering a blade number of 20 close to the optimum value for almost the whole specific speed regime.

5.3.2 Comparison of Experimental Data With Theoretical Analysis

In comparing the calculated N_s-D_s diagram with the one obtained from the test data, differences are observed,

particularly in the low specific speed regime. The experimental iso-efficiency lines of Figure 5, and the theoretical iso-efficiency lines of Figure 1, have been superimposed in Figure 17. The broken lines, representing experimental data, are observed to match very closely at $q_{out} = .5$ for specific speed values above 25. In the same specific speed range but at lower values of q_{out}, the maximum difference between the experimental and theoretical curves is approximately two and one-half percentage points. Considering the simplifying assumptions required in the theoretical analysis, the possible error introduced by using constant empirical factors required and the purpose for which this study is intended, this is quite a tolerable degree of accuracy.

At specific speeds decreasing below 25, the theoretical values were increasingly superior to the experimental values. This is probably partly attributable to the fact that vane thickness ratios, surface roughness ratios, leakage clearance ratios, etc., were assumed to be constant at all specific speeds in the theoretical analysis, which was probably not true in the case of the experimental data. Although it is not a necessary requirement, the test data for the low specific speed pumps did generally represent pumps of smaller flow capacity and, hence, generally, although not universally, of smaller size.

The absolute value of surface roughness, for example, in the impeller passages and diffuser, does not reduce proportionately with the reduction in flow passage dimensions in standard commercial pumps due to economical manufacturing limitations. Hence, the friction factors assumed constant in the theoretical analysis, probably increased with decreasing values of specific speed in the pumps from which test data was gathered.

Another probable cause for differences between experimental and theoretical results in the low specific speed regime stems from the fact that there were far fewer data points in the low specific speed regime, reducing the probability of having truly optimum pump configurations represented by the experimental data. As can be seen from Figures 2m-p, which have a large number of points, the majority of these data points are not optimum.

It must be recognized that bearing and seal friction, considered negligible in the theoretical analysis, become increasingly important in the low specific speed regime, and may make the low specific speed theoretical results slightly optimistic. The fact that the predicted curves check comparatively well with the experimental data in the large

specific speed regime could then be explained by the fact that large specific speed designs usually show a larger blade number than 6, approaching in some cases 12 to 14. In comparing Figure 6 with overlay A of Figure 1, it results that the lines of optimum blade angle are somewhat different in both diagrams, meaning that the calculated data would require a smaller blade angle than the test data implies. This difference again can be explained by the fact that the calculated optimum blade number is considerably higher than the number of blades actually incorporated in the tested pumps. A final conclusion, therefore, regarding the validity of the assumptions of this report and, consequently, the validity of the precalculated N_s-D_s diagrams is not possible at this time. The testing of pumps which show the stipulated geometry will be required before a final verdict on the validity of the assumptions of the component losses can be rendered.

It is therefore reasonable to say that Figure 6 should be used for design calculations which follow conventional design practice. The values predicted in Figure 1 might, however, be obtainable if the geometries stipulated in the overlays can reasonably well be incorporated into the pump design.

The pump data shown in Figure 6 from Reference 4, are obtained from test data of blowers and pumps. No distinction in these test data was made regarding the diffuser design, (i.e., whether a vaneless or vaned annular diffuser was incorporated into the pump. Some clarification of this aspect is provided by Reference 13, which indicates that in the low specific speed regime, vane type diffusers yield better efficiencies than vaneless diffusers, Figure 4, implying that the vaneless type shows efficiencies which are about 5 to 8 points lower than the vane type diffuser in the medium specific speed regime and up to 25 points in the low specific speed regime. This tendency appears reasonable since usually comparatively shallow flow angles are to be expected at diffuser inlet in the low specific speed design due to the small flow factor which renders the vaneless diffuser comparatively inefficient. Hence, the incorporation of guide vanes improves the performance. A more detailed investigation, however, of the particular diffuser designs incorporated in the test data quoted in Reference 13 would be necessary to evaluate this influence numerically. Unfortunately, this detailed information is not quoted.

The analysis yields efficiencies which are higher than the test data shown in Figure 4 for vane diffusers. This difference

is partly explained by the comments in Section 5.2.2 where it was stated that the analysis assumes short vaneless annular diffusers and straight diffusers at the scroll exit.

Another reason for the high efficiency values of the analysis is seen in the high impeller blade number found to be optimum by the analysis (if they can be made sufficiently thin).

It should also be noted that the difference between vane type and vaneless diffusers could be expected to be particularly pronounced in the low specific speed regime, since for this regime low flow factors; i.e., small diffuser angles yield maximum efficiencies. Since the incorporation of guide vanes in the annular diffuser offers the opportunity to make the diffusers flow path "steeper", thus reducing the frictional area (which is not possible for the vaneless type, due to the free vortex pattern) and increasing the diffusion rate, additionally affording a somewhat improved scroll collector design (since now the scroll cross-section becomes larger) it becomes evident that for the specific speed regime of N_S = 10 to 30, the vaned diffuser offers considerable advantages. On the basis of these comments, it appears advisable to interpret the calculated efficiencies presented in the N_S-D_S diagram as being most likely obtainable for pumps with vane type diffusers.

Actually, this aspect merits additional investigation which may prove to be of particular benefit for low specific speed designs.

It means that the diffuser design becomes of critical importance for the efficiency of low specific speed pumps, meaning that the diffuser efficiency determines, to a large degree, the pump efficiency.

Since vaned diffusers have higher efficiencies than vaneless diffusers, the application of a single conical diffuser over only a part of the impeller discharge area (partial emission pumps) should yield acceptably high efficiencies for low specific speed designs. Only little information on the performance of these "partial emission" pumps is found in the unclassified literature. The maximum obtainable efficiency as well as the optimum specific speed regime does not seem to be too well established. Good low specific speed performance, however, is indicated by Reference 27.

Some tentative data are shown by the dashed line in Figure 17a by quoting η_{max} values (for D_{s-opt}). These values indicate a slightly better performance at low specific speeds than full admission vane diffuser pumps, but inferior performance to full admission pumps at specific speeds greater than 15.

It is to be expected that an optimum value for the degree of emission exists and that this value is a function of N_s and D_s. The degree of emission then becomes a major criterion for the optimization, and determines (to a large degree) the optimum

design geometry. In order to determine the optimum degree of emission, a thorough analysis of the flow mechanism in the blocked portion of the pump casing will be necessary. The presently available data are insufficient to perform such detailed analysis.

For even lower specific speeds, the Pitot pump should be expected to yield better performance than the partial emission or the vaned diffuser oump since the Pitot pump will have extremely low windage losses which, according to Figure 15, are comparatively large at small flow factors for conventional centrifugal pumps. Since the windage losses in Pitot pumps occur at the gas side of the rotating drum (see Figure 31), i.e., in a medium in which the density is only 1/1000 of that of liquids, the windage losses are considerably reduced. Hence, Pitot pumps should be capable of exhibiting good efficiencies as long as the probe drag is comparatively small. The more detailed analysis of Pitot pumps, presented in Section 7, seems to confirm this conclusion to some degree. It is to be noted that this conclusion is strictly preliminary due to the lack of sufficient test data.

A treatise on low specific pumps would be incomplete without reference to the "regenerative" or "drag" pump described at various places in the literature (e.g., Reference 25). This

pump type does exhibit very favorable low specific performance at N_s values less than 15, so that this pump performance-wise must be considered a serious competitor for the Pitot pump. The flow mechanism in "regenerative" or "drag" pump is significantly different from the flow mechanism in centrifugal pumps and in some respects not yet too well explored. A detailed treatment of this pump type, particularly an adequate discussion of the flow phenomena occurring in this pump type and, consequently, a treatise on the effect of design geometry on performance, was considered to exceed the scope of the present study program.

Figure 17a shows the efficiency as a function of specific speed, that can be attained with good design. This test data was supplied by the McCulloch Corporation (Reference 26).

5.4 Suction Specific Speed as the Criterion of Optimization for Centrifugal Pumps

As pointed out previously, there are criteria of optimization other than efficiency that may be applied as a restriction to obtain a unique configuration and set of performance characteristics for the family of similar pumps represented by each point on the N_s-D_s diagram. Another criterion which is of especial interest is that of producing maximum suction specific speeds.

In Section 4, suction specific speed was discussed as a convenient parameter for describing limiting cavitation characteristics for pumps. Starting with Equation 4.10 it can be shown that

$$S = 228.5 \frac{\psi}{q_{sv}^{3/4}} \qquad \text{Eq. 5.29}$$

The full derivations of this and the following expressions are given in Section 6.2 but are deleted here for the sake of clarity and continuity.

Since it is possible that preswirl may exist at the condition of maximum S, the absolute angle of the flow at entrance to the impeller α_1, is retained. Considering

the pressure drop due to friction in the inlet section and the reduction in static head resulting from the absolute motion of the fluid in the inlet and the relative motion of the fluid past the pump vanes, the net positive suction head coefficient can be shown to be

$$q_{sv} = \frac{1}{2}\left[\frac{\phi^2}{\sin^2\alpha}(B_1 + B_2 + B_3) + B_3\delta(\delta - 2\phi\cot\alpha)\right] \quad \text{Eq. 5.30}$$

where B_1 is a friction coefficient for the inlet section and B_2 and B_3 are empirical coefficients expressing the loss in static head due to the absolute and relative velocities respectively.

Partial differentiation of q_{sv} with respect to δ, ϕ, and $\cot\alpha$, yields a set of simultaneous equations which, upon solution, results in explicit expressions for ϕ, δ, and α, in terms of ψ, and the empirical coefficients.

$$\phi = \left[\frac{\psi}{2}\,\frac{B_3}{B_4}\left(1 - \frac{B_3}{B_4}\right)\right]^{\frac{1}{3}} \quad \text{Eq. 5.31}$$

$$\delta = \frac{\psi}{\phi^{1/2}} \quad \text{Eq. 5.32}$$

$$\cot\alpha = \frac{B_3}{B_4}\,\frac{\psi}{\phi^{3/2}} \quad \text{Eq. 5.33}$$

where

$$B_4 = B_1 + B_2 + B_3 \qquad \text{Eq. 5.34}$$

Reference 18 indicates values of

$$B_1 + B_2 = 1.1$$

and a value of .2 was selected for B_3. These values of the coefficients yield values of inlet angle $\alpha_1 = 59^\circ$ and suction specific speed S = 541. These values are constant at all values of N_s and D_s. The values of δ and ϕ are shown in Figure 10a, which also gives optimum β_2 and Z for these conditions as calculated by substituting the proper values of δ , ϕ , and α_1, into the efficiency optimization program. Efficiencies are shown in Figure 10b.

It must be conceded that it is possible that the empirical coefficients B_1, B_2, and B_3 are not constant over the entire range, and Shepard and Church (References 8 and 19, respectively) consider that these coefficients have not been accurately determined at present. It is not to be expected, therefore, that there is a high degree of accuracy in these results. Nevertheless, they correspond well with the best suction specific speed values taken from literature as given in Figure 8.

where

$$B_4 = B_1 + B_2 + B_3 \qquad \text{Eq. 5.34}$$

Reference 18 indicates values of

$$B_1 + B_2 = 1.1$$

and a value of .2 was selected for B_3. These values of the coefficients yield values of inlet angle $\alpha_1 = 59^o$ and suction specific speed S = 541. These values are constant at all values of N_s and D_s. The values of δ and ϕ are shown in Figure 18, which also gives optimum β_2 and Z for these conditions as calculated by substituting the proper values of δ, ϕ, and α_1 into the efficiency optimization program. Efficiencies are shown in Figure 19. Since Equation 5.32 shows that δ is a function of ϕ and ψ Equation 5.31 shows that ϕ is a function of ψ for a constant suction specific speed, these two relationships indicate that for any one point on the N_s-D_s diagram there is only one value of each δ and ϕ when suction specific speed is constant. Therefore, the only variables that are left to optimize efficiency at constant suction specific speed are β_2 and Z. The parameters β_2 and Z are inter-related with respect to determining head coefficient, q_{out}, and it can be seen on Figure 10b that the highest efficiencies

for a given value of N_s occur at a q_{out} close to .7. The iso-efficiency lines would curve back to the right in Figure 10b at higher values of q_{out} except the pump is unable to attain these high q_{out} values when the restriction of a constant suction specific speed of 541 is imposed.

Figure 18a shows the parameters β_2 and Z. As mentioned previously, the highest efficiencies for any N_s occur at q_{out} values of about .7, and since β_2 and Z affect q_{out} to a large degree, the optimum values of β_2 and Z are nearly constant over the N_s range investigated.

It must be conceded that it is possible that the empirical coefficients B_1, B_2, and B_3 are not constant over the entire range, and Shepard and Church (References 8 and 19, respectively) consider that these coefficients have not been accurately determined at present. It is not to be expected, therefore, that there is a high degree of accuracy in these results. Nevertheless, they correspond well with the best suction specific speed values taken from literature as given in Figure 8.

Much of the literature suggests values of suction specific speed between 330 and 472, which is somewhat lower than

the value of 541 shown here. However, Figure 8 shows test data points as high as 614, indicating that the value calculated here is a reasonable one. Stepanoff (Reference 4) indicates that suction specific speeds up to 945 are possible with a sacrifice in efficiency, and up to 708 at the best efficiency point. However, special design is required for such high values of suction specific speed, and nowhere in literature have values of the coefficients or the necessary special design considerations been found.

Therefore, it is considered that the values obtained do represent the best that can be done with standard commercial designs with careful attention being given to entrance conditions. Thus, these values do represent the present state of the art in predicting cavitation characteristics.

5.5 Possible Methods for Improving Low Specific Speed Centrifugal Pump Performance

Figures 17 and 17a, and the discussion of section 5.3.2 outline the pump configuration which appears to be most desirable for obtaining high performance of low specific speed centrifugal pumps. One promising possibility lies in increasing the number of impeller blades (and reducing the pump diameter; i.e., the specific diameter) for a given

application. Attention to maintaining surface roughness ratios, leakage clearance ratios, etc., and the use of higher class bearings and seals in the low specific speed regime offers the possibility of an additional boost in centrifugal pump efficiency at specified speeds less than 25.

Further avenues of performance improvements in the low specific speed regime are evidenced in Figure 17a by the preliminary performance of Pitot pumps. It appears likely that efficiencies of 45% with Pitot pumps can be obtained at specific speeds of 10, where the theoretical curve for centrifugal pumps indicates only 40%. A more concise appraisal of the possible pump improvements in this specific speed regime will require additional test information.

It must be recognized that without clever innovations in manufacturing processes, it is unlikely that significant improvements in efficiency could be attained by these means without substantial increases in manufacturing cost. The inherent low power requirements of low specific speed pumps reduce the importance of efficiency in this regime. Thus, for normal commercial applications, economic limitations will confine the iso-efficiency profiles to approximately those shown in Figure 5. However, for applications in which efficiency plays an important role, such as

in missile and space flight applications, substantial increases in manufacturing costs may be justified by increased capability in fulfilling missions.

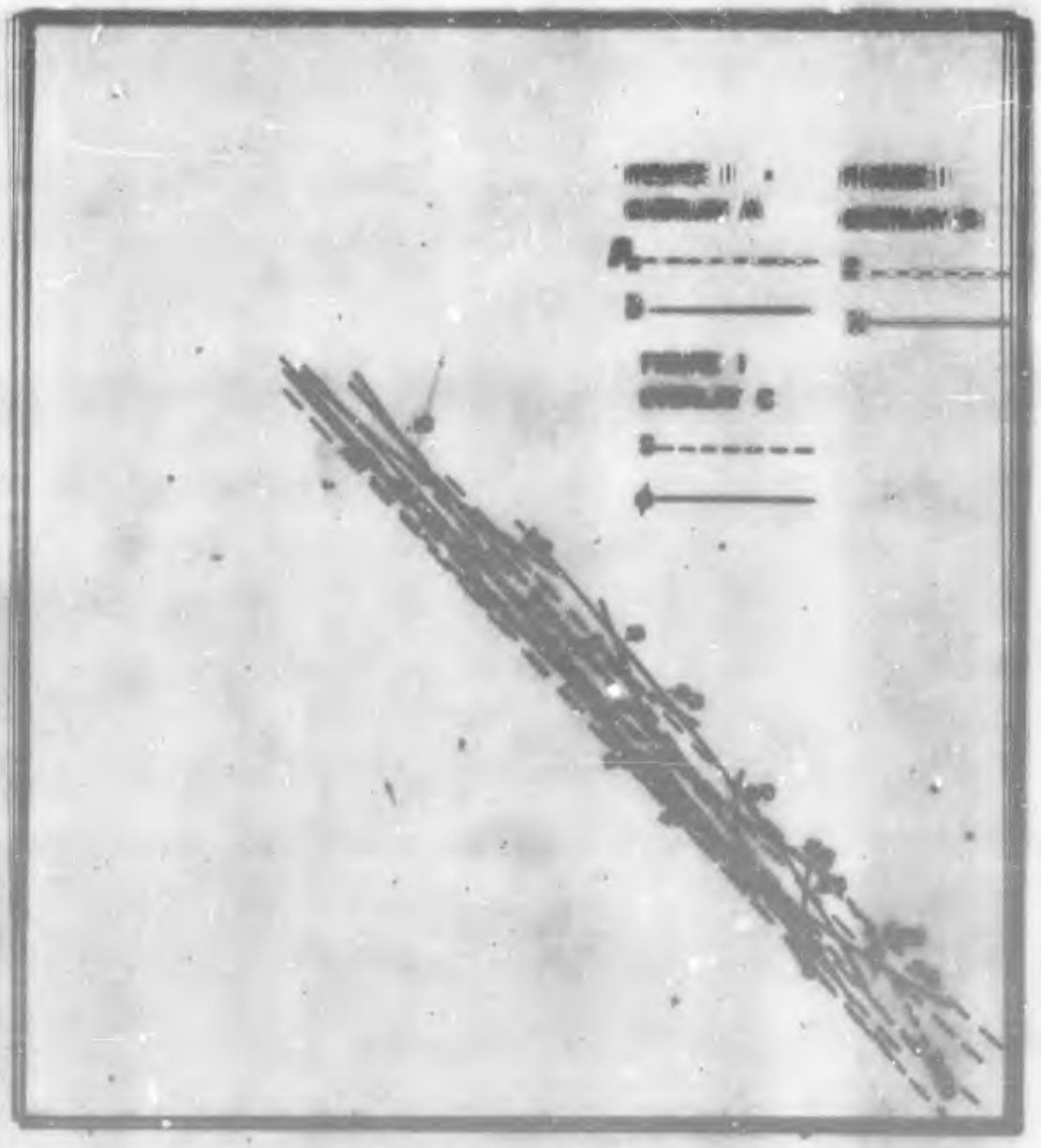

β_2 = IMPELLER EXIT BLADE ANGLE
δ = IMPELLER DIAMETER RATIO

Z = BLADE NUMBER
χ = RATIO OF STRAIGHT DIFFUSER LENGTH TO IMPELLER DIAMETER

δ = SUCTION SPECIFIC SPEED
ϕ = FLOW FACTOR

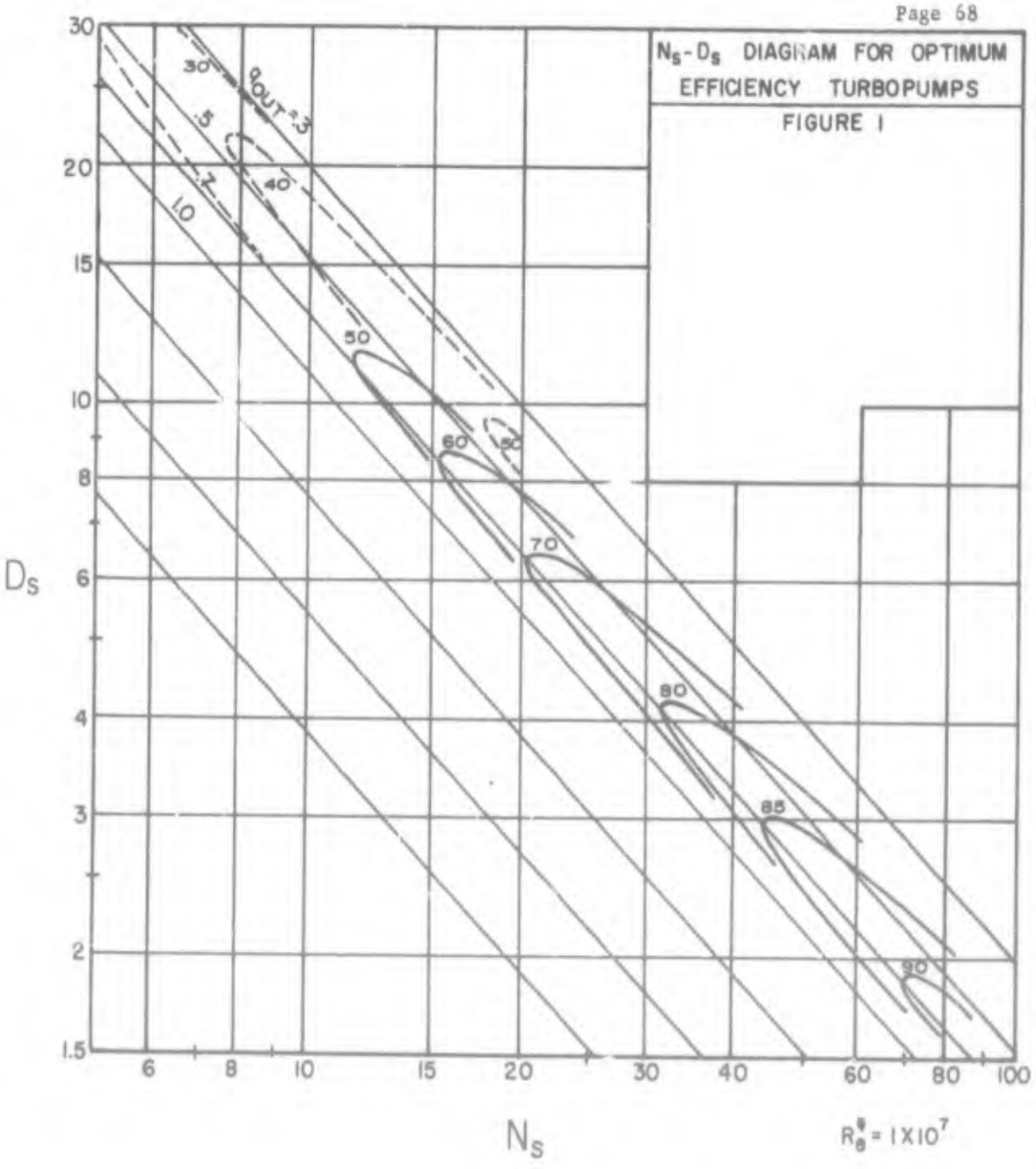

$$Ns = \frac{RPM \; Q^{1/2}}{H^{3/4}}$$

--- PITOT PUMPS
—— CENTRIFUGAL PUMPS

$$Ds = \frac{D \; H^{1/4}}{Q^{1/2}}$$

SUNDSTRAND TURBO

A Division of Sundstrand Corporation

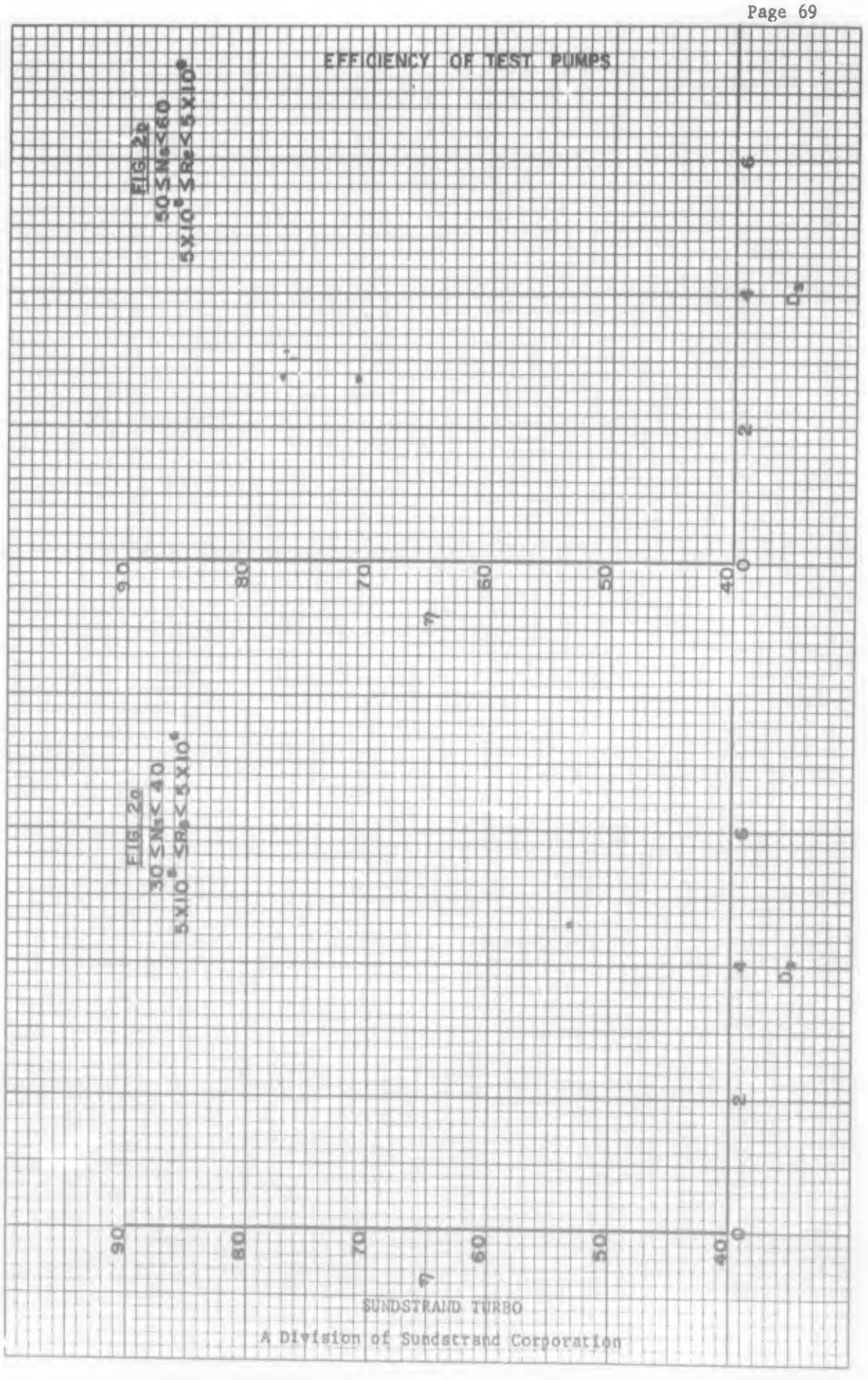
EFFICIENCY OF TEST PUMPS
FIG. 2b
50 ≤ Ns < 60
5X10⁶ ≤ Rs < 5X10⁶
FIG. 2a
30 ≤ Ns < 40
5X10⁶ ≤ Rs < 5X10⁶
Ds
Ds
η
η
90
80
70
60
50
40
0
2
4
6
SUNDSTRAND TURBO
A Division of Sundstrand Corporation

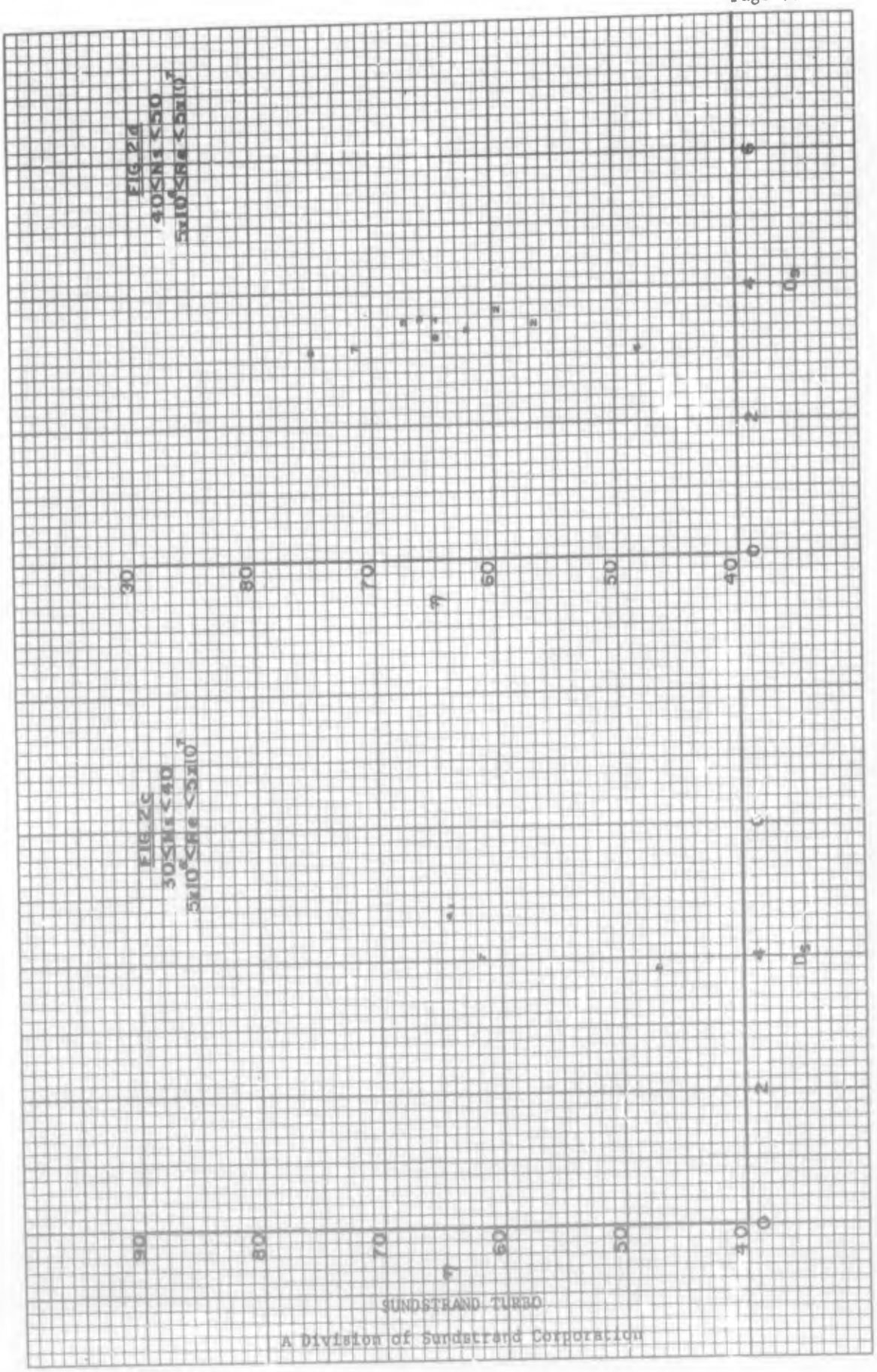
FIG 2d
40≤Nt≤50
5x10⁶≤Re≤5x10⁷
FIG 2c
30≤Nt<40
5x10⁶≤Re≤5x10⁷
30
80
70
60
50
40
90
80
70
60
50
40
6
4
2
0
4
2
0

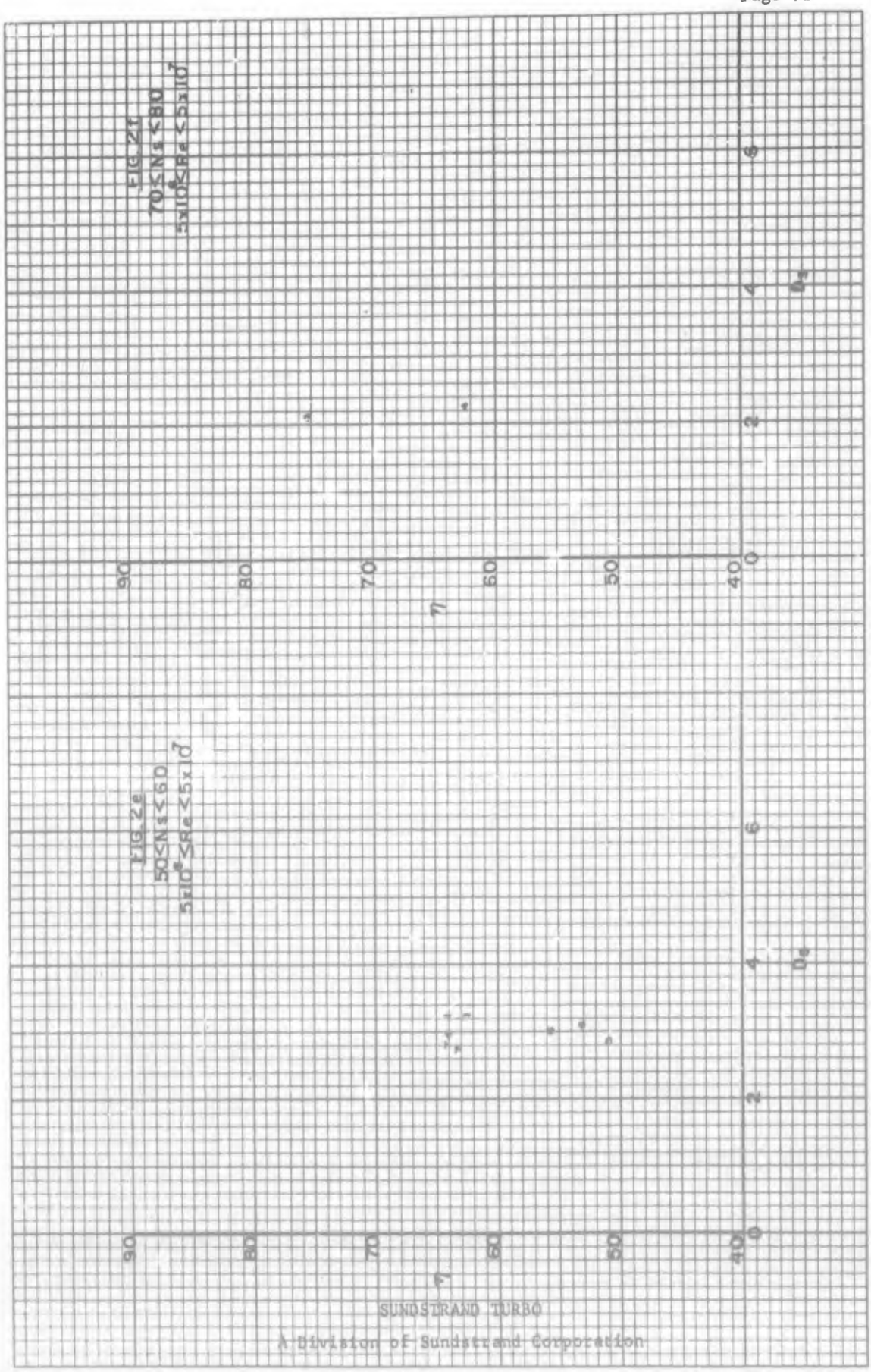
FIG. 2f
70≤Ns≤80
5x10⁶≤Re≤5x10⁷
FIG. 2e
50≤Ns≤60
5x10⁶≤Re≤5x10⁷
90
80
70
60
50
40
0
2
4
6
Ds
Ns
SUNDSTRAND TURBO
A Division of Sundstrand Corporation

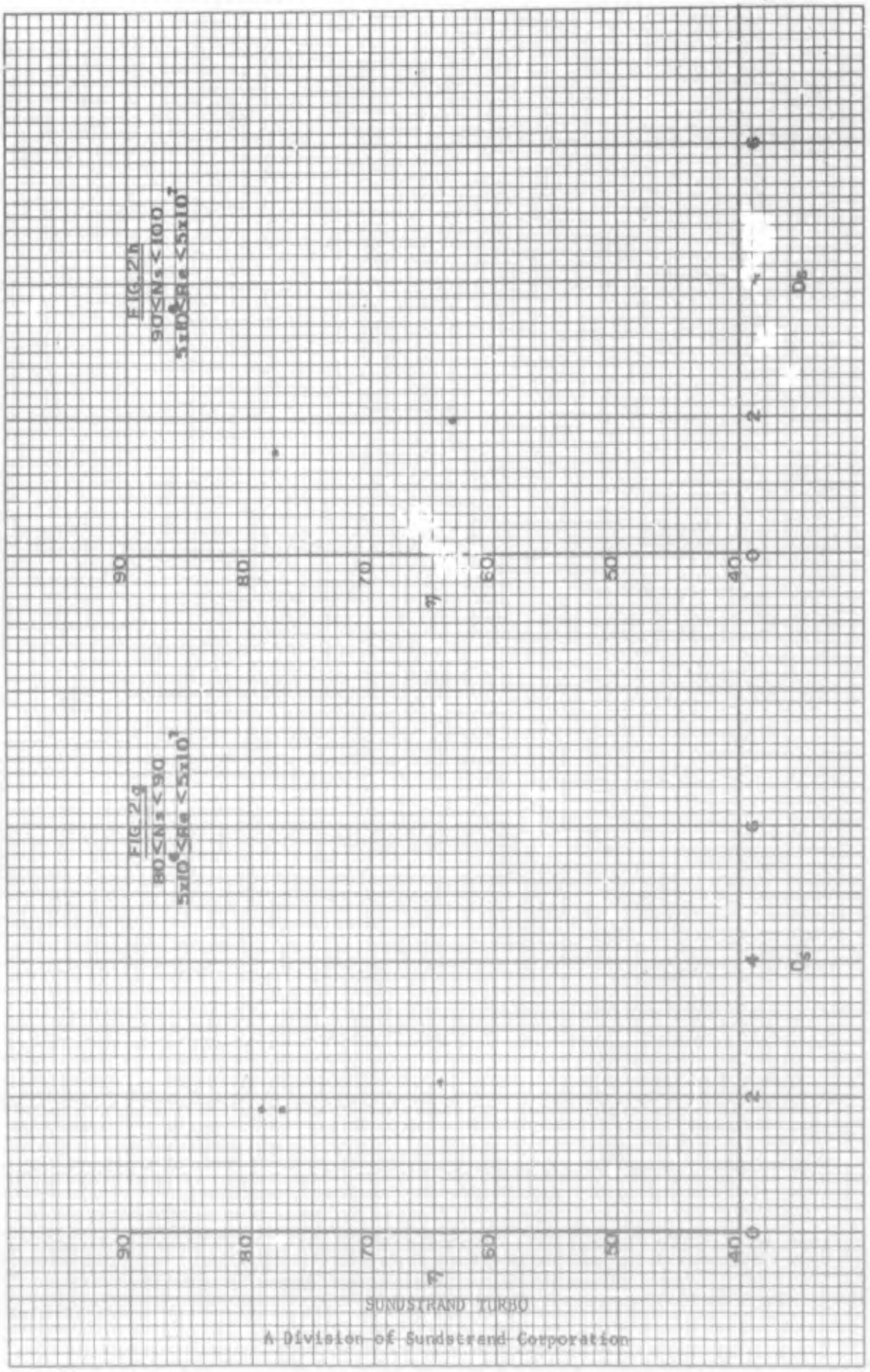
FIG. 2h
90≤Ns<100
5x10⁶≤Re <5x10⁷
FIG. 2g
80≤Ns<90
5x10⁶≤Re <5x10⁷
Ds
Ds
ηt
ηt
90
80
70
60
50
40
6
4
2
0

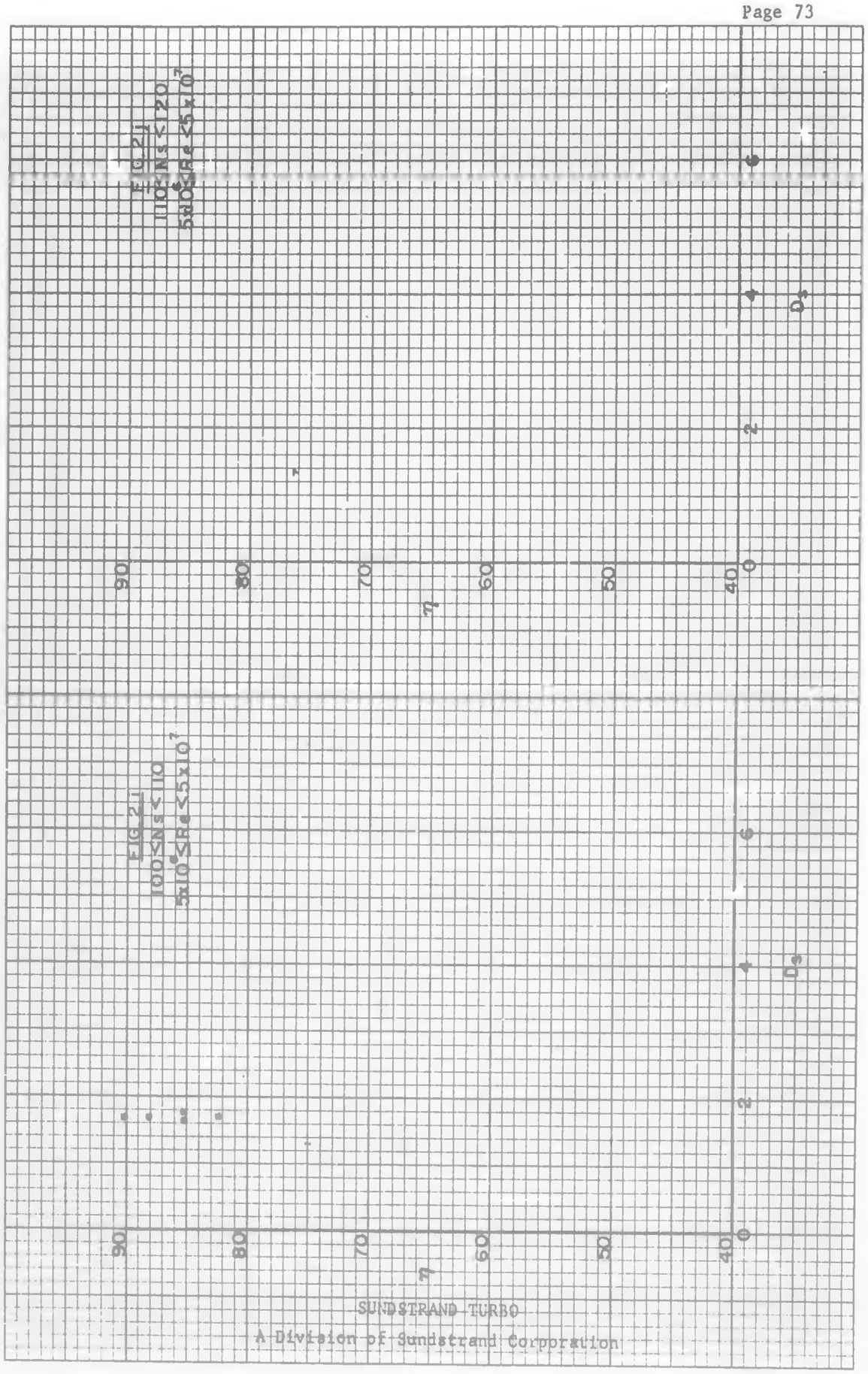
FIG 2J
110≤Ns≤120
5x10³≤Re≤5x10⁷
η
90
80
70
60
50
40
0
2
4
6
Ds
FIG 2J
100≤Ns≤110
5x10⁶≤Re≤5x10⁷
η
90
80
70
60
50
40
0
2
4
6
Ds


FIG 21
10≤Ns≤20
5x10⁵≤Re≤5x10⁶
FIG 24
120≤Ns≤130
5x10⁶≤Re≤5x10⁷
Ds
Ds
90
80
70
60
50
40
0
2
4
6
8

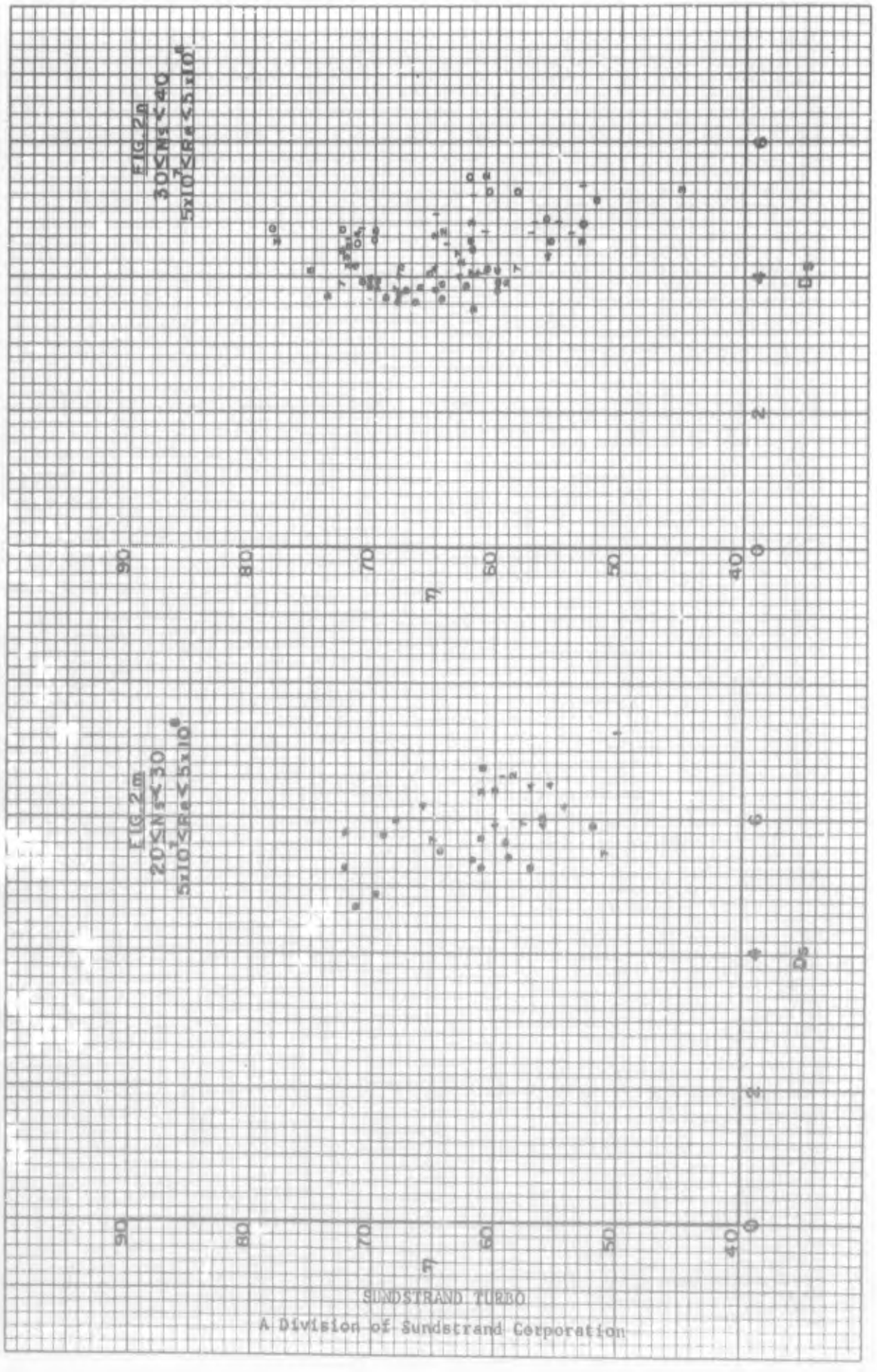
FIG 2m
30≤Ns<40
5x10⁵≤Re<5x10⁶
FIG 2m
20≤Ns<30
5x10⁵≤Re<5x10⁶
η
Ds
90
80
70
60
50
40
0
2
4
6

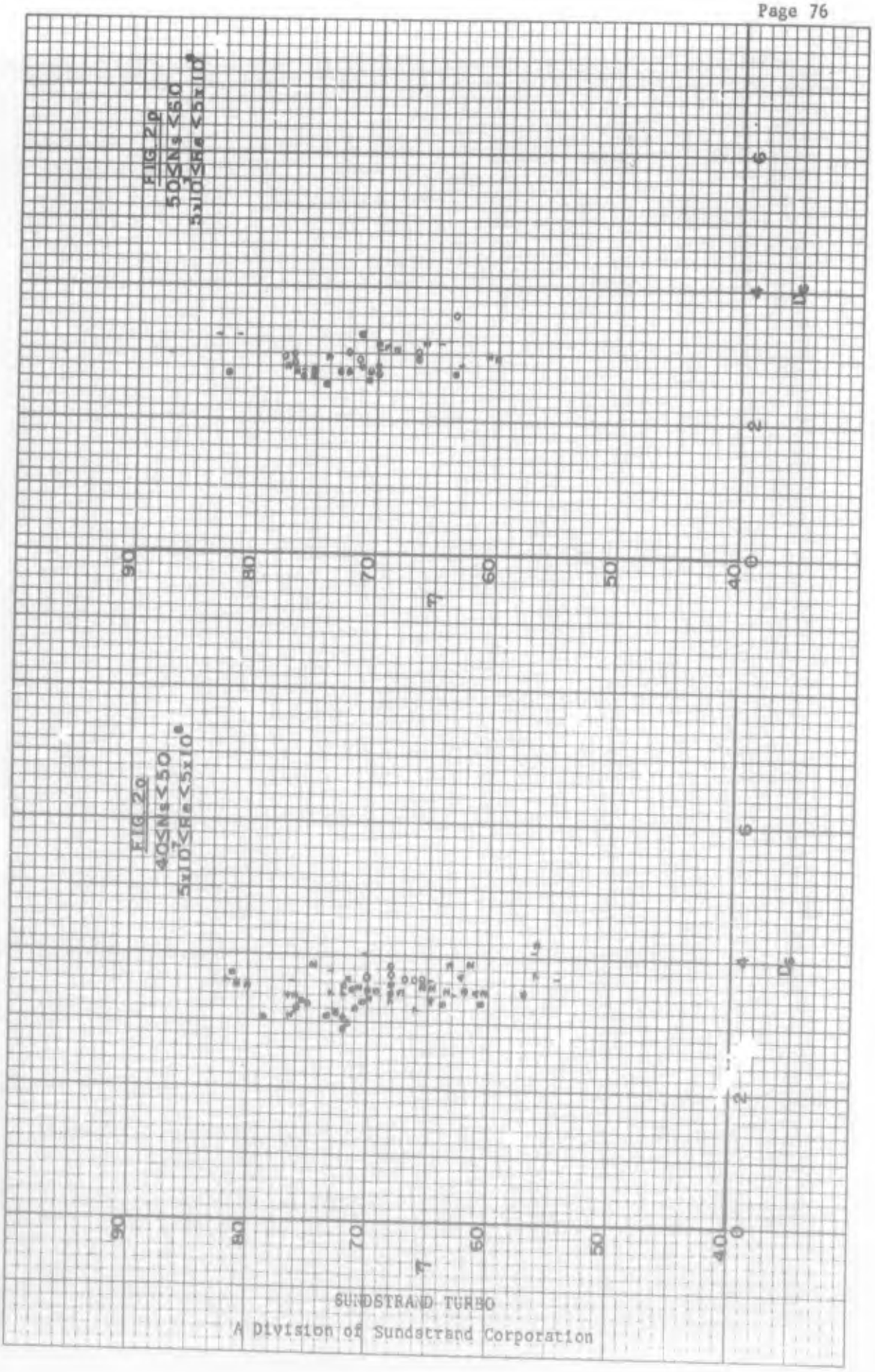
FIG 2b
50≤Ns≤60
5x10⁵≤Re≤5x10⁶
FIG 2a
40≤Ns≤50
5x10⁵≤Re≤5x10⁶
90
80
70
60
50
40
0
2
4
6
10⁶
η
ψ

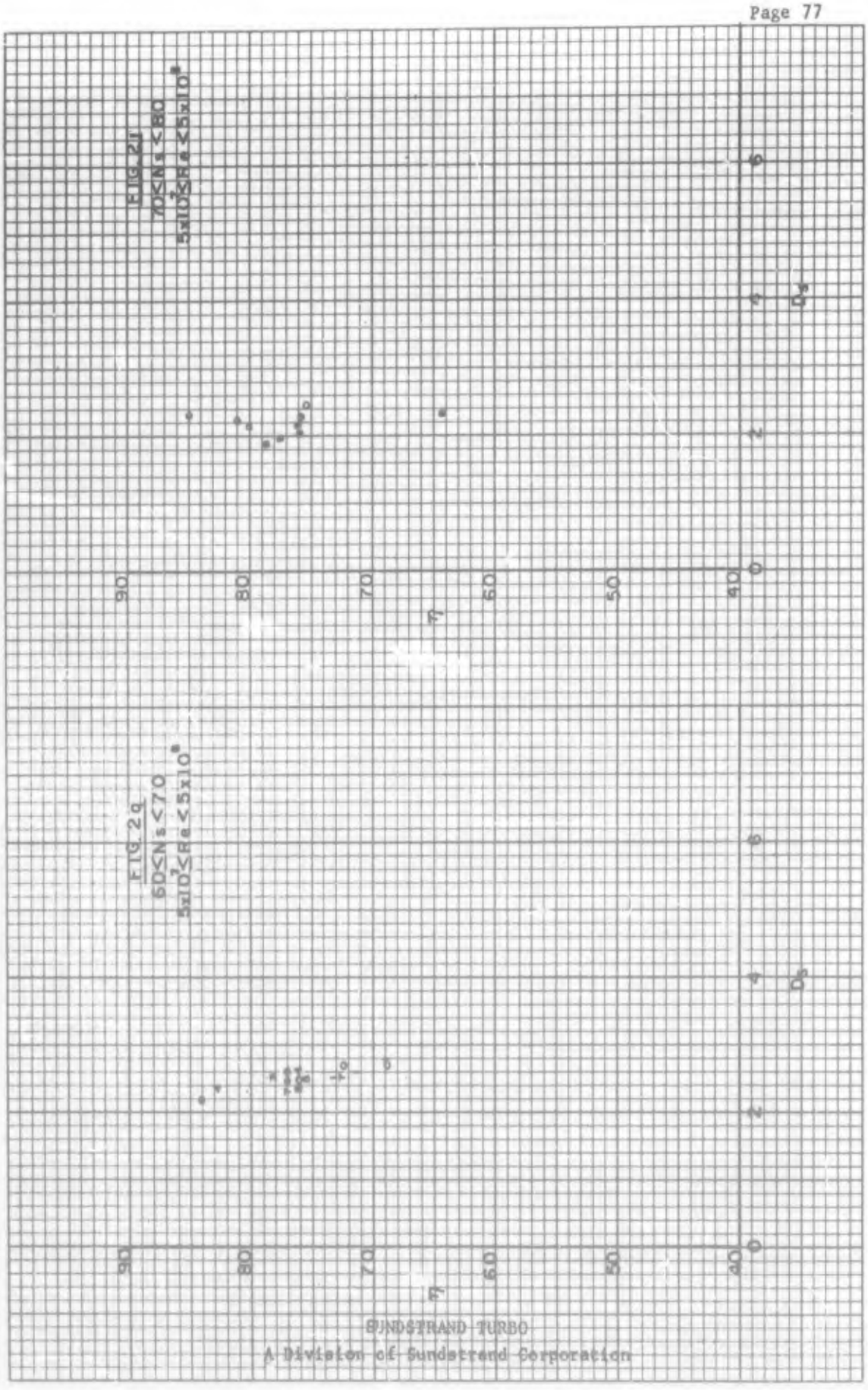
FIG 2I
70≤Ns≤80
5x10⁵≤Re≤5x10⁶
FIG 2g
60≤Ns≤70
5x10⁵≤Re≤5x10⁶
90
80
70
60
50
40
0
2
4
6
Ds
Ns

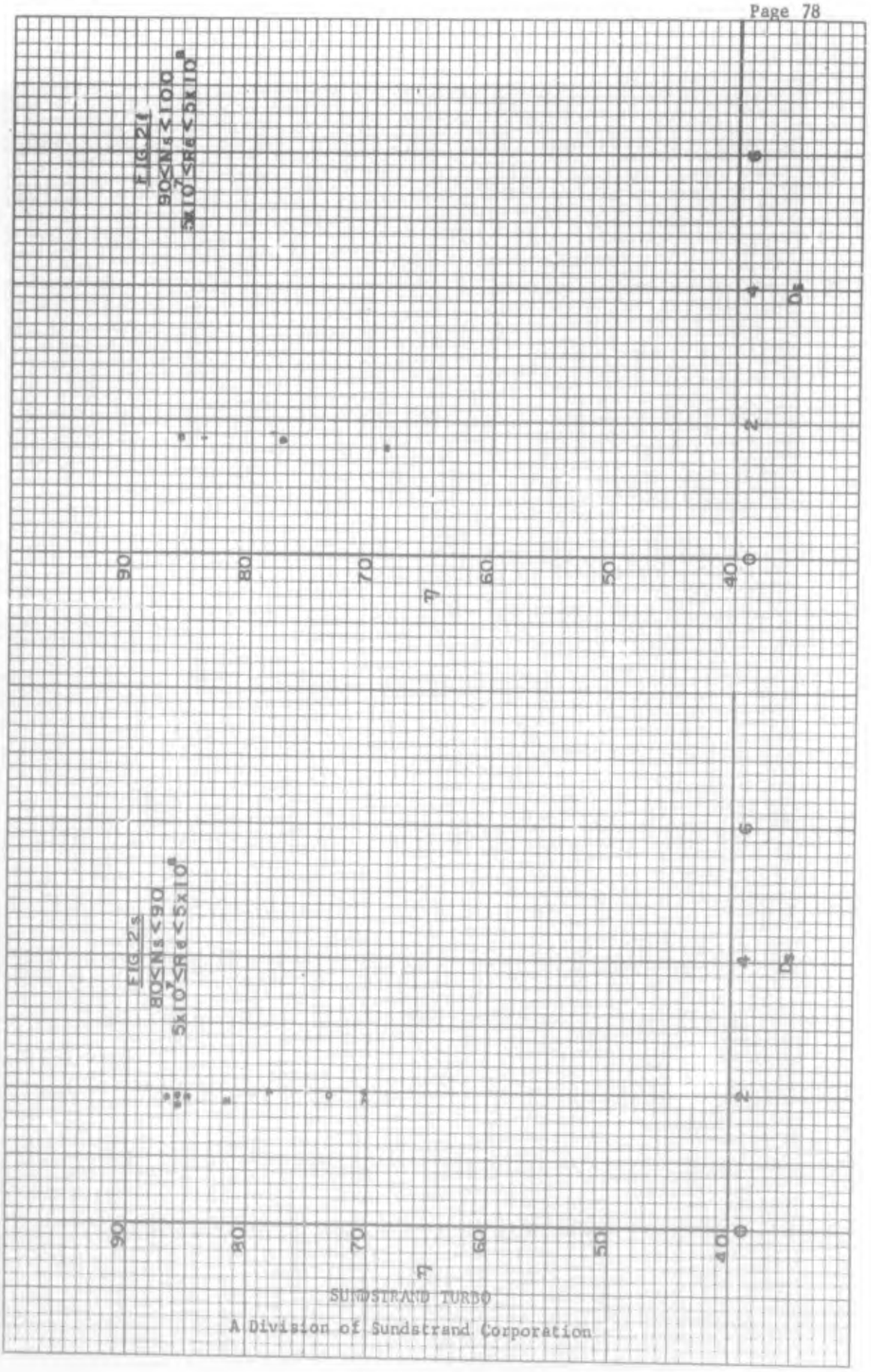

SUNDSTRAND TURBO
A Division of Sundstrand Corporation

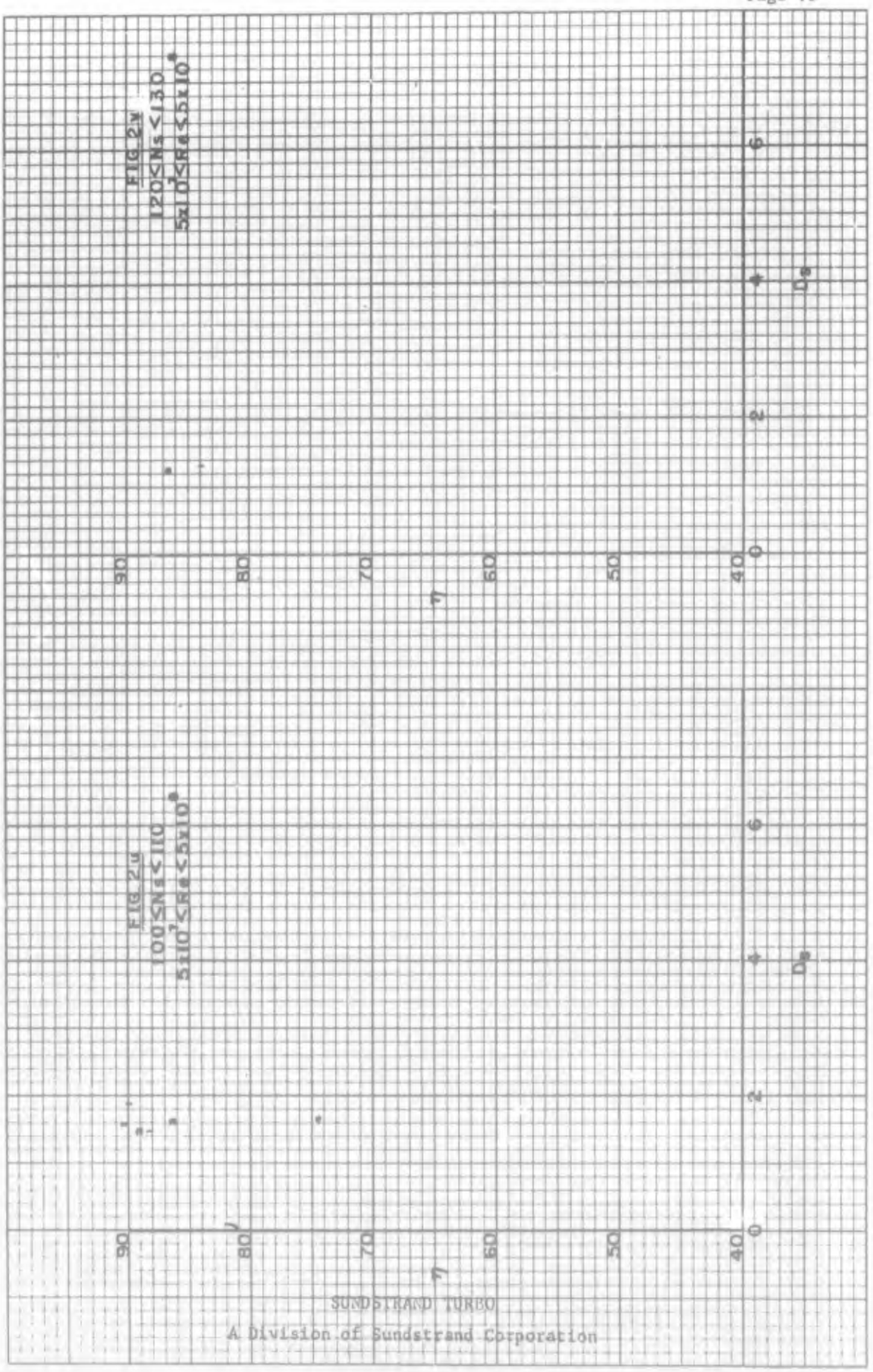
FIG 2W
120≤Ns≤130
5x10³≤Re≤5x10⁶
FIG 2U
100≤Ns≤110
5x10³≤Re≤5x10⁶
90
80
70
60
50
40
30
20
10
6
4
2
0
H
Ds

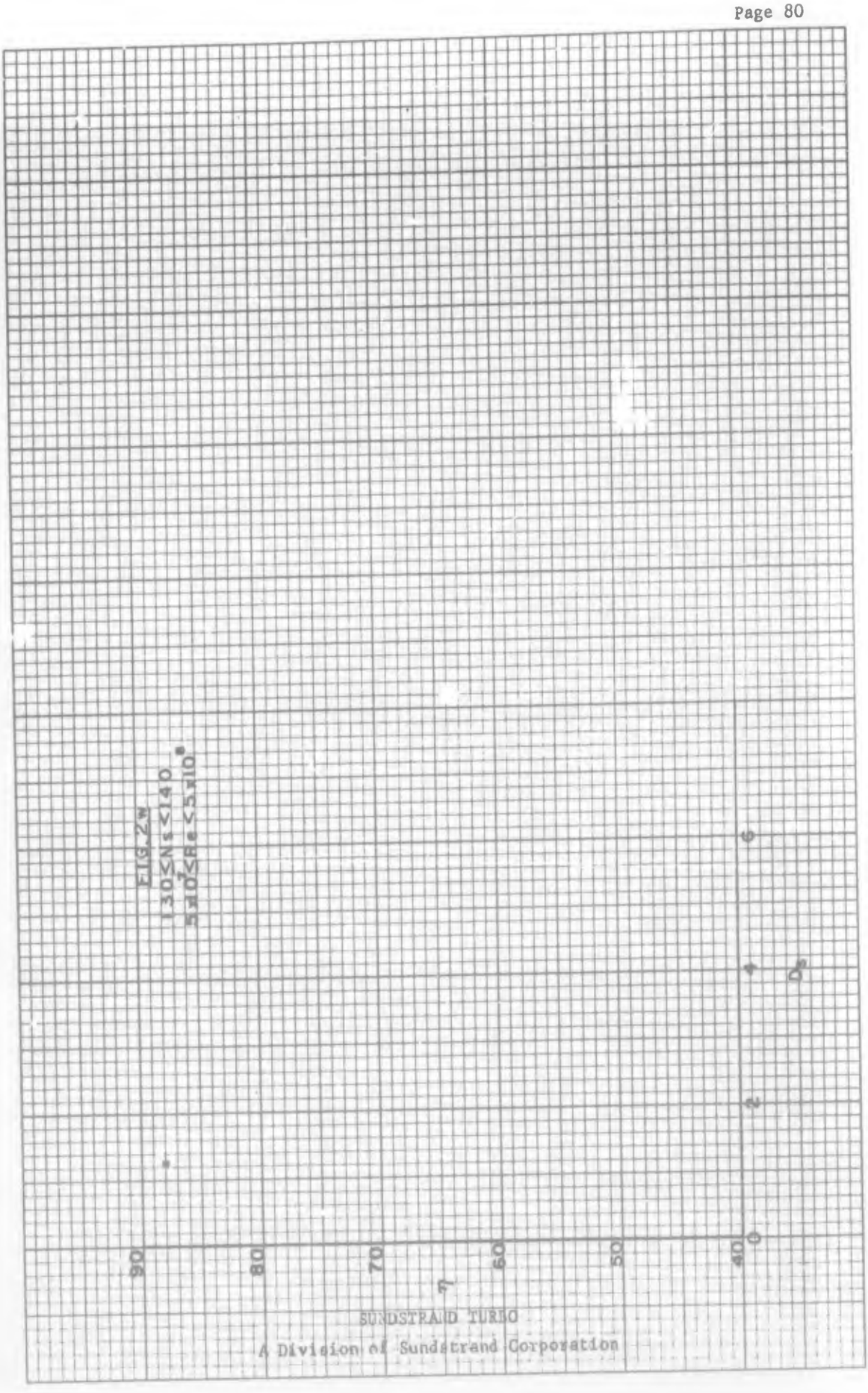
FIG. 2W
130 < Ns < 140
5 x 10^5 < Re < 5 x 10^6
90
80
70
60
50
40
0
2
4
6
Ds
T
SUNDSTRAND TURBO
A Division of Sundstrand Corporation

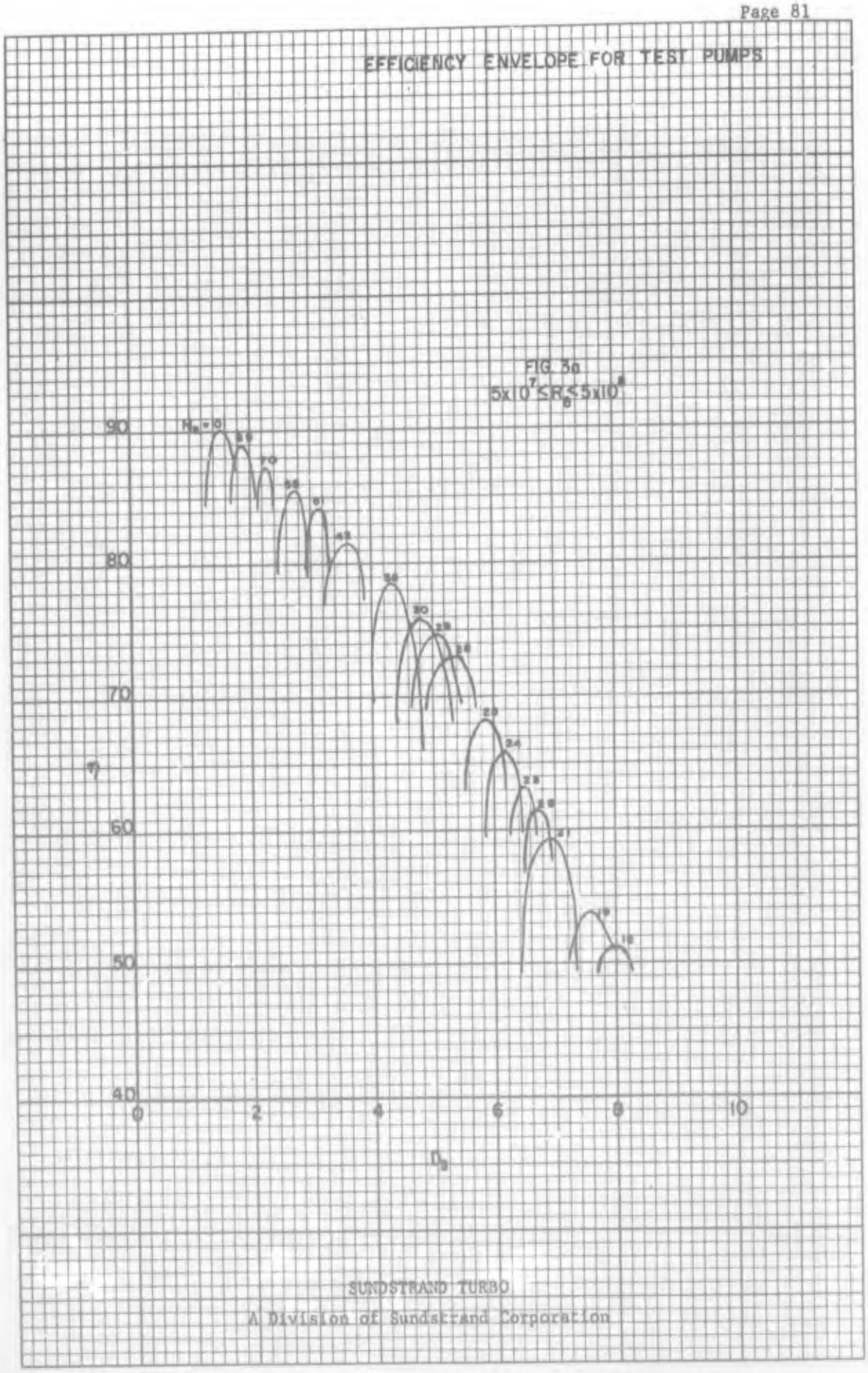
EFFICIENCY ENVELOPE FOR TEST PUMPS
FIG 3a
$5x10^7 \leq R_\theta \leq 5x10^8$
90
80
70
60
50
40
η
0
2
4
6
8
10
D_s
SUNDSTRAND TURBO
A Division of Sundstrand Corporation

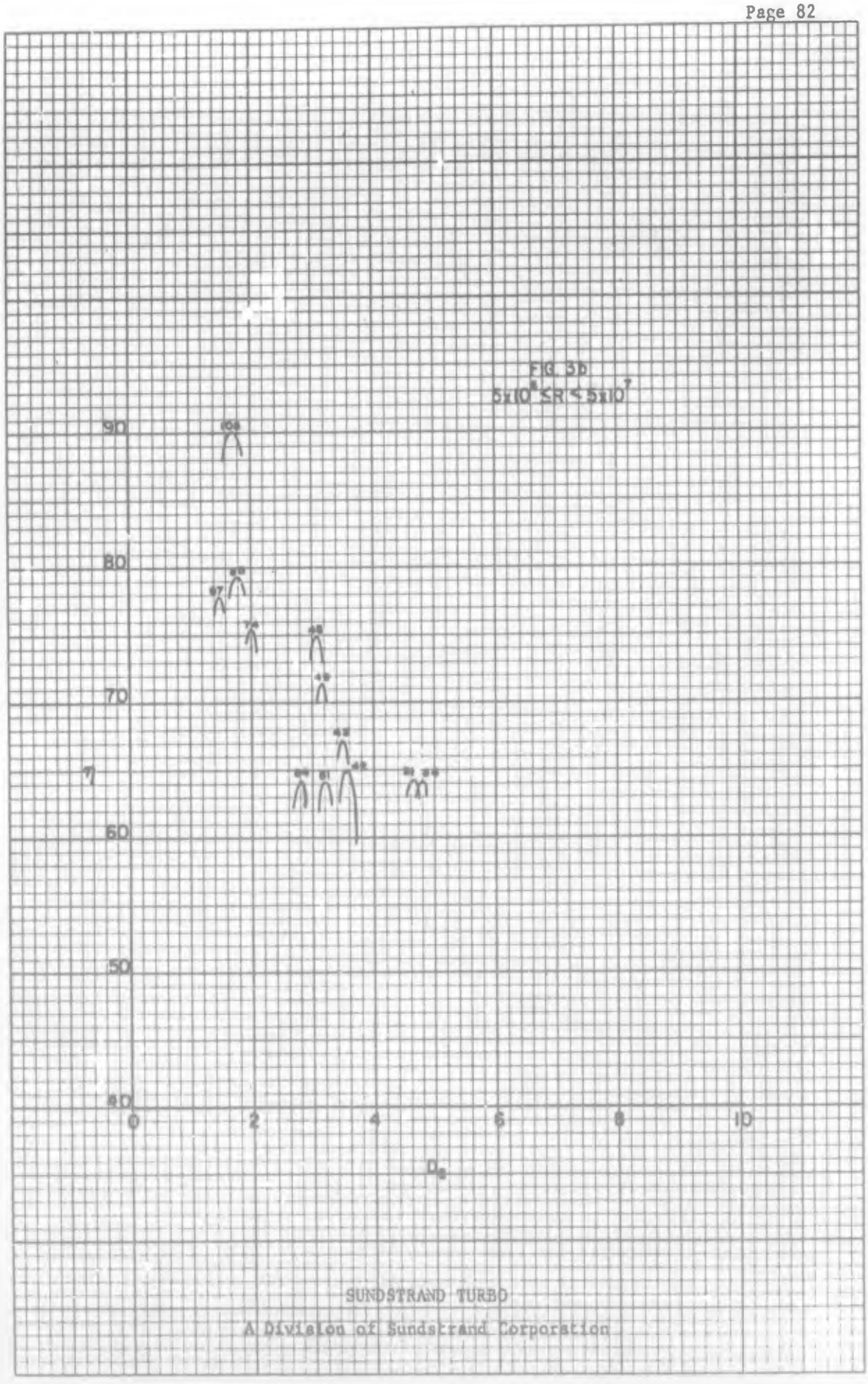
FIG 3D
$5x10^6 \leq R \leq 5x10^7$
90
80
70
60
50
40
0
2
4
6
8
10
D_s

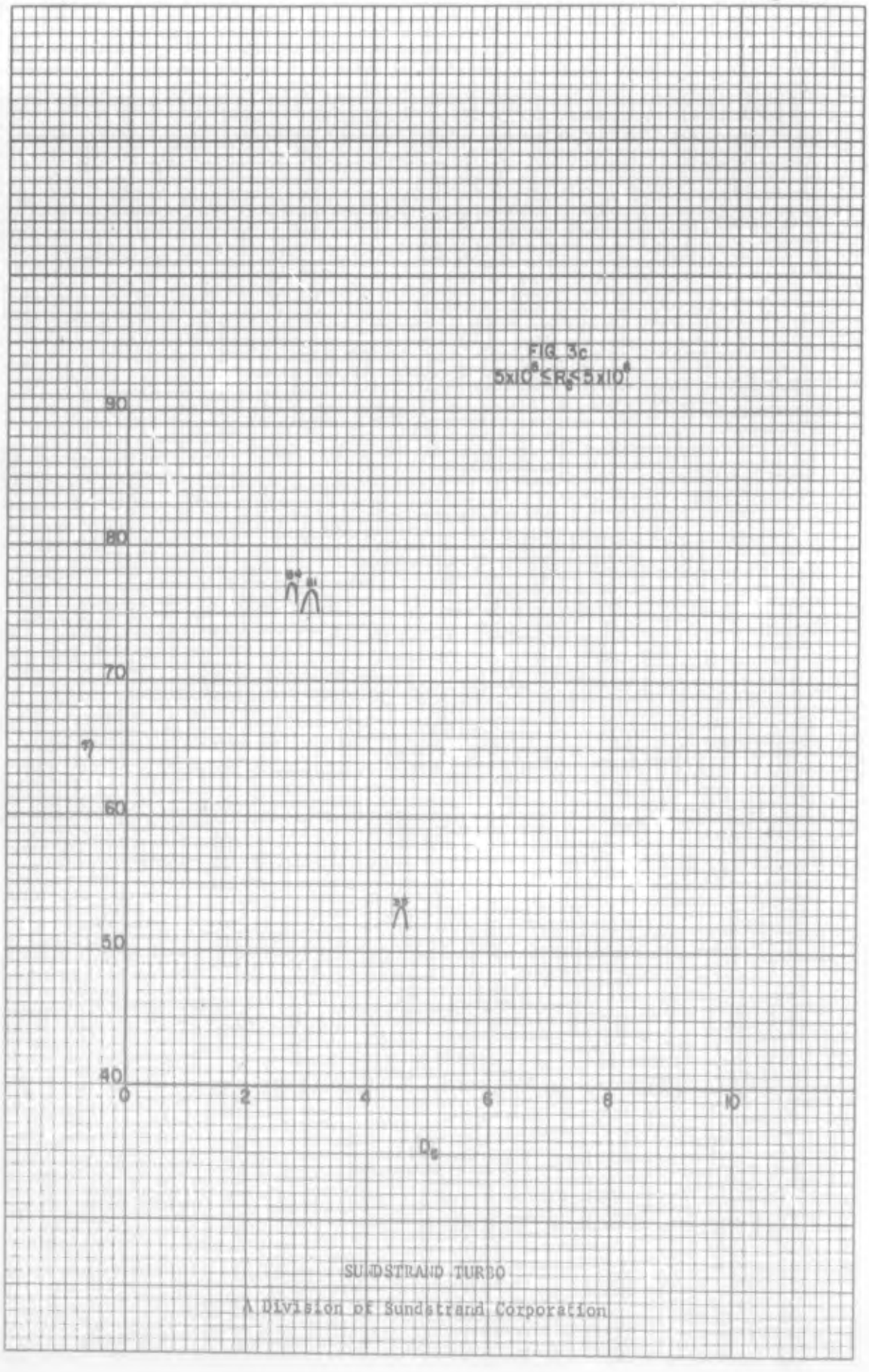
FIG. 3c
$5x10^6 \leq R_e \leq 5x10^7$
90
80
70
60
50
40
η
0
2
4
6
8
10
D_e

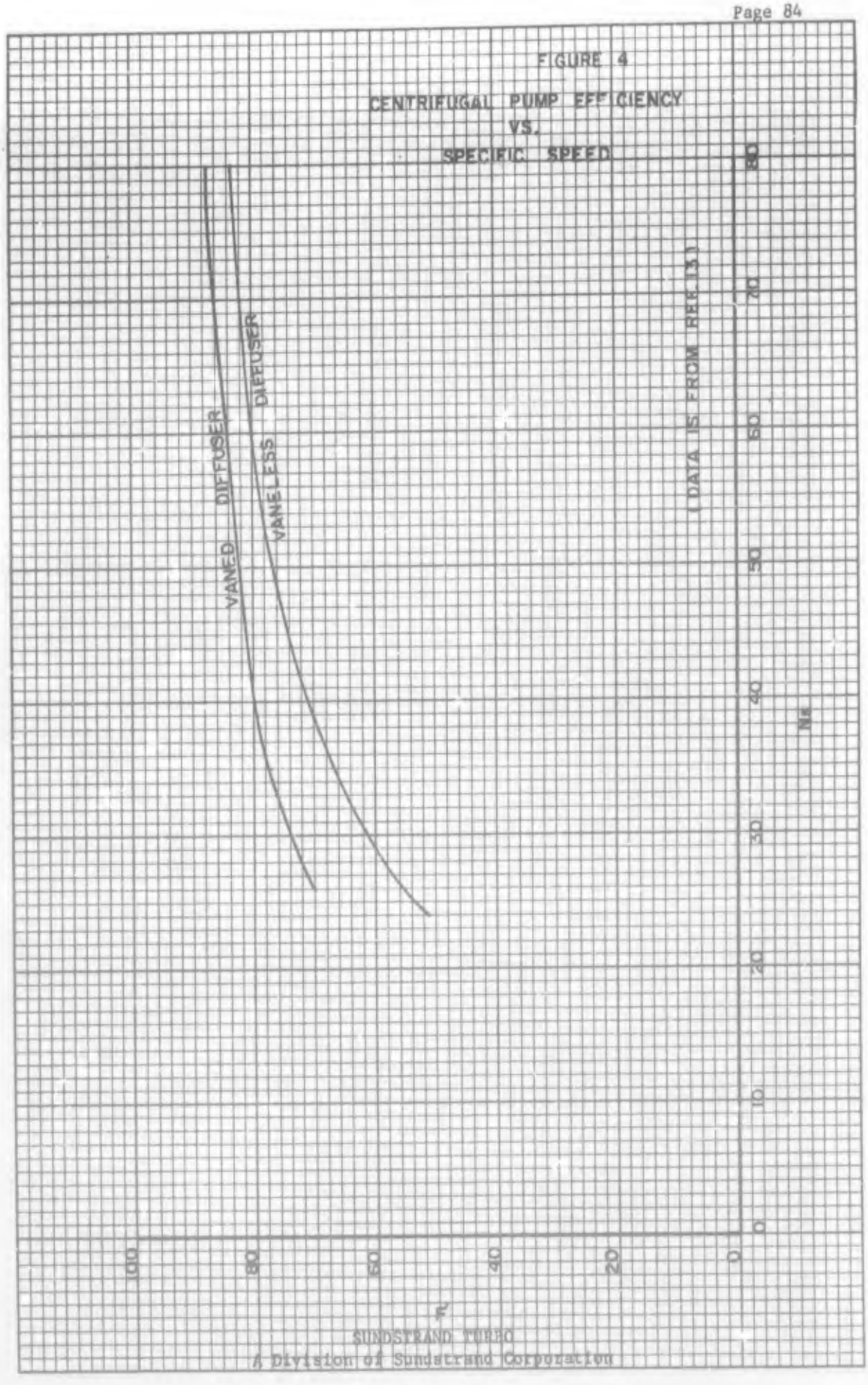
FIGURE 4
CENTRIFUGAL PUMP EFFICIENCY
VS.
SPECIFIC SPEED
VANED DIFFUSER
VANELESS DIFFUSER
(DATA IS FROM REF. 13)
Ns
100
80
60
40
20
0
0
10
20
30
40
50
60
70
80

EFFICIENCY OF TEST PUMPS

FIG. 5

$5 \times 10^7 \leq R_s < 5 \times 10^8$

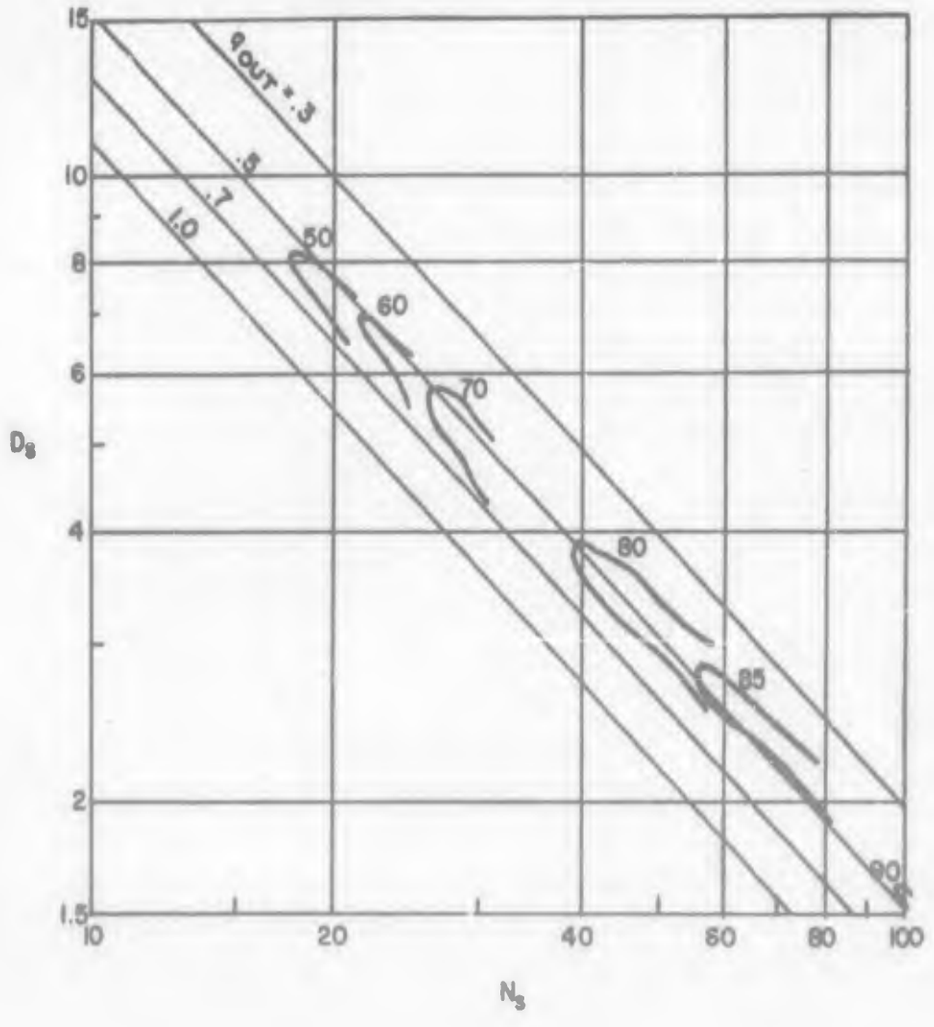

PUMP PARAMETERS
VS.
SPECIFIC SPEED FROM TEST DATA

FIG. 6

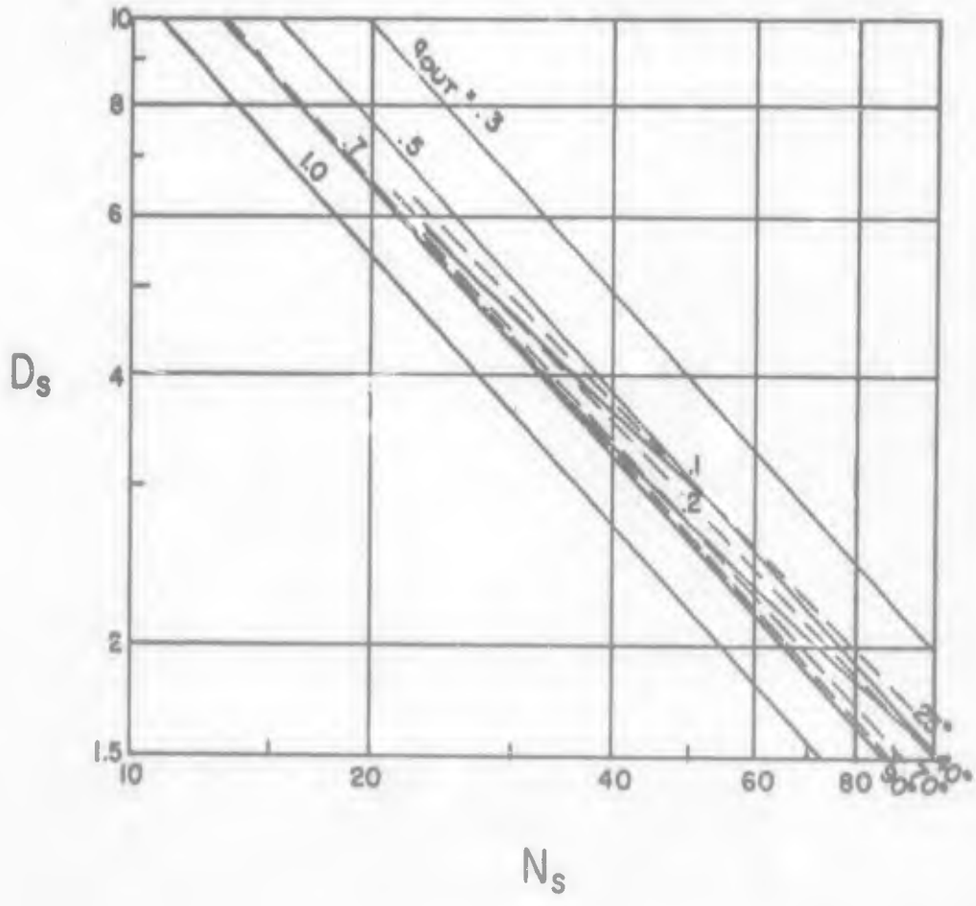

———BLADE ANGLE β_2
———DIAMETER RATIO δ
(FROM STEPANOFF)

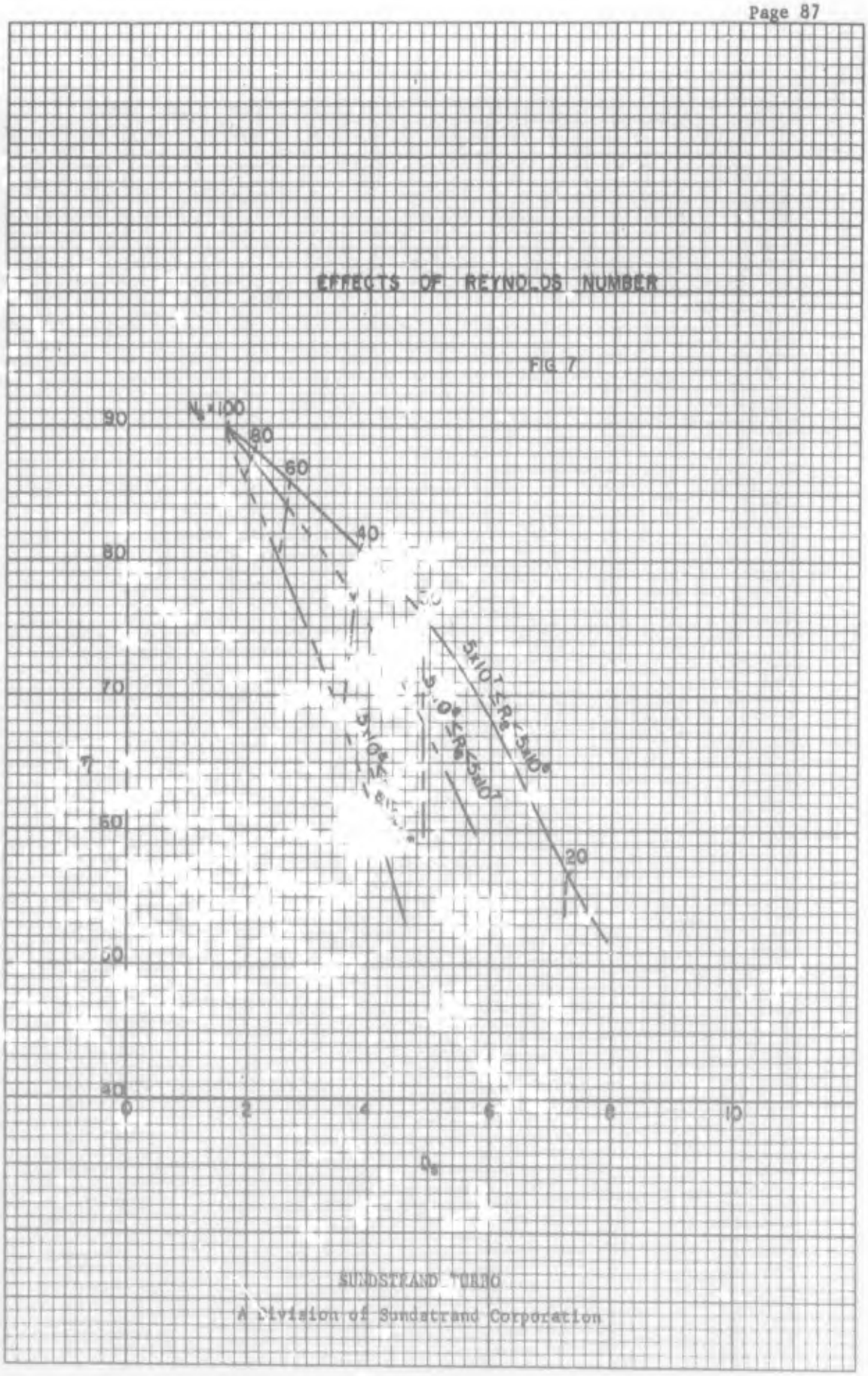
EFFECTS OF REYNOLDS NUMBER
FIG 7
$N_s \times 100$
90
80
60
40
30
70
50
20
10
0
2
4
6
8
10
D_s
$5\times10^7 \leq R_e < 5\times10^8$
$5\times10^6 \leq R_e < 5\times10^7$
$5\times10^5 \leq R_e < 5\times10^6$

FIGURE 7a
EXPONENT FOR REYNOLDS NUMBER
CORRECTION FACTOR

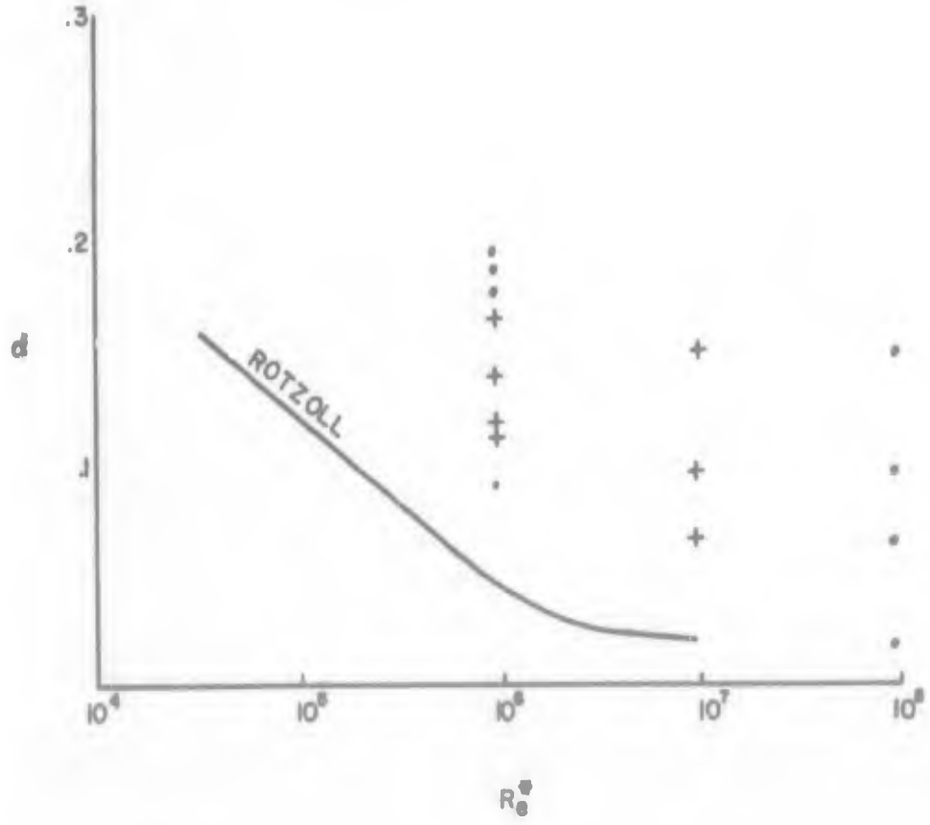

FIGURE 7b

SOURCES OF ENERGY LOSSES IN CENTRIFUGAL PUMPS.

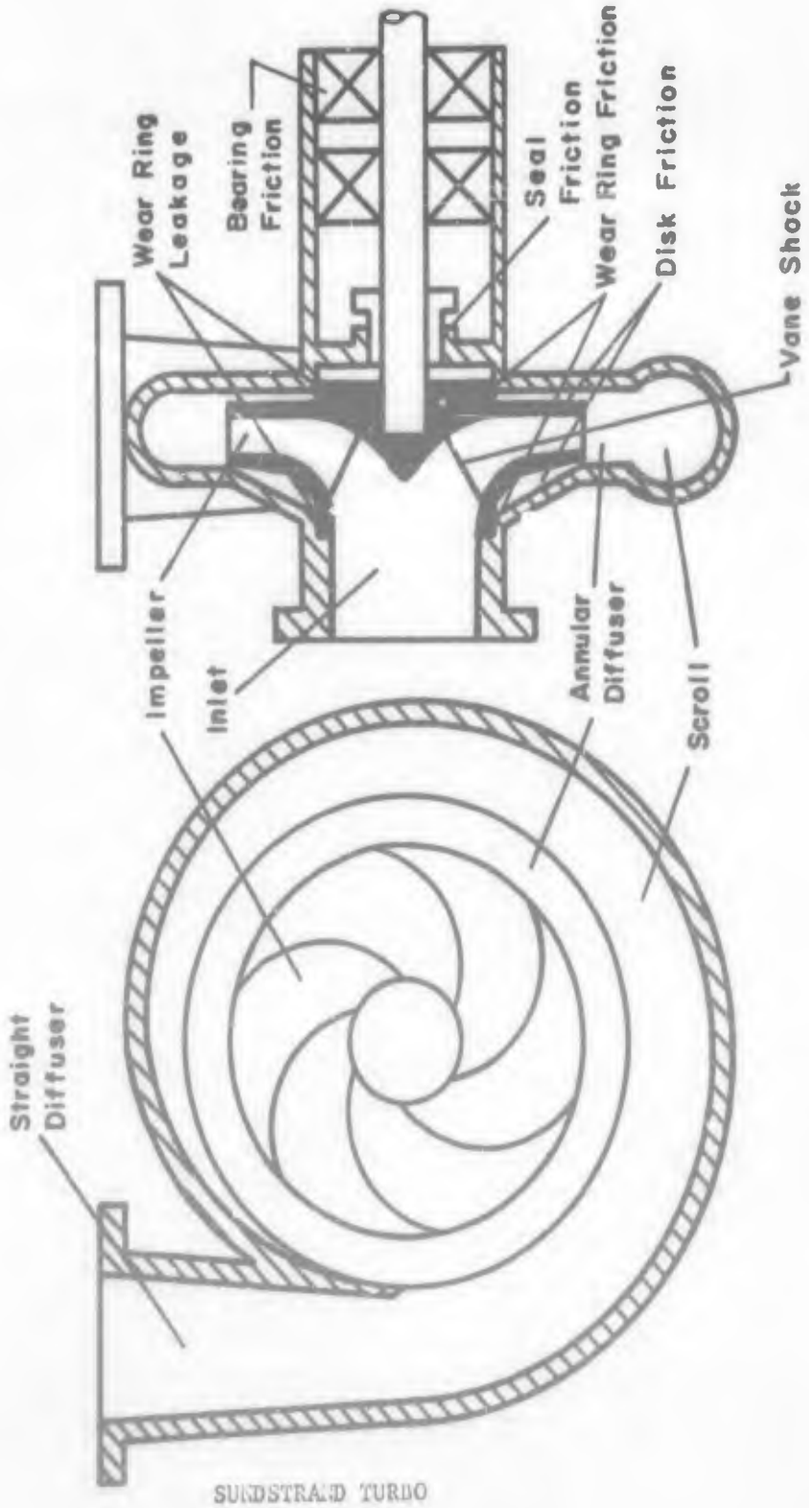

SUNDSTRAND TURBO

A Division of Sundstrand Corporation

FIG. 8

SUCTION SPECIFIC SPEED FROM TEST DATA

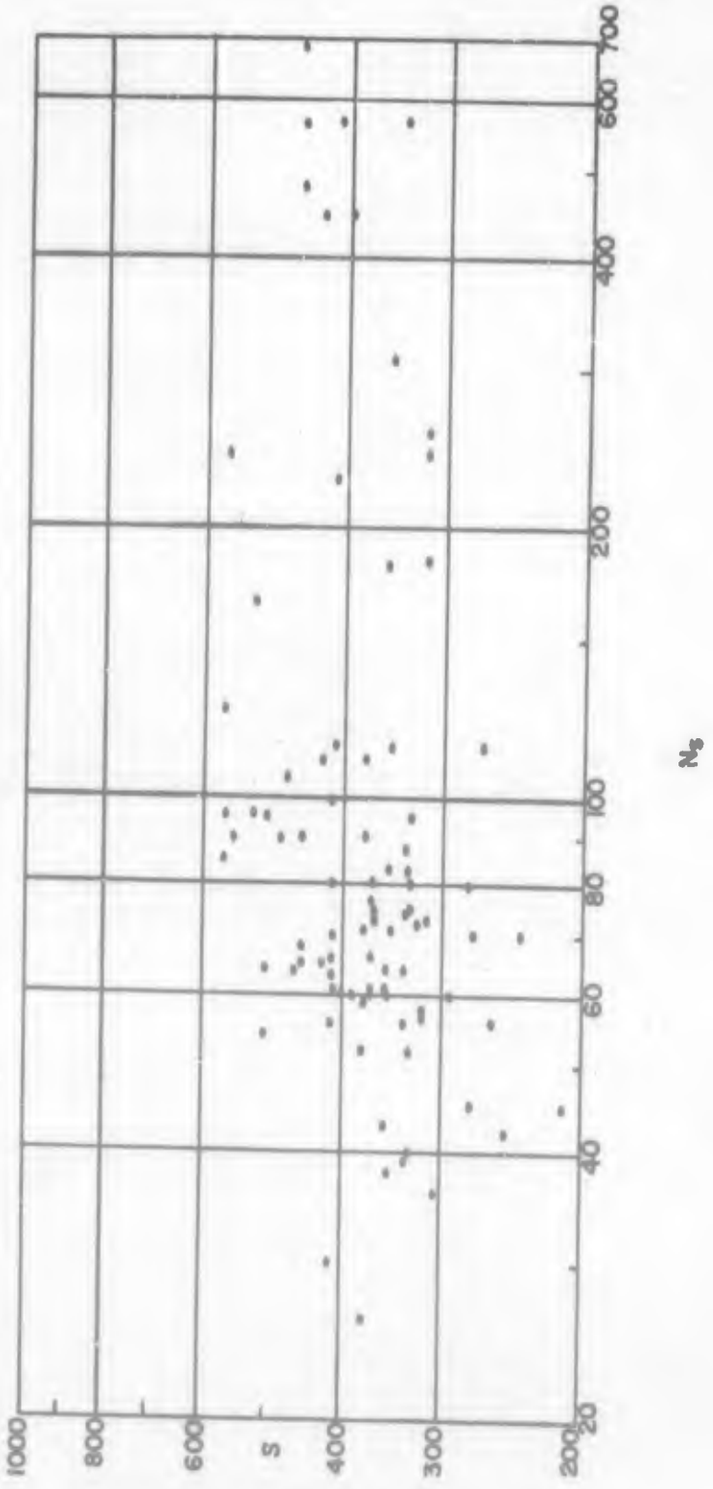

SUNDSTRAND TURBO

A Division of Sundstrand Corporation

FIGURE 9
SCHEMATIC OF IMPELLER SHOWING VELOCITY DIAGRAMS

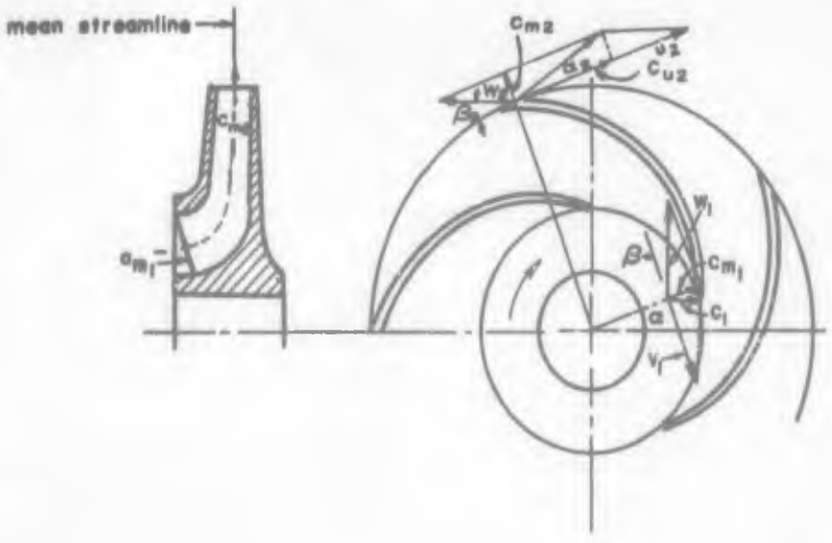

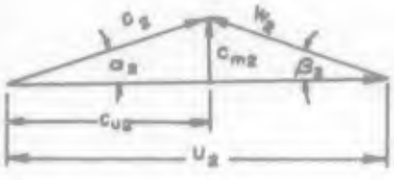

EXIT VELOCITY

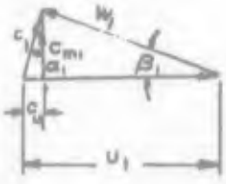

INLET VELOCITY

VELOCITY DIAGRAMS ARE FOR A SLIP FACTOR OF UNITY AND ARE AT THE MEAN STREAMLINE

SUNDSTRAND TURBO

A Division of Sundstrand Corporation

FIGURE 10
THEORETICAL HEAD
COEFFICIENT

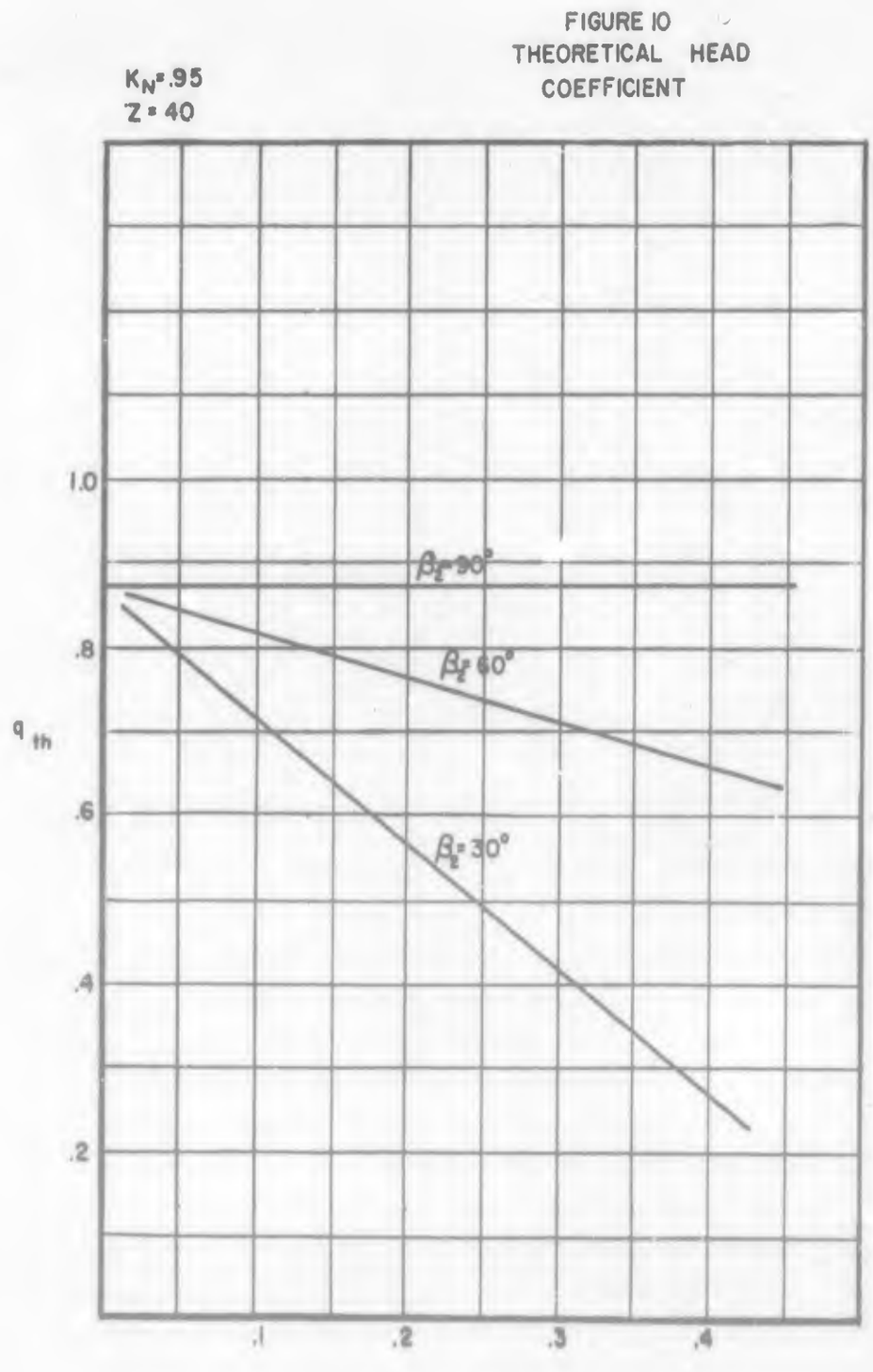

SUNDSTRAND TURBO

A Division of Sundstrand Corporation

$K_j = 1.0$

$R_e^M = 1 \times 10^7$

$\tau = 0$

FIGURE 11

IMPELLER HEAD LOSS COEFFICIENT

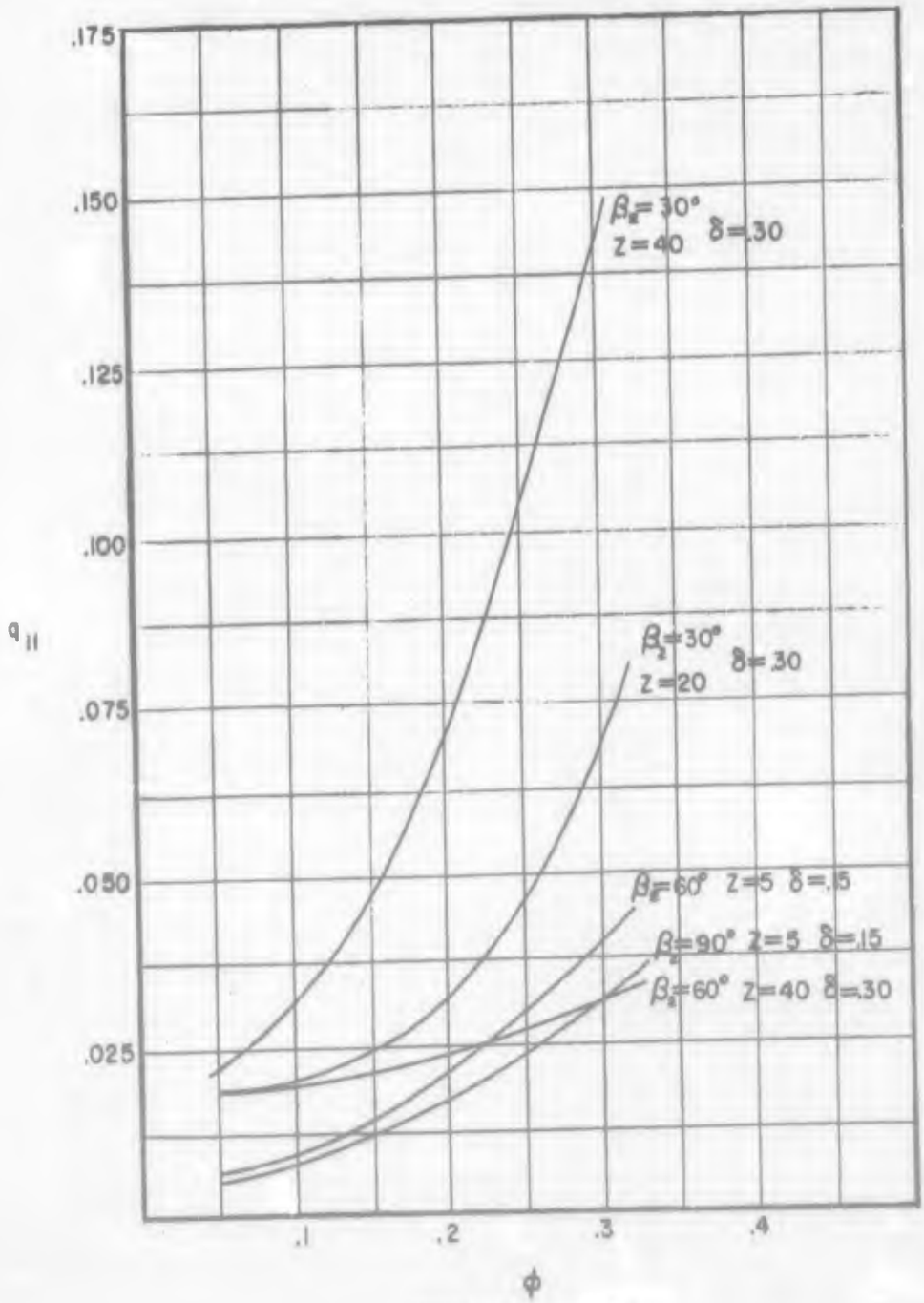

FIGURE 12

ANNULAR DIFFUSER HEAD COEFFICIENT

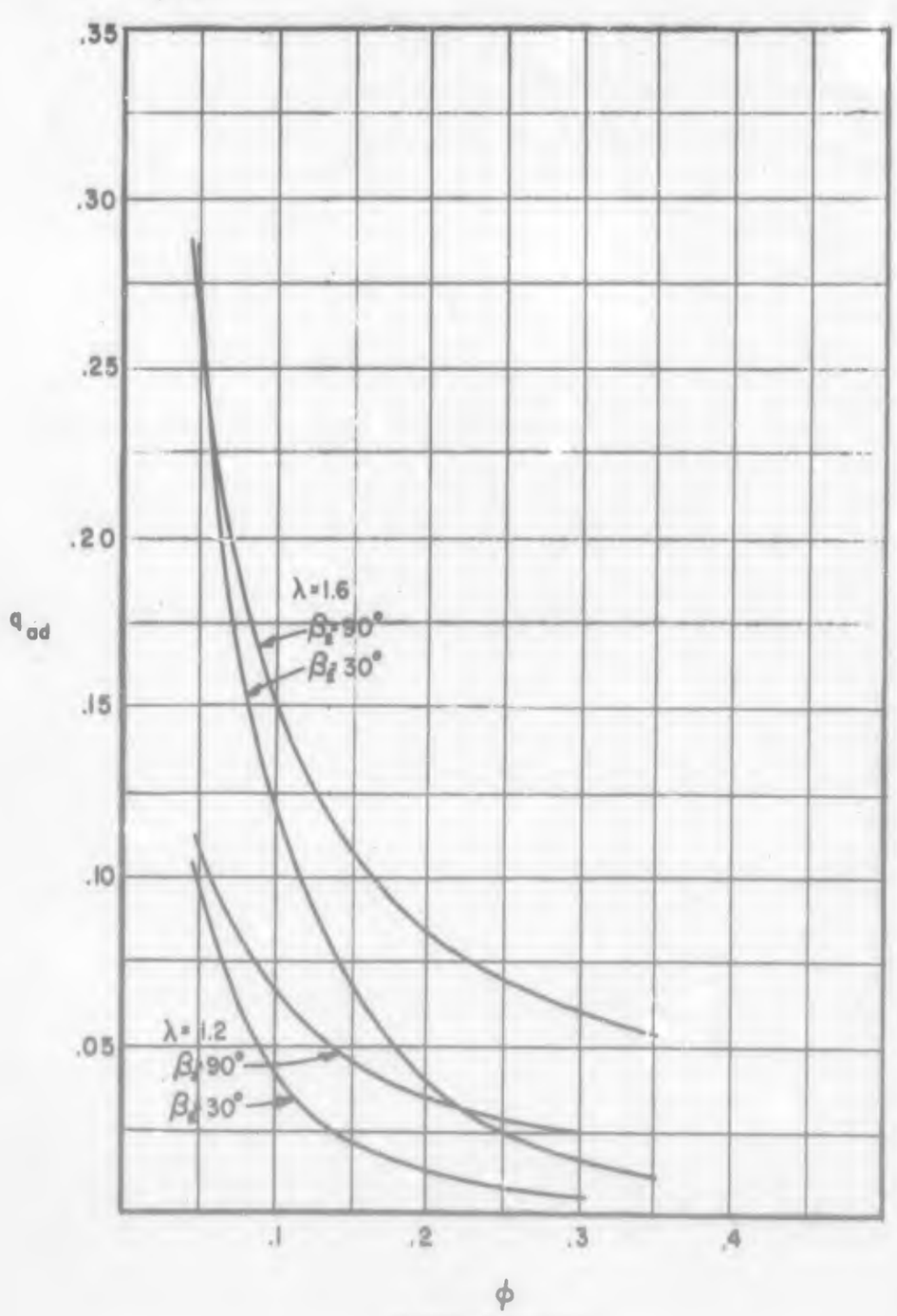

SUNDSTRAND TURBO

A Division of Sundstrand Corporation

FIGURE 13
SCROLL HEAD LOSS COEFFICIENT

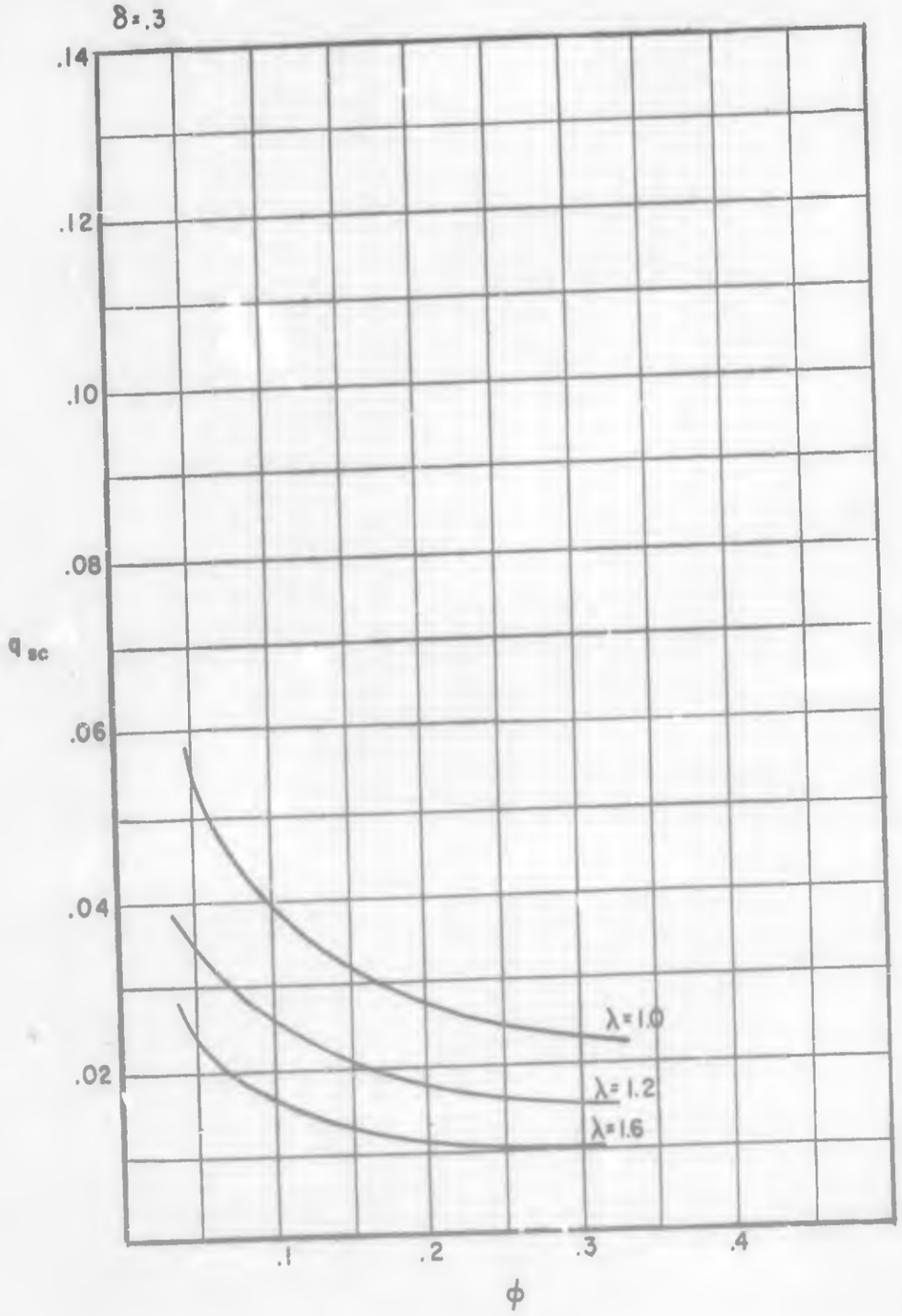

SUNDSTRAND TURBO

A Division of Sundstrand Corporation

FIGURE 14
STRAIGHT DIFFUSER HEAD
LOSS COEFFICIENT

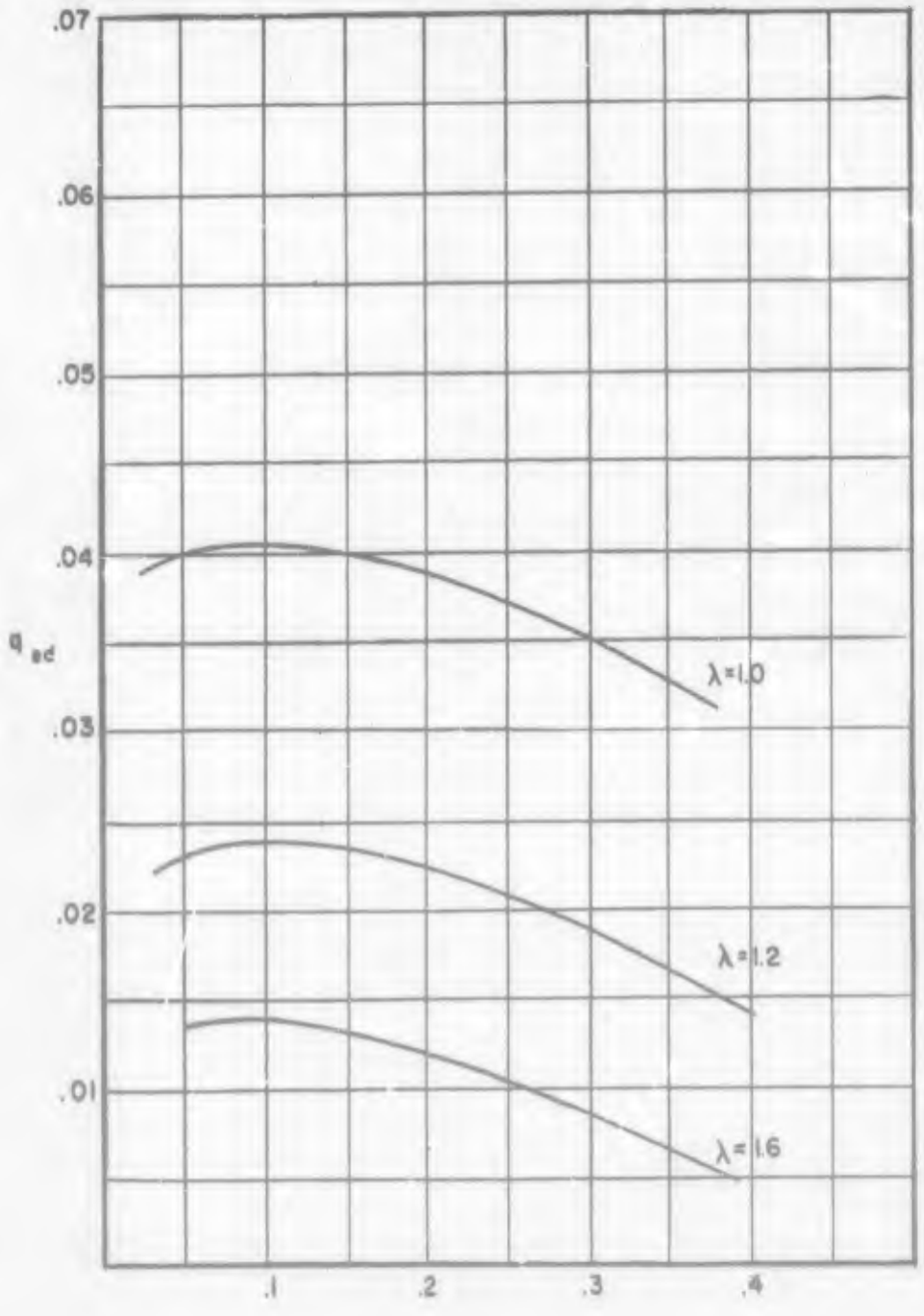

FIGURE 15

DISK FRICTION AND WEAR
RING FRICTION HEAD
COEFFICIENTS

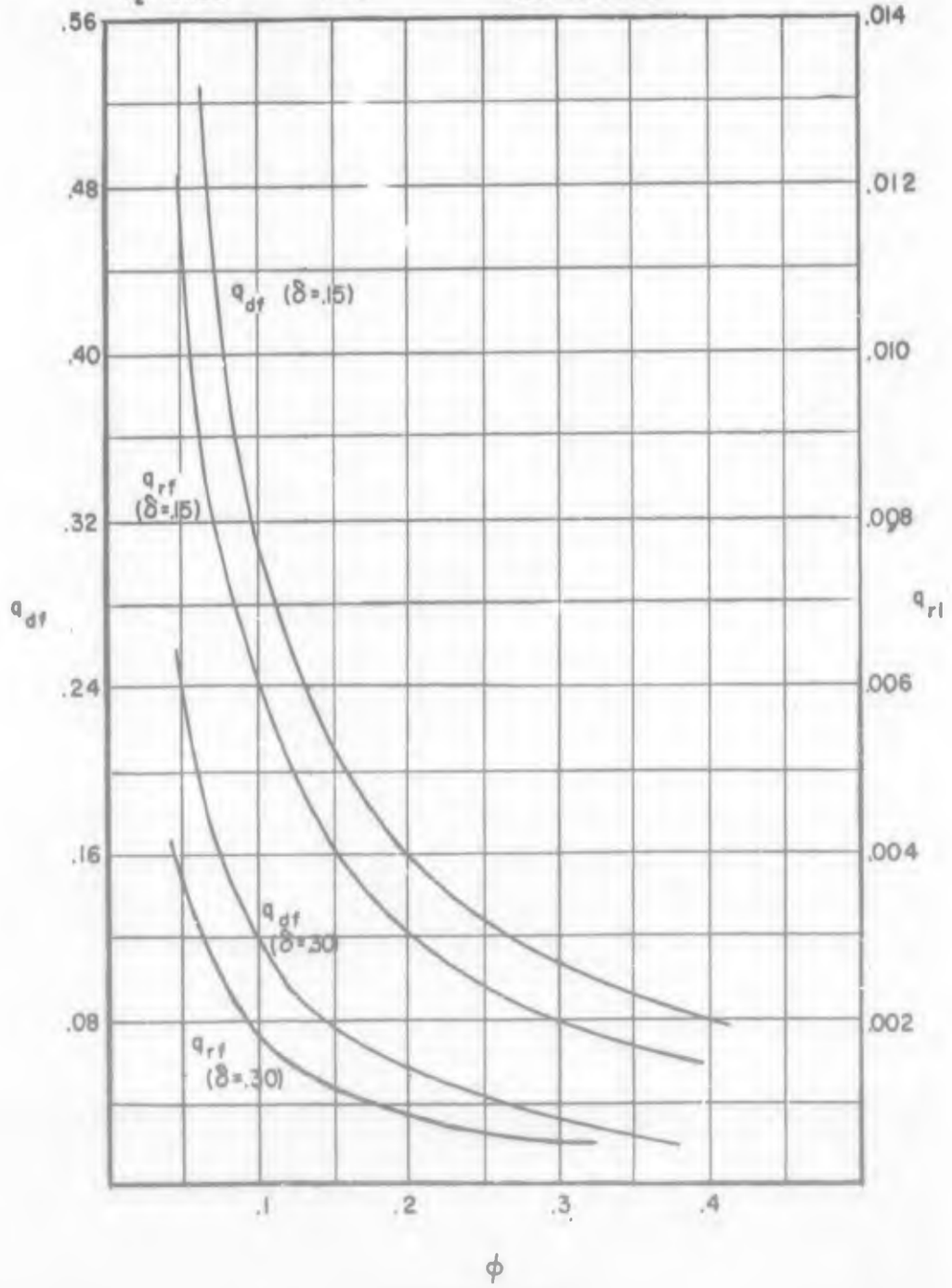

SUNDSTRAND TURBO

A Division of Sundstrand Corporation

FIGURE 16
WEAR RING LEAKAGE HEAD LOSS COEFFICIENT

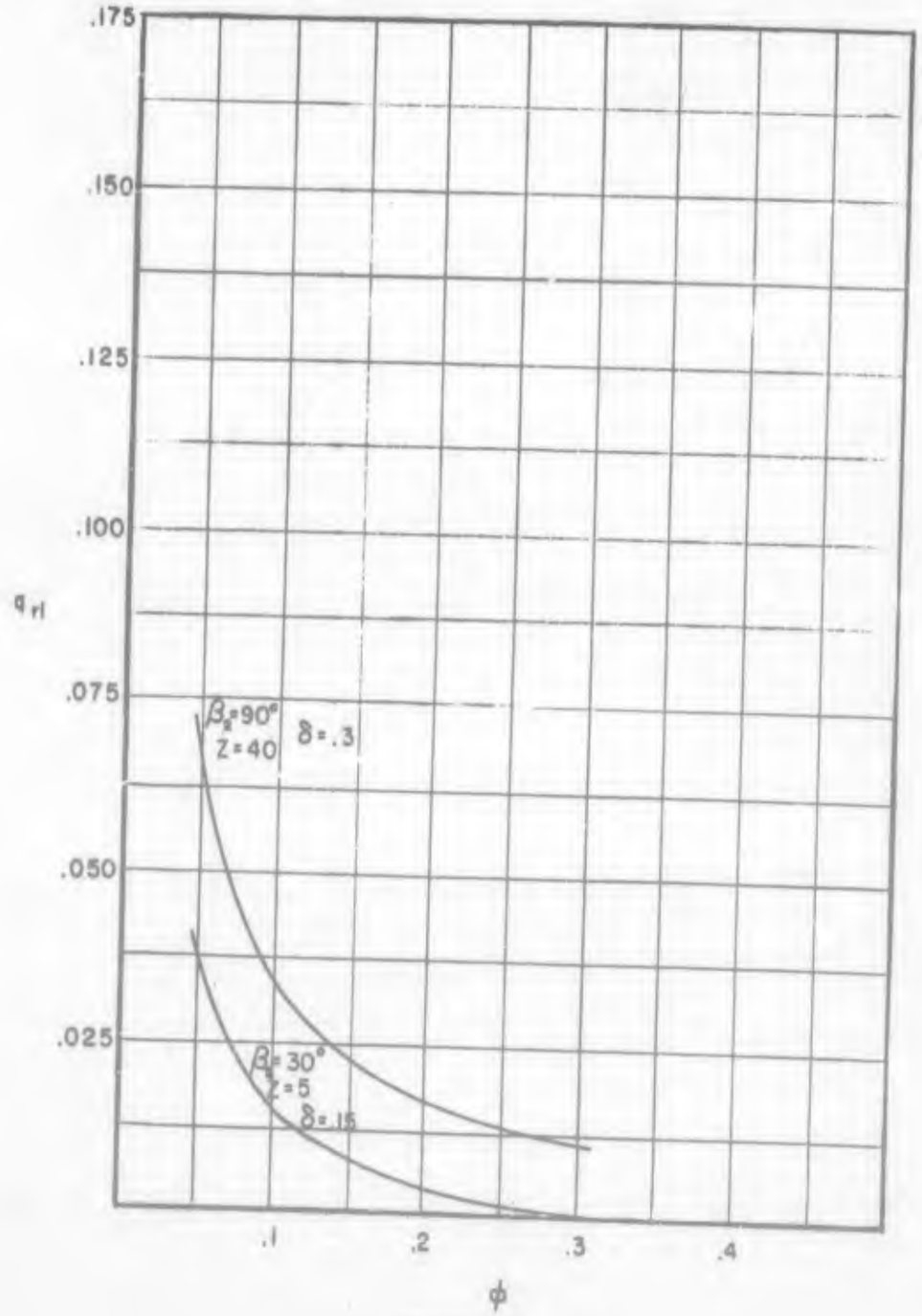

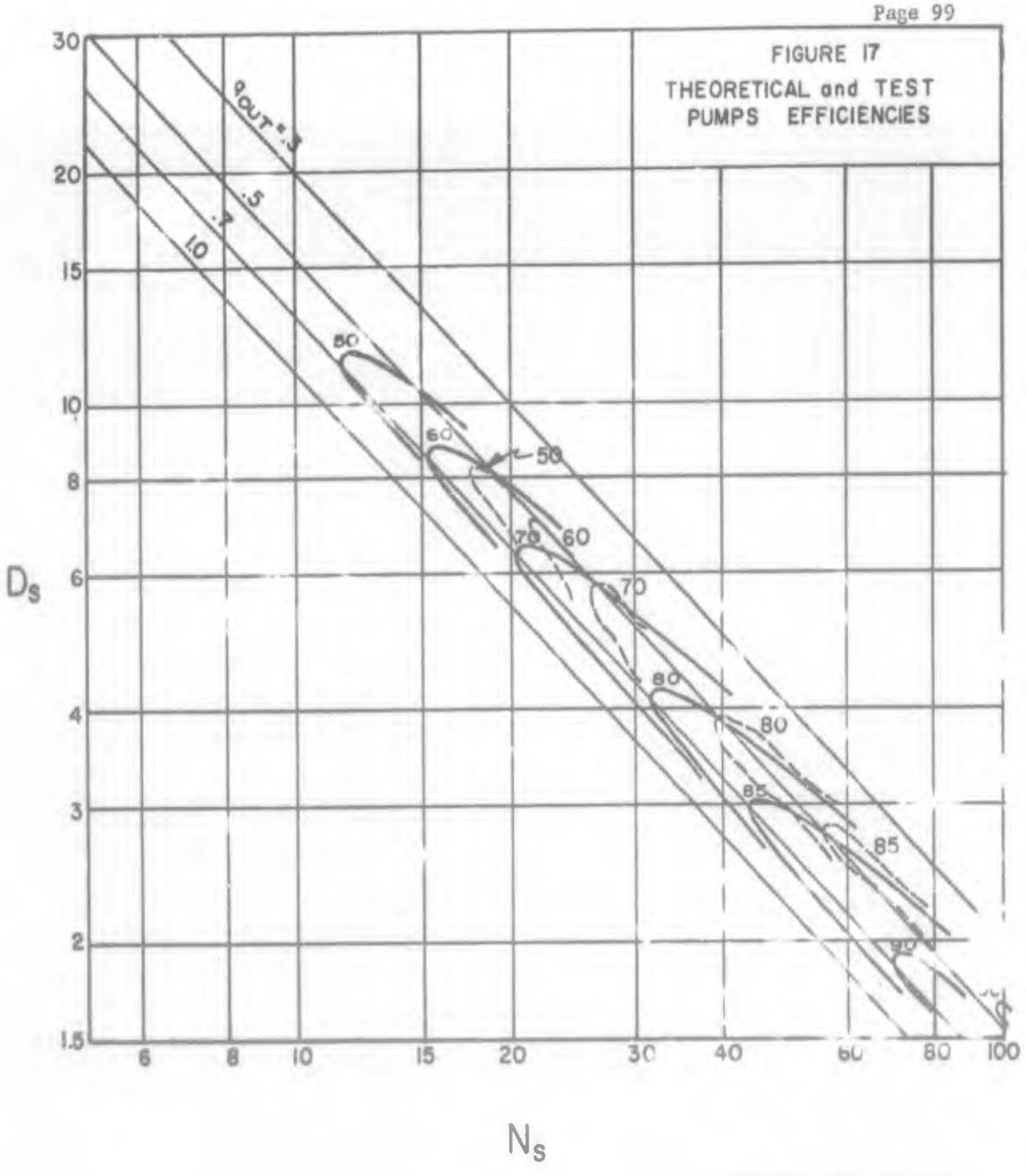
FIGURE 17
THEORETICAL and TEST
PUMPS EFFICIENCIES
Q_{OUT}=.3
.5
.7
1.0
50
60
50
70
60
70
80
80
85
85
90
30
20
15
10
8
6
4
3
2
1.5
D_S
6
8
10
15
20
30
40
60
80
100
N_S
THEORETICAL PUMPS
TEST PUMPS

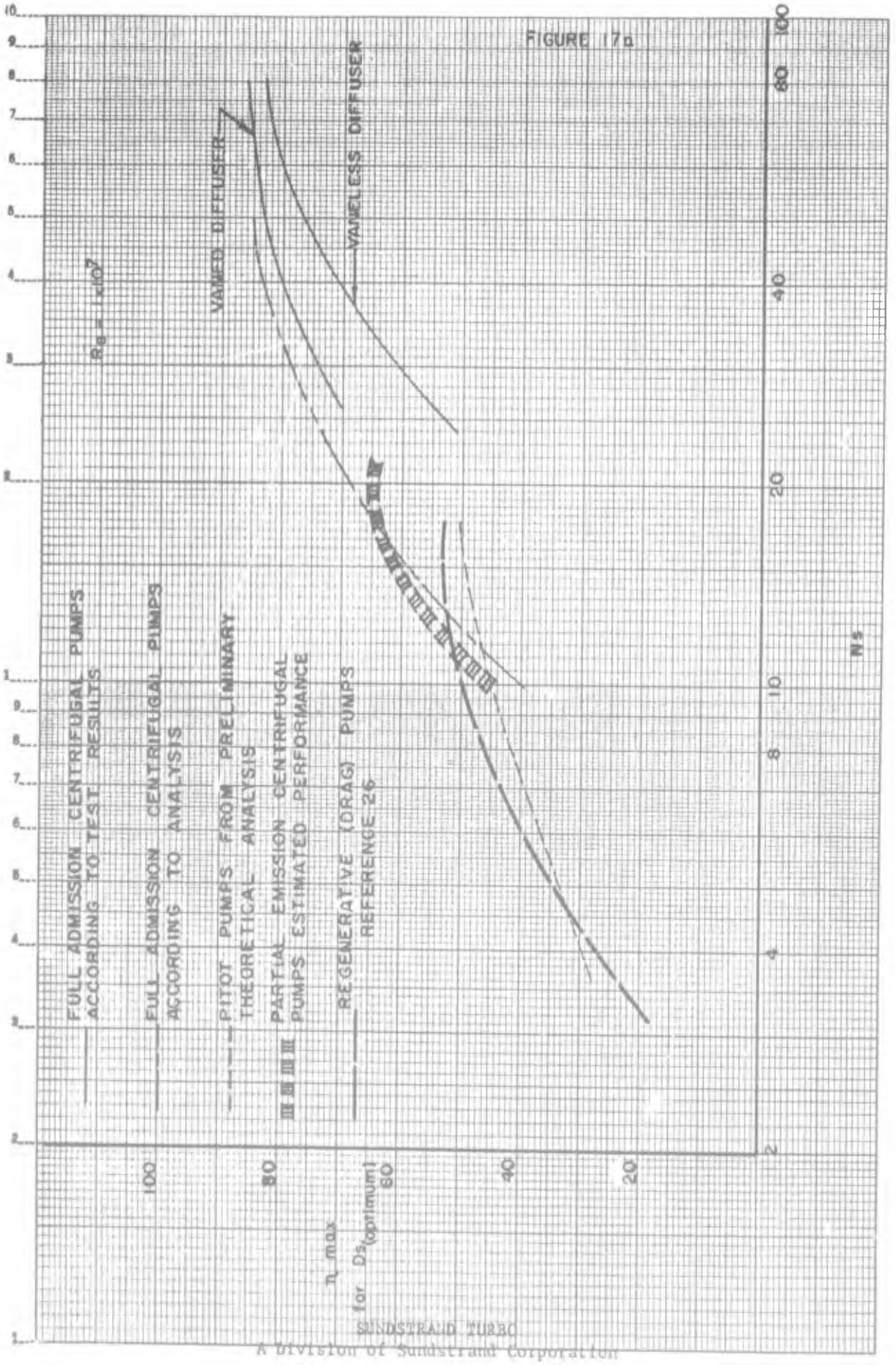
FIGURE 17a
VANED DIFFUSER
VANELESS DIFFUSER
$R_e = 1 \times 10^7$
FULL ADMISSION CENTRIFUGAL PUMPS
ACCORDING TO TEST RESULTS
FULL ADMISSION CENTRIFUGAL PUMPS
ACCORDING TO ANALYSIS
PITOT PUMPS FROM PRELIMINARY
THEORETICAL ANALYSIS
PARTIAL EMISSION CENTRIFUGAL
PUMPS ESTIMATED PERFORMANCE
REGENERATIVE (DRAG) PUMPS
REFERENCE 26
η_{max} for D_s (optimum)
Ns

FIG. 18a

GEOMETRIC PARAMETERS FOR OPTIMUM SUCTION SPECIFIC SPEED

$R_{\delta}^{*} = 1 \times 10^{7}$ S = 541

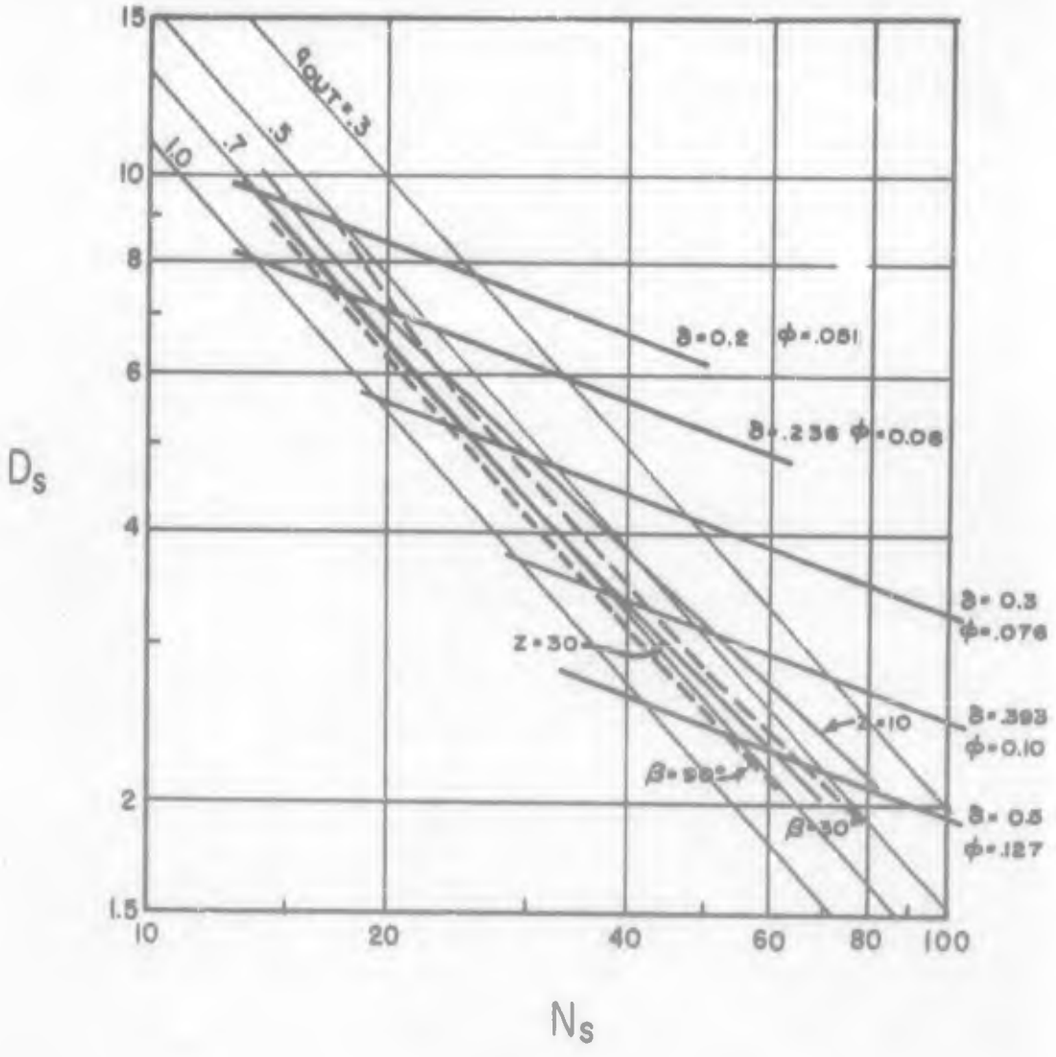

FIG. 18b
$N_s - D_s$ DIAGRAM FOR OPTIMUM
SUCTION SPECIFIC SPEED

$S = 541$ $\quad R_e^{\blacklozenge} = 1 \times 10^7$ $\quad \alpha_1 = 59^0$

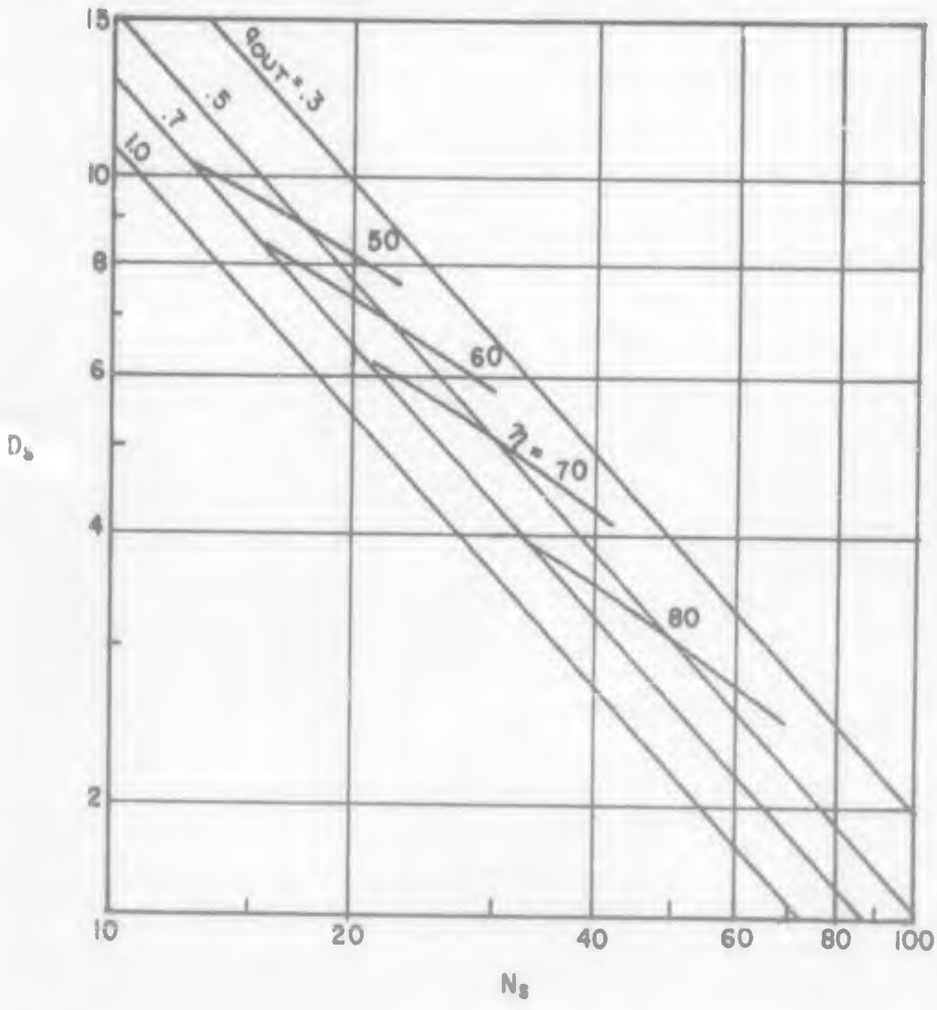

6. DERIVATIONS OF THE CENTRIFUGAL PUMP EQUATIONS

6.1 Efficiency Equation

6.1.1 Theoretical Head Coefficient

The theoretical head has been defined as the actual energy transfer taking place between the impeller and the fluid. The energy transfer between an impeller and the fluid traversing it may be analyzed for idealized conditions by application of Newton's laws of motion to the fluid flow. A typical impeller is shown schematically in Figure 9, together with a vectorial representation of the fluid and impeller velocities at entrance to and at exit from the impeller. For idealized conditions, it is assumed that steady flow exists; that is, the mass rate of flow is constant and no fluid is stored in the impeller, and that the velocity of the flow is uniform across any finite area perpendicular to the flow. Since only the fluid entering and leaving the impeller is capable of exerting an external force upon it, consideration of the velocities at entrance and at exit permits evaluation of the energy transfer taking place. Further, the radial and axial components of

these velocities create loads on the bearings, but do not contribute to the driving torque required (except as a function of bearing friction), and hence, only the tangential components of the velocities need to be considered.

Since the moment of momentum of the fluid passing through the impeller is changed only as a result of the moment or torque exerted between impeller and fluid, the energy transfer may be evaluated by analyzing the change in moment of momentum of the fluid traveling the impeller. According to Newton's third law, the driving torque equals the difference between moment of momentum at exit and entrance,

$$T = \frac{G}{g}(r_2 \ C_{u2} - r_1 \ C_{u_1}) \qquad \text{Eq. 6.1}$$

Where T is the torque in pound-feet, G is the weight rate of flow in pounds per second, r_1 and r_2 are the mean radii of the inlet and outlet areas respectively, C_{u_1} and C_{u_2} are the tangential components of the absolute flow velocities at inlet and outlet respectively and g is the standard gravitational constant.

The energy transfer is the product of torque and angular velocity of the impeller ω, in radians per second:

$$E = T\omega = \frac{G\omega}{g}\left(r_2 C_{u2} - r_1 C_{u1}\right) \qquad \text{Eq. 6.2}$$

The peripheral velocity of the wheel U, at any point is equal to the radius times the angular velocity. Thus,

$$E = \frac{G}{g}\left(U_2 C_{u2} - U_1 C_{u1}\right) \qquad \text{Eq. 6.3}$$

The energy transfer per unit of weight flow is obtained by dividing E by G, resulting in the well known Euler equation,

$$\frac{E}{G} = H_{th} = \frac{1}{g}\left(U_2 C_{u2} - U_1 C_{u1}\right) \qquad \text{Eq. 6.4}$$

where H_{th} is the energy transferred per unit of weight flow, or theoretical head, with units of $\frac{\text{ft-lb}}{\text{lb}}$ or ft.

Equation 6.4 expresses explicitly the relationship between the energy transfer per unit of mass flow and the velocities in the vector diagram of Figure 9.

It is generally agreed by most investigators that, without the influence of inlet guide vanes, there should be essentially no preswirl in the inlet flow; that is, C_{u1} is nearly equal to zero, when operating at or near the best efficiency point. Since maximum efficiency for swirlfree inlet conditions (no inlet guide vanes) is the criteria of optimization under consideration, only the conditions at the best efficiency point are concerned, C_{u1} is assumed to equal zero, and the theoretical head becomes

$$H_{th} = \frac{U_2 \, C_{u2}}{g} \qquad \text{Eq. 6.5}$$

Referring again to the velocity diagram of Figure 9,

$$C_{u2} = U_2 - W_{u2} \qquad \text{Eq. 6.6}$$

$$= U_2 - C_{m2} \cot \beta'_2 ,$$

where C_{m2} is the meridional component of absolute flow velocity at impeller exit, that is, that component lying in a plane passing through the axis of rotation, and β_2 is the angle that the flow makes with the tangent to the impeller. Substituting Equation 6.6 into 6.5,

$$H_{th} = \frac{1}{g} \left(U_2^2 - U_2 \, C_{m2} \cot \beta'_2 \right) \qquad \text{Eq. 6.7}$$

Among the idealizing assumptions, it was stipulated in the derivations of Equation 6.7 that the flow is uniform, both as to magnitude and direction, over the entire impeller outlet area. References 4, 7 and 8, among others, indicate that the flow is not uniform over the impeller outlet flow area and discuss correction factors which account for the effect on H_{th}. H_{th} represents the actual energy transfer occurring between the impeller and the fluid, and was calculated from the difference of moment of momentum of the impeller inlet and outlet flows, assuming uniformity over the entire flow area. But the moment of momentum of the fluid is variable at different points in the impeller outlet area, so it is necessary to integrate across the flow area in order to determine the actual H_{th}. It should be noted that the resulting reduction in H_{th} does not represent an energy loss, but indicates the inability of the impeller to absorb, transmit, and impart the energy. Wislicenus (Reference 7 pf. 335) has derived a correction factor based upon a sinusoidal variation with respect to axial position of the meridional component of the flow velocity, as shown in Figure 19, a uniform velocity distribution in the peripheral direction and a constant

value of β_2'. Integrating over the entire area he obtains

$$H_{th} = \frac{1}{g}\left[U_2^2 - \frac{\pi}{8}^2 \; U_2 \; C_{m2\,av} \cot\beta_2'\right] \qquad \text{Eq. 6.8}$$

Thus, the subtractive term of the equation for H_{th} is increased by a factor of $\frac{\pi}{8}^2 = 1.234$.

Stepanoff (Reference 4, pf. 49) performs a similar derivation, assuming a linear rather than a sinusoidal velocity profile as shown in Figure 20. Integrating over the flow area, he derives another expression for H_{th}.

$$H_{th} = \frac{1}{g}\left\{U_2^2 - \left[1 + \frac{(C_a - C_b)}{12\,C_{m2av}^2}\right] U_2 \; C_{m2av} \cot\beta_2'\right\} \qquad \text{Eq. 6.9}$$

Both Wislicenus and Stepanoff assume that β_2' is constant. This would require that the tangential component of the flow velocity C_{u2} would vary as a direct function of C_{m2}. Test data in Reference 9 indicates that this is not necessarily accurate, but that variations may occur in β_2' as well as in C_{m2}.

Following the same approach, but using different assumptions, another correction for H_{th} may be derived. In Figure 21

the assumed velocity distribution of both the meridional and the tangential components of the flow are illustrated. These consist of a linear distribution topped with a sinusoidal distribution. Although this does not exactly match the profiles shown in Reference 9, the random characteristic of the experimental data would preclude the possibility of exact duplication. But the velocity profile assumed should yield fairly representative results. Figure 22 shows an element of flow issuing from the impeller of width dx and of circumferential length πD_2. If the meridional component of velocity for the incremental element of the flow is C_{m2}', the volume flow rate across the incremental area is,

$$dQ = \pi D_2 \, C_{m2}' \, dx \qquad \text{Eq. 6.10}$$

The flow element has a tangential velocity component, C_{u2}', which is not uniform over the impeller outlet area, but varies as a function of its axial position. Assuming that the maximum tangential velocity is C_{u2} and the minimum value is $(1 - \Pi) C_{u2}$, then the difference between the maximum and minimum is ΠC_{u2}. The variation in C_{u2}' is assumed to follow a sine function across the axial extent of the outlet area, so that the tangential velocity of any

incremental flow element is given by, (see Fig. 22 for notations)

$$C_{u2}' = C_{u2} - n\,C_{u2} + n\,C_{u2}\sin\left[\pi\frac{X}{b}\right] \qquad \text{Eq. 6.11}$$

$$= C_{u2}\left[1 - n + n\sin\left[\pi\frac{X}{b}\right]\right.$$

The meridianal component of the flow follows a similar function, but of different magnitude. In the case of the meridianal velocity, it is desirable to relate the function to the mean rather than the maximum value of C_{m2}. The mean height of a sine function is $\frac{2}{\pi}$, therefore, the meridianal velocity of any incremental flow element is,

$$C_{m2}'' = C_{m2} - \frac{2}{\pi}k\,C_{m2} + k\,C_{m2}\sin\left[\pi\frac{X}{b}\right] \qquad \text{Eq. 6.12}$$

$$= C_{m2}\left[1 - \frac{2k}{\pi} + k\sin\left[\pi\frac{X}{b}\right]\right.$$

From Eq. 6.5, the head developed in any incremental element would be,

$$dP = \gamma\,H_{th}'\,dQ \quad \text{where } \gamma = \text{density.} \qquad \text{Eq. 6.13}$$

The power absorbed by the fluid or imparted by the rotor for the incremental element is

$$H_{th}'' = \frac{U_2\,C_{u2}'}{g} \qquad \text{Eq. 6.14}$$

Combining Equations 6.10 to 6.14 and integrating yields

$$P = \gamma\frac{U_2}{g}C_{u2}\,Q\left[1 - n\left(1 - \frac{2}{\pi}\right) + kn\left(\frac{1}{2} - \frac{4}{\pi^2}\right)\right. \qquad \text{Eq. 6.15}$$

The mean theoretical output head H_{th} is equal to the power, P, divided by the weight rate of flow, G.

$$H_{th} = \frac{P}{G} = \frac{U_2}{g} C_{u2} \left(1 - .363n + .0945\, kn\right) \qquad \text{Eq. 6.16}$$

$$= K_n U_2 C_{u2}$$

where

$$K_n = 1 - .363n + .0945\, kn \qquad \text{Eq. 6.17}$$

If it is assumed that k = .4 and n = .15, the resulting value for K_n is .95.

From Equations 6.7 and 6.16, the theoretical head is

$$H_{th} = \frac{K_n}{g} \left[U_2^2 - U_2 C_{m2} \cot \beta_2'\right] \qquad \text{Eq. 6.18}$$

If it is assumed that the flow is guided perfectly by the impeller vanes, then the flow angle β'_2 would be equal to the vane angle β_2. However, investigations of real pumps indicate that the flow is not guided perfectly by the blades and, furthermore, that β'_2 is variable at different points around the periphery of this pump, complicating the use of Equation 6.18. A widely accepted solution to the problem is to introduce an empirically determined slip factor m, and to base the calculation of H_{th} on the blade

angle, β_2. Thus,

$$H_{th} = \frac{K_n}{g}\left[U_2^2 + U_2 C_{m2} \cot\beta_2'\right] = \frac{K_n}{mg}\left[U_2^2 - U_2 C_{m2} \cot\beta_2\right] \quad \text{Eq. 6.19}$$

Considerable work has been done to obtain a satisfactory expression for the slip factor in terms of pump geometry. Five different expressions found in the literature and converted to the notation of this report are listed in Table 2.

TABLE 2

EQUATIONS FOR SLIP

Originator	Equation for m	Reference
Stodola	$\dfrac{1}{1 - \dfrac{\sin\beta_2}{Z\left[1 - K_1\phi\cot\beta_2\right]}}$	10
Meisel	$\dfrac{1}{1 - \dfrac{.72\ Z\ S_{u2}}{\pi\ r_2^2}}$	11
Busemann	$\dfrac{1 - K_1\phi\ \cot\beta_2}{h_o - C_{h1}\ K_1\phi\ \cot\beta_2}$	7

TABLE 2 --(Continued)

EQUATIONS FOR SLIP

Originator	Equation for m	Reference
Eckert	$1 + \frac{\pi \sin \beta_2}{2Z\,(1-\delta)}$	12
Pfleiderer	$1 + \frac{1 + .6 \sin\beta_2}{Z\,(1+\delta)\left[\chi^2 - .25\,(1-\delta^2)\right]^{\frac{1}{2}}}$	13

X is shown in Figure 25

The first two expressions by Stodola and Meisel do not take into account the very important effect of blade length. Dr. Stodola, in discussing Reference 11, mentions the inaccuracy of his own expression, and also points out that Meisel's expression gives zero effect at $\beta_2 = 90°$, a result that is contrary to experience. The remaining expressions are compared in Figure 23. Test data and the corresponding sources are given in Table 3. When compared with the test data, the spread of Eckert's curves suggests that his expression is too strongly influenced by changes in blade angle. The expressions by Busemann and Pfleiderer both agree fairly well with the test data and with each other.

TABLE 3

β_2 deg.	Z	δ	Test Value of m	Pfleiderer m	Busemann m	Pfleiderer % Error	Busemann % Error	Ref.
90	18	.541	1.153	1.18 *	1.09	2.5 *	5.5	5
24	7	.568	1.38	1.373 *		4.8 *		6
30	2	.574	3.5	3.35 +	3.9 ◊	4.3 +	11.4 ◊	7
30	4	.574	1.97	2.175 +	1.9 ◊	10.1 +	3.5 ◊	7
30	6	.574	1.64	1.783 +	1.5 ◊	8.5 +	8.5 ◊	7
40	4	.604	1.74	1.678 +	1.90 ◊	3.5 +	9.2 ◊	8
40	6	.604	1.47	1.451 +	1.53 ◊	1.4 +	4.1 ◊	8
40	8	.604	1.33	1.338 +	1.38 ◊	.4 +	6.0 ◊	8
40	12	.604	1.21	1.226 +	1.23 ◊	1.3 +	1.7 ◊	8
40	16	.604	1.15	1.69 +	1.18 ◊	1.7 +	2.6 ◊	8
20	6	.636	1.64	1.784	1.48 ◊	8.8 +	9.8 ◊	9
20	6	.594	1.77	1.784 +	1.48 ◊	0.8 +	16.4 ◊	9

+ corrected for x but not for δ; * corrected for δ but not for x;

◊ not corrected for δ.

Shepherd (Ref. 8) and Wislicenus (Ref. 7) both indicate that the Busemann slip factor is fairly well substantiated. However, the Pfleiderer slip factor expresses essentially the same tendencies and magnitudes, and it shows even better agreement with test data than the expression by Busemann. A somewhat different approach to the slip concept is presented in Ref. 22. This concept was stimulated by the fact that the assumptions involved in the above discussed approaches are not entirely satisfactory for explaining the actual flow mechanism causing the slip, since detailed investigations on compressor characteristics have led to the conclusion that the slip also is a function of the flow factor as evidenced by many test data. Ref. 22 assumes that the reason for the apparent slip is flow separation at the suction side of the blade which causes the relative impeller leaving component to assume a direction which produces a smaller peripheral component than the one which would result when the flow would adhere to the blades. This effect is assumed to exist in addition to the relative vortex in the impeller channel. It is furthermore assumed that both effects influence each other by assuming, for example, that the influence of the relative eddy in the flow channel decreases with decreasing axial channel width

and that the influence of the relative flow eddy is additionally diminished by the separation of the flow on the suction side of the blade. In evaluating the available data on the above basis, the slip is expressed by the relation

$$\frac{1}{m} = 1 - \left(1 - \frac{1}{m_{20}}\right)\frac{20}{Z}$$

whereby m_{20} represents the slip for a blade number of 20. This relation is assumed to be valid for blade numbers between 14 and 28. The slip at the reference blade number is then expressed as a function of flow factor, blade angle, and channel geometry in a diagram as reproduced in Fig. 24 This diagram shows that the slip increases with decreasing blade angles, increasing flow factors and decreasing ratios of b_1/b_2.

It has to be conceded that this presentation most likely represents all the different influences on the slip and that the equations proposed by Messrs. Busemann and Pfleiderer are approximations which do not duly account for all the influences which affect the somewhat complicated flow mechanism involved in the slip concept. It is, however, also apparent that the data presented in Fig. 24 have only limited validity and may not be applicable for extremely

small blade numbers. Since it is the intent of this study to also deal with pumps of comparatively small blade numbers, the approximate concept of Pfleiderer is used in this report for the calculation of the slip in spite of the apparent shortcomings. Furthermore, the form of the slip correction by Pfleiderer lends itself more readily to the kind of mathematical manipulation that is employed in this analysis.

Thus

$$m = 1 + \frac{1 + .6 \sin\beta_2}{Z(1+\delta)\left[\chi^2 + .25(1-\delta)^2\right]^{1/2}} \qquad \text{Eq. 6.20}$$

The slip factor by Pfleiderer contains an additional geometric parameter χ, which is defined in Figure 25 as

$$\chi = \frac{h}{D_2} \qquad \text{Eq. 6.21}$$

It should be possible to evaluate an optimum value for χ as a function of the other parameters through the use of the potential flow theory. However, considering the approximate nature of the evaluation of m, such an analysis would probably unduly complicate the form of the equation. Observation of common pump designs indicates that χ is a strong function of δ. In the low end of the specific

speed regime with which we are concerned, δ is generally small and the axial extent of the impeller inlet portion, represented by χ, is also small. With increasing specific speed, as the mixed flow regime is approached, δ and χ both increase. Scaling from pictures of pumps in the literature representing a range of δ and χ values, the following approximate evaluation for χ was obtained:

$$\chi = .5\delta^2 \qquad \text{Eq. 6.22}$$

Substituting Eq. 6.22 into Eq. 6.20 yields

$$m = 1 + \frac{1 + .6 \sin\beta_2}{.5Z\,(1+\delta)\left[\delta^4 + (1-\delta)^2\right]^{\frac{1}{2}}} \qquad \text{Eq. 6.23}$$

It is recognized that Equation 6.22 is strictly an approximation, and it would be desirable to know the magnitude of the error that is introduced by such an approximation, and also to obtain an indication of the accuracy of Eq. 6.22 itself. Figure 26 shows the magnitude of the error in the slip factor m introduced by approximating χ with Equation 6.22, assuming that the actual value of χ differs by 50% from its calculated approximation. The error reduces with reducing β_2, reducing δ and increasing

blade number. In Table 4 several values of χ, scaled from the illustrations, are given, together with the percent deviation resulting from using Equation 6.22 for approximate values. The error in χ is considerably less than was assumed in calculating Figure 26. Thus, it appears that the error introduced by approximating χ as a function of δ is reasonably small in the range of pump configurations in which we are interested, and the approximation is certainly more accurate than assuming a constant mean value of χ.

Equation 6.23 represents a rather complicated function of δ which will be difficult to handle mathematically. Figure 27 shows the actual function and a linear approximation over the range of δ values in which we are interested. The maximum error introduced by the linear approximation of the δ term is on the order of 2% which is certainly reasonable in view of the improvement in the form of the equation. Thus, the expression for m reduces to

$$m = 1 + \frac{1 + .6 \sin\beta_2}{5Z(1-.2833\delta)} \qquad \text{Eq. 6.24}$$

In view of the simplification made in the slip factor equation, it would be expedient to check the final form of Equation 6.24 with the test data. The test data is shown

in Table 4, with the percent error also being indicated, and the data is compared in Figure 28. On the average, the accuracy of the expression is not materially affected, except in the case of a very low blade number of 2. Substitution of Equation 6.24 into Equation 6.19 yields a mathematical expression with which H_{t_h} may be quantitatively evaluated and if divided by H_{ref} yields

$$q_{th} = \frac{.95(1-K_1\phi\cot\beta_2)}{1+\frac{1+.6\sin\beta_2}{.5\,Z(1-.28338)}}$$

TABLE 4

β_2 deg	Z	δ	x	m'	m''	m_t	E_m	m_c	E_x	ref.	x_c
90°	18	.51	.0216	1.239	1.206	1.153	7.2	1.122	+	3	.130
24	7	.535	.164	1.408	1.413	1.38	2	1.387	13	6	.143
30	2	.54	0	2.835	2.51	3.5	19	3.10	*	7	.146
30	4	.54	0	1.917	1.755	1.97	2.8	1.80	*	7	.146
30	6	.54	0	1.612	1.503	1.64	1.8	1.53	*	7	.146
40	4	.568	.193	1.761	1.805	1.74	1.1	1.782	16	8	.162
40	6	.568	.193	1.507	1.536	1.47	2.3	1.499	16	8	.162
40	8	.568	.193	1.380	1.403	1.33	3.7	1.352	16	8	.162
40	12	.568	.193	1.254	1.268	1.21	3.6	1.222	16	8	.162
40	16	.568	.193	1.190	1.201	1.15	3.3	1.161	16	8	.162
20	6	.6	0	1.627	1.467	1.64	.9	1.48	*	9	.18
20	6	.559	0	1.583	1.467	1.79	11.5	1.655	*	9	.156

x = h/D, where h is the axial distance from inlet to outlet mean stream line

m' = slip factor calculated on actual δ and x

m'' = slip factor calculated on simplified equation of δ and x

m_t = actual test value of slip factor

m_c = test value of slip factor corrected by factor $\frac{m''}{m'}$

E_m = % of error between m' and m_t, based on m_t

E_x = % deviation of x from x_c, based on x

x_c = calculated value of x from, $x_c = .5\,\delta^2$

* - value of x follows test requirements rather than normal design practice.

\+ - does not appear consistent with design practice.

6.1.2 Impeller Loss Coefficient

The impeller flow losses may be divided into three categories:

a. Incidence losses occurring along the leading edges of the vanes.

b. Flow losses due to friction.

c. Diffusion losses due to any reduction in relative velocity which might occur between impeller inlet and outlet.

a. Incidence Losses - One of the assumptions is that, at the best efficiency point, the inlet portion of the vanes is designed for incidence free entry. Therefore, the incidence losses are negligible. However, the flow losses will be analyzed on the basis of logarithmic spiral vanes, and for such a vane shape, the best efficiency point does not occur at an incidence free entry condition for a purely radial impeller. The introduction of an inducer section presupposes that there is a departure from the purely radial and logarithmic spiral

configuration at the innermost part of the vane, permitting the vane to be designed for incidence free entry. Thus, it is justifiable to assume that the incidence losses may be neglected for design point performance characteristics.

b. Flow Losses - The flow loss is assumed to be of the same form as expressed by the Darcy equation for straight pipes,

$$H_{ls} = \frac{fLW_a^2}{D_a^* 2g} \qquad \text{Eq. 6.25}$$

with correction being made for the fact that the impeller passageways are not straight, but contain a right angle bend. In Equation 6.25, H_{ls} is the impeller head loss assuming a straight impeller channel, f is a friction factor, L is the length of the passage, W_a is the root-mean-square relative velocity and D_a^* is the hydraulic diameter. The hydraulic diameter, which is necessary to make the equation applicable to rectangular flow channels, is equal to four times the cross-sectional area of the flow passage divided by the wetted perimeter.

The effect of the curve in the impeller channel will be treated in a manner similar to that used for pipe bends and elbows; namely, equating the bend loss to an equivalent length of straight pipe. Hence, it is necessary first to determine the flow loss with the assumption that the impeller passageway is essentially straight. If the fluid were allowed to travel outward between two parallel plates, representing the front and back shrouds, in a free vortex it would follow a logarithmic spiral. Logarithmic spiral vanes, or reasonable approximatives thereof, have been found to be quite satisfactory vane configurations. Hence, the analysis of the flow losses in the impeller will assume logarithmic spiral vanes.

Assuming that the channel length is L, that the position along L is given by the distance l and that the velocity varies linearly along L, then the relative velocity W at any point is,

$$W = W_1 (1 + al) \qquad \text{Eq. 6.26}$$

where W_1 is the relative velocity at impeller entrance and $\underline{a}$ is a constant relating W to 1. Referring to Figure 9, the flow is assumed to traverse a straight radial impeller along a logarithmic spiral path from d_e to D_2. The losses in such an impeller will be analyzed first, and allowances will be made for losses resulting from the inducer section later. The length of a logarithmic spiral from d_e to D_2 is

$$L = \frac{(d_e - D_2)}{2 \sin \beta_2} \qquad \text{Eq. 6.27}$$

since the definition of a logarithmic spiral requires that β = constant, and is, therefore, equal to β_2.

D_1 may be related to D_2, δ , and τ , by assuming that the impeller inlet flow area outside d_e is equal to the flow area inside d_e or

$$\frac{\pi}{4}\left(d^2 - d_e^2\right) = \frac{\pi}{4}\left(d_e^2 - d_h^2\right)$$

Thus,

$$d_e = D_2 \delta \left[\frac{1 + \tau^2}{2}\right]^{1/2} \qquad \text{Eq. 6.28}$$

The vane thickness is neglected, as it would have comparable effects in both areas. Substituting Equation 6.28 into Equation 6.27 yields

$$L = \frac{D_2 \left[1 - \delta \left(\frac{1+r^2}{2} \right)^{1/2} \right]}{2 \sin \beta_2} \qquad \text{Eq. 6.29}$$

The value of $\underline{a}$ may be evaluated from the consideration that, at any point along L, the relative velocity is given by

$$W = \frac{C_m}{\sin \beta} \qquad \text{Eq. 6.30}$$

Since β is constant for a logarithmic spiral and is, in fact, equal to β_2, W is directly proportional to C_m at all points along the flow path. Thus, by definition

$$K_i = \frac{C_{m2}}{C_{m1}} = \frac{W_2}{W_1} \qquad \text{Eq. 6.31}$$

The end conditions, W_1 and W_2, provide a relationship between K_i and $\underline{a}$, since from Equation 6.26

$$W_2 = W_1 \ (1 + aL) \qquad \text{Eq. 6.32}$$

So,

$$a = \frac{K_1 - 1}{L}$$

Eq. 6.33

Since we are concerned with flow losses which, according to Equation 6.25 are a function of the square of the relative velocity, or introducing Equation 6.30 of the meridional component of velocity, it is desired to evaluate C_{ma}^2 in such a way that the result is the same as if integrating over the entire length, let

$$C_{ma}^2 = \int_0^L \frac{C_m^2 \, dl}{L}$$

Since,

$$C_m^2 = C_{m1}^2 (1 + al)^2$$

Eq. 6.34

$$C_{ma}^2 = C_{m1}^2 \int_0^L (1 + al)^2 \, dl$$

Eq. 6.35

$$= C_{m1}^2 \left(1 + aL + \frac{a^2 l^2}{3}\right)$$

Substituting Equation 6.33 into 6.34 yields

$$C_{ma}^2 = \frac{C_{mi}^2}{3}\left(K_i^2 + K_i + 1\right) \qquad \text{Eq. 6.36}$$

It would be desirable to calculate the Reynolds number and the hydraulic diameter at the point where $C_m = C_{ma}$. From Equation 6.34,

$$C_{ma} = C_{mi}\left(1 + a l_a\right)$$

where l_a is the distance along the channel length L where $C_m = C_{ma}$.

Rearranging and solving for l_a,

$$l_a = \frac{\frac{C_{ma}}{C_{mi}} - 1}{a} \qquad \text{Eq. 6.37}$$

Substituting from Equations 6.33 and 6.36,

$$l_a = \frac{L}{K_i - 1}\left[\left(\frac{K_i^2 + K_i + 1}{3}\right) - 1\right] \qquad \text{Eq. 6.38}$$

The equation for a log spiral of length l_a in terms

of the limiting diameters, D_1 and d_e, is

$$l_a = \frac{D_a - d_h}{2 \sin \beta_2} \qquad \text{Eq. 6.39}$$

Equating 6.38 and 6.39, solving for D_a and introducing L from Equation 6.29 yields

Eq. 6.40

$$D_a = D_2 \left\{ \frac{1 - \delta \left(\frac{1+\tau^2}{2} \right)^{1/2}}{K_1 - 1} \left[\left(\frac{K_1^2 + K_1 + 1}{3} \right)^{1/2} - 1 \right] + \delta \left(\frac{1+\tau^2}{2} \right)^{1/2} \right\}$$

$$= D_2 J$$

where

Eq. 6.41

$$J = \frac{1 - \delta \left(\frac{1+\tau^2}{2} \right)^{1/2}}{K_1 - 1} \left[\left(\frac{K_1^2 + K_1 + 1}{3} \right)^{1/2} - 1 \right] + \delta \left(\frac{1+\tau^2}{2} \right)^{1/2}$$

Having determined D_a, it is now possible to evaluate D_a^* and R_e at the point a where $C_m = C_{ma}$. From conditions of continuity,

$$Q = C_{ma} \; A_{ma} = C_{ma}(\pi D_a - Zt)\, b_a = W_a \, A_a$$

where A_{ma} is the flow area perpendicular to C_{ma}, A_a is the flow area perpendicular to W_a and t is the thickness of the vanes. Since $W_a = C_{ma}/\sin \beta_2$,

$$A_a = A_{ma} \sin\beta_2 = (\pi D_a - Zt) b_a \sin\beta_2 \qquad \text{Eq. 6.42}$$

where b_a is the channel depth at point a. A_a represents the total flow area. The area of any individual impeller passageway is obtained by dividing the total area by the number of vanes. Thus, the hydraulic diameter of each individual passageway is

$$D_a^* = \frac{4(\pi D_a - Zt)\, b_a \sin\beta_2}{2Z\left[\left(\frac{\pi D_a - Zt}{Z}\right)\sin\beta + b_a\right]} \qquad \text{Eq. 6.43}$$

The vane depth, b_a, may be evaluated from conditions of continuity. At point a, the volume flow is given

by,

$$Q = C_{me}\ b_e\ (\pi D_e - Zt)$$

$$= C_{mi}\left(\frac{K_1^2 + K_1 + 1}{3}\right)^{1/2} D_2\left(\pi J - Z\,\frac{t}{D}\right) b_e \qquad \text{Eq. 6.44}$$

where t is the vane thickness. At the inlet, the volume flow is given by

$$Q = C_{mi}\left[\frac{\pi\, D_2^2 \delta^2\,(1-\tau^2)}{4}\right] \qquad \text{Eq. 6.45}$$

Equating Equations 6.44 and 6.45, and solving for b_e,

$$b_e = \frac{\pi D_2 \delta (1-\tau)}{4\left(\frac{K_1^2+K_1+1}{}\right)(\pi J - Z\frac{t}{D_2})} \qquad \text{Eq. 6.46}$$

All of the terms in Equation 6.25 have now been evaluated with the exception of the friction factor, f.

Blasius' law, as applied to pipes, would evaluate

f as,

$$f = \frac{.316}{R_e^{\frac{1}{4}}} \qquad \text{Eq. 6.47}$$

where R_e is the Reynolds number of the passageway and is given by the equation

$$Re = \frac{\rho W_a D_a^*}{\mu} = \frac{\rho C_{m1} \sqrt{\frac{K_1^2 + K + 1}{3}} D_a^*}{\mu \sin\beta_2} \qquad \text{Eq. 6.48}$$

Substituting b_a from Equation 6.46 into Equation 6.43, and inserting the resulting D_a^* into Equation 6.48, evaluates R_e.

$$R_e = \frac{\rho C_{m1} \pi D \delta^2 (1-\tau^2)}{\left[\frac{2(\pi J - Z\frac{1}{D})}{Z} \sin\beta + \frac{\pi \delta^2 (1-\tau^2)}{2(\frac{K_1^2 + K_1 + 1}{3})}\right]} \qquad \text{Eq. 6.49}$$

It is desirable to relate the flow passage Reynolds number to the pump Reynolds number by evaluating D_2

in terms of R_e^*, and substituting into Equation 6.49,

$$D_2 = \frac{R_e^* \mu}{\rho U_2} \qquad \text{Eq. 6.50}$$

Combining the above equations into Equation 6.32 and dividing by the reference head, the straight impeller loss coefficient is obtained.

$$q_{1s} = \frac{.0189\phi^{1.75}\left[1-\delta\left(\frac{1+\tau^2}{2}\right)^{\frac{1}{2}}\right]\left(\frac{K_1^2+K_1+1}{3}\right)^{1.5}}{R_e^{*\frac{1}{4}}(1-\tau^2)^{1.25}\sin^4\beta} \qquad \text{Eq. 6.51}$$

$$\left\{Z\left[\frac{2(\pi J - Z\frac{t}{D})\sin\beta}{Z\delta^2} + \frac{\pi(1-\tau^2)}{2\left(\frac{K_1^2+K_1+1}{3}\right)^{\frac{1}{2}}(\pi J - Z\frac{t}{D})}\right]\right\}^{1.25}$$

A quantitative evaluation of the losses introduced by the change in direction of flow from an axial to a radial direction was not found in the literature. In order to obtain an approximate evaluation of this loss, empirical data for the losses in pipe elbows

was extrapolated with a number of simplifying assumptions. Losses in pipe elbows are given on Page 6-39 of Reference 14 in terms of an equivalent length of straight pipe. It is assumed that the losses in the curved portion of the impeller passageway may similarly be represented in terms of an equivalent length of the straight radial passageway already evaluated above.

By dividing the equivalent lengths given in Reference 14 by their corresponding pipe diameters, a dimensionless representation is found which has a small degree of variation, and an average value of equivalent pipe length over pipe diameter of approximately 12 is obtained. However, the flow in a centrifugal pump impeller is aided in its turn from an axial to a radial direction by the centrifugal forces acting upon the fluid. Thus, the loss could be expected to be somewhat smaller than would be likely to occur in pipe fittings. Thus, an average value of 4 will be assumed for the ratio of equivalent length of impeller channel to impeller channel hydraulic diameter. Therefore, the impeller loss previously evaluated assuming a straight radial impeller must be increased

by a factor of

$$N_{ic} = 1 + \frac{4D_a^*}{L} \qquad \text{Eq. 6.52}$$

Introducing L and D_a^* from Equations 6.29 and 6.43 respectively,

$$N_{ic} = 1 + \frac{8T(1-\tau^2)\sin^2\beta}{Z\left(\frac{k_1^2+k_1+1}{3}\right)^{1/2}\left[1-\delta\left(\frac{1+T^2}{2}\right)^{1/2}\right]\left[\frac{2(\pi J - Z\frac{t}{D})\sin\beta}{Z\delta^2+} + \frac{\pi(1-\tau^2)}{2\left(\frac{k_1^2+k_1+1}{3}\right)^{1/2}\left(\pi J - Z\frac{t}{D}\right)}\right]}$$

Eq. 6.53

Due to the approximate nature of N_{ic} and considering the complexity Equation 6.53 would create if introduced as a factor multiplied times q_{is}, as given in Equation 6.51, it would be justifiable to attempt to introduce some simplifying assumptions. For $\tau = 0$, and δ ranging from .1 to .3, the right hand term in the denominator may be

evaluated,

$$.79 < \left[1 - 8\left(\frac{1+r^2}{2}\right)\right] < .93$$

An average value would be .86. Furthermore, if it is assumed that b_a/D_2 is small compared with π, J, sin β_2/Z, allowing b_a/D_2 to be set to zero in the denominator, Equation 6.53 becomes

$$N_{ic} = 1 + \frac{16 \frac{b_a}{D_2} \sin\beta_2}{.86} \qquad \text{Eq. 6.54}$$

If $b_a/D_2 = .0215$ and $\beta_2 = 90^c$,

$$N_{ic} = 1.4 \qquad \text{Eq. 6.55}$$

Applying this factor to Equation 6.51 yields,

$$q_{isc} = N_{ic}\ q_{is} = 1.4\ q_{is}, \qquad \text{Eq. 6.56}$$

thus evaluating the flow losses in the impeller.

c. Diffusion Losses - As the fluid traverses the impeller passageways, a change in relative velocity may occur. If the relative velocity is reduced,

diffusion losses will occur which reduce the output head of the pump. This loss in head is given by

$$H_{id} = N_{id} \frac{W_1^2 - W_2^2}{2g} \qquad \text{Eq. 6.57}$$

From the velocity triangles of Figure 9,

$$W_1^2 = C_{m1}^2 + \delta^2 U_2^2 \qquad \text{Eq. 6.58}$$

$$W_2^2 = \frac{K_1^2 C_{m1}^2}{\sin^2 \beta_2} \qquad \text{Eq. 6.59}$$

Substituting Equations 6.53 and 6.54 into 6.52, gives the diffusion head loss in the impeller as

$$H_{id} = \frac{N_{id} \left(C_{m1}^2 + \delta^2 U_2^2 - \frac{K_1^2 C_{m1}^2}{\sin^2 \beta_2} \right)}{2g} \qquad \text{Eq. 6.60}$$

Dividing by the reference head results in the impeller diffusion head loss coefficient

$$q_{id} = \frac{N_{id}}{2} \left[\phi^2 \left(1 - \frac{K_1^2}{\sin^2 \beta_2} \right) + \delta^2 \right] \qquad \text{Eq. 6.61}$$

Negative values of this loss are, of course, impossible and must be excluded.

$$N_{Id} \approx 0.4$$

The head loss coefficient for the impeller is the sum of the head loss coefficients given in Equations 6.56 and 6.61.

$$q_{II} = 1.4\, q_{Is} + q_{Id} \qquad \text{Eq. 6.62}$$

where q_{Is} is given by Equation 6.51. The literature does not contain much with which to substantiate this evaluation of the losses in the impeller. However, when it is compared with similar evaluations by other investigators, this evaluation of the impeller loss is found to be of the same order of magnitude and to demonstrate the same qualitative tendancies, and is discussed further in Section 5.2.2 of the report.

6.1.3 Annular Diffuser Loss Coefficient

In the annular diffuser portion of the pump, it is assumed that the flow losses are also represented by a

function similar to the Darcy equation, so that the flow loss is given by

$$H_{ad} = \frac{f L_{ad}}{D_{ad}^*} \frac{C_{ad}}{2g} \qquad \text{Eq. 6.63}$$

where C_{ad} is the absolute velocity in the annular diffuser, L_{ad} is the length of the flow path, D_{ad}^* is the hydraulic diameter of the annular diffuser and f is a friction factor.

It can be shown by potential flow theory and by experimental studies that the streamlines in the annular diffuser follow approximately a logarithmic spiral path, assuming the sides of the diffuser are parallel. Thus, a logarithmic spiral path will be assumed for this study, and the length of the flow path L_{ad} is given by

$$L_{ad} = \frac{D_x - D}{2 \sin \alpha_2} = \frac{D(\lambda - 1)}{2 \sin \alpha_2} \qquad \text{Eq. 6.64}$$

It is possible to evaluate $\sin \alpha_2$ in terms of β_2 and ϕ. Referring to the outlet velocity triangle in

Figure 9,

$$C_2^2 = \left[K_1^2 C_{m1}^2 + \frac{1}{m_2} \left(U_2 - \frac{K_1 C_{m1}}{\tan\beta_2} \right)^2 \right] \qquad \text{Eq. 6.65}$$

$$= K_1^2 C_{m1}^2 \left[1 + \frac{1}{m^2} \left(\frac{1}{\phi K_1} - \frac{1}{\tan\beta_2} \right)^2 \right]$$

and

$$\sin\alpha_2 = \frac{C_{m2}}{C_2} = \frac{K_1 \; C_{m1}}{\left[K_1^2 C_{m1}^2 + \frac{1}{m^2} \left(U_2 - \frac{K_1 C_{m1}}{\tan\beta_2} \right)^2 \right]^{1/2}} \qquad \text{Eq. 6.66}$$

$$= \frac{1}{\left[1 + \frac{1}{m^2} \left(\frac{1}{\phi K_1} - \frac{1}{\tan\beta_2} \right)^2 \right]^{1/2}}$$

The mean velocity in the annular diffuser may be obtained by integration in the same fashion as for the mean relative velocity in the impeller as given by Equation 6.36, whereupon C_{ad}^2 is found to be

$$C_{ad}^2 \quad C_2^2 \left(\frac{1}{\lambda 2} + \frac{1}{\lambda} + 1 \right) \qquad \text{Eq. 6.67}$$

The hydraulic diameter of the annular diffuser is equal to four times the cross-sectional area divided by the

wetted perimeter. Evaluated at the midpoint, the hydraulic diameter is,

$$D_{ad}^{*} = \frac{4\left[\frac{\pi (D_2 + D_3) b_2}{2}\right]}{2\left[\frac{\pi (D_2 + D_3)}{2}\right]} = 2 b_2 \qquad \text{Eq. 6.68}$$

From conditions of flow continuity, and neglecting the effect of blade thickness, b_2 may be evaluated as

$$b_2 = \frac{d^2}{4 K_1 D_2} = \frac{D_2 \delta^2}{4 K_1} \qquad \text{Eq. 6.69}$$

Assuming again the relationship suggested by Blasius, the friction factor may be defined as,

$$f = \frac{.316}{Re_{ad}^{1/4}} \qquad \text{Eq. 6.70}$$

In order to evaluate Re_{ad} for the annular diffuser, it is found that using b_2 as the characteristic dimension furnishes a reasonably good match with experimental data. Hence, Re_{ad} may be defined as,

$$Re_{ad} = \frac{\rho b_2 C_{ad}}{\mu} \qquad \text{Eq. 6.71}$$

Solving Equations 4.9 and 6.71 for μ and equating,

$$\frac{b_2 C_{ad}}{Re_{ad}} = \frac{U_2 D_2}{R_e^*}$$

Rearranging,

$$Re_{ad} = \frac{b_2 C_{ad} R_e^*}{U_2 D_2}$$

Introducing Equations 6.64 through 6.72 into 6.63, and dividing by the reference head U_2^2/g, a head loss coefficient for the annular diffuser is obtained.

$$q_{ad} = \frac{.0854\ \phi^{1.75}(\lambda-1)\left[1+\frac{1}{m^2}\left(\frac{1}{\phi K_i}-\frac{1}{\tan\beta_2}\right)^2\right]^{1.375}\left(\frac{1}{\lambda^2}+\frac{1}{\lambda}+1\right)^{.875} K_i^3}{R_e^{*1/4}\ \delta^{2.5}} \qquad \text{Eq. 6.73}$$

In order to account for the fact that the flow through the annular diffuser is less than that through the impeller by an amount equal to the ring leakage, the flow factor must be adjusted by a factor

$$\left(1-\frac{q_{rl}}{q_{th}}\right)$$

Thus, the head loss coefficient for the annular diffuser is given by,

$$q_{ad} = \frac{.0854\,\phi^{1.75}\left(1-\frac{q_{rl}}{q_{th}}\right)^{1.75}(\lambda-1)\left[1+\frac{1}{m^2}\left(\frac{1}{\phi K_1}-\frac{1}{\tan\beta_2}\right)^2\right]^{1.375}\left(\frac{1}{\lambda^2}+\frac{1}{\lambda}+1\right)^{.875}K_1^{\,2}}{R_e^{*1/4}\,\delta^{2.8}}$$

Data from the literature with which to substantiate the head loss in the annular diffuser is not readily available. However, this function is quantitatively of the same magnitude and qualitatively represents the same tendancies as described by other investigators.

6.1.4 Scroll Losses

The equation for the losses in the scroll is assumed to be of the same form as for the flow losses previously analyzed; i.e.,

$$H_{sc} = \frac{f L_{sc}}{D_{sc}^*} \frac{C_{sc}^2}{2g} \qquad \text{Eq. 6.75}$$

A generalized analysis covering all possible shapes of scroll cross-section would be very difficult to perform. The investigations reported in Reference 15 indicate that the shape of the scroll cross-section does not affect the losses in the scroll to any appreciable extent. Therefore, for simplicity, a circular scroll cross-section will be assumed. Figure 29 gives the notation used in the analysis of the scroll losses.

Scrolls for pumps have long been designed with the assumption of conservation of angular momentum across the scroll area, and this design criteria has been found to give good performance. Reference 13 performs an analysis for the outlet diameter of a circular cross-section scroll. The

volume flow at the discharge of the pump is given by

$$Q = \int_{r_x}^{R} \frac{C_{u_2} r_2}{r} b_{sc} \, dr$$

$$= C_{u_2} r_2 \, 2\pi \left(e - \sqrt{e^2 - i^2} \right) \qquad \text{Eq. 6.76}$$

Solving for i,

$$i = \frac{Q}{2\pi C_{u_2} r_2} + \left(\frac{Q r_2}{\pi C_{u_2} r_2} \right)^{1/2} \qquad \text{Eq. 6.77}$$

Since i, at the outlet, is the radius of the scroll cross-section,

$$d = 2i = \frac{Q}{\pi C_{u_2} r_2} + \left(\frac{2 Q D_2}{\pi C_{u_2} r_2} \right)^{1/2} \qquad \text{Eq. 6.78}$$

From conditions of continuity, neglecting vane blockage,

$$Q = C_{m_1} D_2^2 \delta^2 \frac{\pi}{4} (1 - \tau^2) \qquad \text{Eq. 6.79}$$

Recognizing that

$$C_{u_2} = \frac{C_{m_1} K_i}{m} \left(\frac{1}{\phi K_i} - \cot \beta_2 \right) \qquad \text{Eq. 6.80}$$

which, substituted into 6.78, yields

$$d_4 = 2D_2\left\{\frac{m(1-\tau^2)\delta^2}{4K_1\left(\frac{1}{\phi K_1}-\cot\beta_2\right)} + \left[\frac{m\lambda(1-\tau^2)\delta^2}{4K_1\left(\frac{1}{4K_1}-\cot\beta_2\right)}\right]^{1/2}\right\} \quad \text{Eq. 6.81}$$

The velocity most characteristic of the performance of a straight conical diffuser is found to be at the throat or inlet area. It will be assumed that the velocity C_3 from the annular diffuser into the scroll will be the characteristic velocity for the scroll. From conditions of continuity and from Equation 6.65,

$$C_3 = \frac{C_2}{\lambda} = \frac{C_{m1}K_1}{\lambda}\left[1+\frac{1}{m^2}\left(\frac{1}{\phi K_1}-\cot\beta_2\right)^2\right]^{1/2} \quad \text{Eq. 6.82}$$

If C_3 is the characteristic velocity in the scroll, then the hydraulic diameter would be the diameter of an imaginary flow channel, not actually existing in the pump, that would pass the pump volume flow at a velocity C_3.

$$Q = \frac{\pi}{4} D_{sc}^{\ 2}\ C_3 \quad \text{Eq. 6.83}$$

Rearranging and introducing Equations 6.79 and 6.81,

$$D_{sc}^{*} = D_2 \left\{ \frac{\lambda (1-\tau^2) \beta^2}{K_1 \left[1 + \frac{1}{m^2} \left(\frac{1}{\phi K_1} - \cot\beta_2 \right)^2 \right]^{1/2}} \right\}^{1/2} \qquad \text{Eq. 6.84}$$

The length of the scroll is very nearly

$$L_{sc}' = \pi D_3 \qquad \text{Eq. 6.85}$$

Since the fluid is entering the scroll around the entire periphery of the annular diffuser, only an infinitesimal part of the flow travels this full length, and on the other hand, an equal infinitesimal part of the flow travels zero distance. Thus, it will be assumed that the whole flow travels only one-half of the total scroll length, or

$$L_{sc}'' = \frac{\pi D_3}{2} \qquad \text{Eq. 6.86}$$

The flow is known to follow a helical path in the scroll, induced by the radial velocity of the incoming fluid.

If the fluid flows in a helix of constant angle α_3, then the mean length of the flow path would be

$$L_{sc} = \frac{\pi D_s}{2 \cos \alpha_3} \qquad \text{Eq. 6.87}$$

By definition of λ and assuming $\cos \alpha_3 = .977$,

$$L_{sc} = \frac{\pi D_s \lambda}{.5550} \qquad \text{Eq. 6.88}$$

The Reynolds number for the scroll, evaluated at the fictitious D_{sc}^* is,

$$Re_{sc} = \frac{\rho C_s D_{sc}^*}{\mu} \qquad \text{Eq. 6.89}$$

Introducing the defining equation of pump Reynolds number, R_e^*, and rearranging,

$$Re_{sc} = \frac{R_e^* C_s D_{sc}^*}{U_s D_s} \qquad \text{Eq. 6.90}$$

Substituting from Equations 6.82 and 6.84,

$$Re_{sc} = R_e \phi \delta \left\{ \frac{K_1 \left[1 + \frac{1}{m^2} \left(\frac{1}{\phi K_1} - \cot \beta_2 \right)^2 \right]^{1/2} (1 - \tau^2)}{\lambda} \right\}^{1/2} \qquad \text{Eq. 6.91}$$

Experimental data from References 9 and 15 would indicate that the friction factor would be represented satisfactorily by the equation

$$f = \frac{.57}{Re_{sc}^{1/4}} \qquad \text{Eq. 6.92}$$

Introducing the appropriate expressions derived above into Equation 4.83 and dividing by the reference head U_2^2/g of [illegible]n expression for a head loss coefficient for the scroll

$$q_{sc}'' = \frac{.54 \quad .78 \quad K_1^{2.375}\left[1 + \frac{1}{m^2}\left(\frac{1}{\phi K_1} - \cot\beta_2\right)^2\right]^{1.188}}{\delta^{1.25} \quad R_e^{*1/4} \quad \lambda^{1.4375} \quad (1-\tau^2)^{.625}} \qquad \text{Eq. 6.93}$$

In order to account for the fact that the flow through the scroll is less than that through the impeller, a factor of $\left(1 - \frac{q_{rl}}{q_{th}}\right)$

must be applied to the flow factor ϕ. Hence, the corrected equation for the head loss coefficient for the scroll is,

$$q_{sc} = \frac{.546\phi^{1.75}\left(1-\frac{qrl}{qth}\right)^{1.75} K_1^{2.375}\left[1+\frac{1}{m^2}\left(\frac{1}{\phi K_1}-\cot\beta_2\right)^2\right]^{1.188}}{\delta^{1.25}\ R_e^{*1/4}\ \lambda^{1.4375}\ (1-r^2)^{.625}}$$

Eq. 6.94

6.1.5 Straight Diffuser Losses

In order to provide a uniform basis for comparison, it is assumed that the outlet velocity C_5 from the pump is equal to the meridional velocity at inlet to the impeller C_{m1}. A straight conical diffuser is assumed to diffuse the flow from C_4 to $C_5 = C_{m1}$. Considerable work has been done to obtain efficiency values for conical diffusers. The efficiency of a

straight conical diffuser is given by

$$\eta_{sd} = \frac{\frac{C_4^2 - C_5^2}{2g} - gC_4^2}{\frac{C_4^2 - C_5^2}{2g}} \qquad \text{Eq. 6.95}$$

in which

$$\xi_{sd} = \left(\frac{C_4^2}{2g}\right)$$

is equal to the head loss in the straight diffuser.

Thus, upon rearranging,

$$H_{sd} = \xi_{sd} \frac{C_4^2}{2g} = \frac{(1 - \eta_{sd})(C_4^2 - C_{m1}^2)}{2g} \qquad \text{Eq. 6.96}$$

Assuming conservation of angular momentum in the scroll permits evaluation of C_4.

$$C_4 \quad \frac{D_2 \lambda}{2} + \frac{d_4}{2} = \frac{C_2 D_2}{2} \qquad \text{Eq. 6.97}$$

Thus, rearranging,

$$C_4 = \frac{C_2 D_2}{D_2 \lambda + d_4} \qquad \text{Eq. 6.98}$$

Introducing Equations 6.81 and 6.98 into 6.96, and dividing by the reference head U_2^2/g,

$$q_{sd} = \frac{\phi^2\left[1+\frac{1}{m^2}\left(\frac{1}{\phi K_1}-\cot\beta_2\right)^2\right](1-\eta_{sd})}{2\left\{\lambda+2\left[\frac{m(1-\tau^2)\delta^2}{4K_1\left(\frac{1}{\phi K_1}-\cot\beta_2\right)}+\left[\frac{m\lambda(1-\tau^2)\delta^2}{4K_1\left(\frac{1}{\phi K_1}-\cot\beta_2\right)}\right]^{1/2}\right]^2\right\}} - \frac{\phi^2(1-\eta_{sd})}{2}$$

Eq. 6.99

In order to account for the fact that the flow through the straight diffuser is less than that through the impeller by the amount of the wear ring leakage, the flow factor must be adjusted by a factor of

$$1-\frac{q_{rl}}{q_{th}}$$

Hence, the corrected equation for the head loss

coefficient for the straight diffuser is,

$$q_{sd} = \frac{\phi^2\left(1-\eta_{sd}\right)}{2}\left(1-\frac{q_{r1}}{q_{th}}\right)^2$$

Eq. 6.100

$$\left\{\frac{K_1^2\left[1+\frac{1}{m^2}\left(\frac{1}{\phi K_1}-\cot\beta_2\right)^2\right]}{\left\{\lambda+2\left[\frac{m(1-\tau^2)\,\delta^2}{4K_1\left(\frac{1}{\phi K_1}-\cot\beta_2\right)}+\left(\frac{m\lambda(1-\tau^2)\,\delta^2}{4K_1\left[\frac{1}{\phi K_1}-\cot\beta_2\right]}\right)^{1/2}\right]\right\}^2}-1\right\}$$

The value of η_{sd} is not affected greatly by changes in area ratio, A_5/A_4 from 2 to 10 if the divergence angle is approximately 10^o, and the efficiency of a straight conical diffuser for this condition can be as high as .90 from Reference 16. This would assume fairly uniform velocity in the entrance flow, which would not normally occur in the outlet from a scroll. In order to account for velocity variation in the flow entering the straight diffuser, η_{sd} will be assumed equal to .87.

6.1.6 Wear Ring Leakage Losses

For simplicity, it will be assumed that there are two wear rings located at the impeller eye diameter $d = \delta D_2$. The leakage area would be

$$A_{rl} = \frac{\pi \delta D_2 \Lambda}{2} \qquad \text{Eq. 6.101}$$

where Λ is the ring clearance. The leakage flow past one ring is

$$Q_{rl} = C_{rl} A_{rl} \sqrt{2 g H_{rl}} \qquad \text{Ec. 6.102}$$

where C_{rl} is a leakage coefficient and H_{rl} is the head drop across the leakage path.

The head drop across the leakage path will be equal to the static head developed in the impeller, minus the impeller head loss and minus the head developed by centrifugal force in the rotating fluid outside the shroud surrounding the impeller. The theoretical head, H_{th}, and the impeller head loss, H_{il}, have already been evaluated. The head developed in the clearance around the shroud may be evaluated by assuming that the average velocity of the fluid in the shroud clearance space is

one-half the peripheral velocity of the impeller. The differential equation for the head developed over an incremental element of radius dR is,

$$dH_r = \frac{R\omega_{r1}}{2}\, dR \qquad \text{Eq. 6.103}$$

where ω_{r1} is the angular velocity of the fluid in the clearance space around the impeller. Integrating the above gives

$$H_r = \int_{d/2}^{D/2} \frac{\omega_{r1}^2}{2g}\, R dR = \frac{\omega_{r1}^2}{2g}\left(\frac{D_2^2}{4} - \frac{d^2}{4}\right) \qquad \text{Eq. 6.104}$$

Since

$$\omega_{r1} = \frac{\omega}{2} \qquad \text{Eq. 6.105}$$

where ω is the angular velocity of the impeller,

$$H_r = \frac{\omega^2}{8g}\left(\frac{D_2^2}{4} - \frac{d^2}{4}\right) = \frac{U_2^2}{8g}\left(1 - \delta^2\right) \qquad \text{Eq. 6.106}$$

If H_o is the difference in head from the impeller eye to its outside diameter, then the head across the leakage

space is

$$H_{rl} = H_o - H_r$$

$$= H - \frac{U_2^2}{8g}\left(1-\beta^2\right) \qquad \text{Eq. 6.107}$$

The head at the outside of the impeller will be

$$H_o = H_{th} - H_{ll} - \frac{C_2^2}{2g} \qquad \text{Eq. 6.108}$$

From the outlet velocity triangle of Figure 9, it can be shown that

$$C_2^2 = \frac{1}{m^2}\left(U_2^2 + W_2^2 - 2U_2W_2\cos\beta_2\right) \qquad \text{Eq. 6.109}$$

Since

$$W_2 = \frac{C_{m2}}{\sin\beta_2} = \frac{K_1\phi U_2}{\sin\beta_2} \qquad \text{Eq. 6.110}$$

then

$$\frac{C_2^2}{2g} = \frac{U_2^2}{2m^2g}\left(1 + \frac{K_1^2\phi^2}{\sin^2\beta_2} - \frac{2K_1\phi}{\tan\beta_2}\right) \qquad \text{Eq. 6.111}$$

Substituting Equation 6.111 into 6.108

$$H_o = H_{th} - H_{ll} - \frac{U_2^2}{2gm^2}\left(1 + \frac{K_1^2\phi^2}{\sin^2\beta_2} - \frac{2K_1\phi}{\tan\beta_2}\right) \qquad \text{Eq. 6.112}$$

Then,

$$H_{rl} = H_{th} - H_{ll} - \frac{U_2^2}{2gm^2}\left(1 + \frac{K_1^2\phi^2}{\sin^2\beta_2} - \frac{2K_1\phi}{\tan\beta_2}\right) - \frac{U_2^2}{8g}\left(1-\beta^2\right)$$

Eq. 6.113

The power loss due to leakage is the mass flow times the energy input

$$P_{rl} = \gamma Q_{rl} \; H_{th} \qquad \text{Eq. 6.114}$$

and the energy loss per pound of flow for one ring is

$$\frac{H_{rl}}{2} = \frac{P_{rl}}{Q\gamma} = \frac{Q_{rl} \; H_{th}}{Q} \qquad \text{Eq. 6.115}$$

The leakage coefficient may be approximated by

$$C_{rl} = \left(f \frac{K_2}{K_1} + 1.5 \right) \qquad \text{Eq. 6.116}$$

where k_1 and k_2 are defined by Equations 6.147 and 6.145 respectively.

Combining the above equations, and dividing by the reference head, U_2^2/g, the leakage loss coefficient is,

$$q_{rl} = \frac{2K_1 q_{th}}{\phi(1-\tau^2)\left(\frac{K_2}{K_1} f + 1.5\right)^{\frac{1}{2}}} \qquad \text{Eq. 6.117}$$

$$\left\{ 2\left[q_{th} - q_{ll} - \frac{1}{2m^2}\left(1 + \frac{K_1^2\phi^2}{\sin^2\beta_2} - \frac{2K_1\phi}{\tan\beta_2}\right) - \frac{1-\delta^2}{8} \right] \right\}$$

The Reynolds number of the leak path is

Eq. 6.118

$$Re_{rl} = \frac{K_1 R_e^* \delta}{\left(\frac{K_1}{K_2} f + 1.5\right)^{\frac{1}{2}}} \left[q_{th} - q_{ll} - \frac{1}{m^2}\left(1 + \frac{K_1^2\phi^2}{\sin^2\beta_2} - \frac{2K_1\phi}{\tan\beta_2} \right) - \frac{1-\delta^2}{8} \right]^{\frac{1}{2}}$$

For turbulent flow, $Re_{r1} \geq 1250$,

$$f = \frac{1}{1.8\, Re_{r1}^{.298}} \qquad \text{Eq. 6.119}$$

For laminar flow, $Re_{r1} < 1250$,

$$f = \frac{64}{Re_{r1}} \qquad \text{Eq. 6.120}$$

In the wear ring leakage tests reported in Reference 4, the test pump was a 3" pump with 4-1/8" wear rings. Diametral clearances ranged from .0129 to .039 inches. The lowest figure represents a k_1 value of .0029, which appeared to be in line with the experimental data compiled for centrifugal pumps. A "k_2" value of .166 appears to be representative of commercial practice.

6.1.7 Disc Friction Losses

Following Reference 17, the power absorbed through disc friction can be expressed by an equation of the form

$$P_{df} = \frac{C_d}{Re_{df}} \gamma \frac{U_2^3 D_2^2}{8g} (1-\beta^5) \qquad \text{Eq. 6.121}$$

Dividing by the mass flow and the reference head gives,

$$q = \frac{P_{df} g}{\gamma Q U_2^2}$$

$$= \frac{C_d (1-\delta^3)}{2\pi\phi \, Re_{df}^n \, (1-\tau^2)\delta^2} \qquad \text{Eq. 6.122}$$

Reference 17 also gives

$$Re_{df} = \frac{\rho U_2 D_2}{2\mu} \qquad \text{Eq. 6.123}$$

Thus, from the definition of R_e^*,

$$Re_{df} = \frac{1}{2} R_e^* \qquad \text{Eq. 6.124}$$

Therefore,

$$q_{df} = \frac{C_d (1-\delta^3)}{2^{1-n}\pi\phi R_e^{*n} (1-\tau^2)\delta^2} \qquad \text{Eq. 6.125}$$

Reference 17 gives $C_d = 1.300$ and $n = .50$ for laminar flow and $C_d = .0418$, and $n = .20$ for turbulent flow. The transition between laminar and turbulent flow occurs at $R_e^* = 2.2 \times 10^5$. Most centrifugal pumps will operate in the turbulent region. Letting

$$C_{df} = \frac{C_d}{2^{1-n} \pi R_e^{*n}} \qquad \text{Eq. 6.126}$$

then

$$q_{df} = \frac{C_{df} (1-\delta^3)}{\phi \delta^2 (1-\tau^2)} \qquad \text{Eq. 6.127}$$

Using the values from Reference 17 would yield a value of

$$C_{df} = 3.06 \times 10^{-4} \quad \text{for} \quad R_e^* = 10^7$$

However, the results of other investigators vary by nearly 100% above and below this value. A value of

$$C_{df} = 3.7 \times 10^{-4} \qquad \text{Eq. 6.128}$$

seems to present a good match with overall performance data.

6.1.8 Ring Friction Losses

Figure 30 shows an element of fluid between two wear rings. The outer ring is assumed to be stationary, while the inner ring rotates with an angular velocity ω. It is further assumed that inertia forces and viscosity changes in the fluid due to heating in the wear ring space are negligible. Furthermore, only those forces having a moment about the center of rotation will affect the power required to drive the pump and, hence, only those forces need to be considered. The sum of the forces acting upon the element is equal to zero for steady state conditions. The forces consist of two pressure forces and two shear forces. Thus, assuming the depth of the element perpendicular to the paper to be b_r, the sum of the forces is,

$$b_r (P+\Delta P)\Delta R \cos\left(\frac{\Delta\theta}{2}\right) - b_r P\Delta R \cos\left(\frac{\Delta\theta}{2}\right) + \nu R\Delta\theta b_r$$

Eq. 6.129

$$-(\nu+\Delta\nu)(R+\Delta R)\Delta\theta b_r = 0$$

Rearranging,

$$\cos\left(\frac{\Delta\theta}{2}\right)\frac{\Delta P}{\Delta\theta} - \left(\nu + R\,\frac{\Delta\nu}{\Delta R} - \Delta\nu\right) = 0 \qquad \text{Eq. 6.130}$$

As Δ_R and Δ_θ approach zero, Equation 6.13C approaches a limit

$$\frac{dP}{d\theta} - \left(\nu + R\,\frac{d\nu}{dR}\right) = 0 \qquad \text{Eq. 6.131}$$

Due to the symmetry of the element and the forces acting on it,

$$\frac{dP}{d\theta} = 0 \qquad \text{Eq. 6.132}$$

Thus,

$$\nu + R\,\frac{d\nu}{dR} = Q \qquad \text{Eq. 6.133}$$

Integrating

$$\ln \nu = -\ln R + \ln B_1 \qquad \text{Eq. 6.134}$$

Thus

$$\nu = \frac{B_1}{R} \qquad \text{Eq. 6.135}$$

The shear force at any point is

$$\nu = \mu \frac{du}{dR} \qquad \text{Eq. 6.136}$$

where $\frac{du}{dR}$ is the rate of change in velocity with respect to radius. Equating Equations 6.135 and 6.136 and rearranging,

$$dU = \frac{B_1}{\mu} \frac{dR}{R} \qquad \text{Eq. 6.137}$$

Integrating,

$$U = \frac{B_1}{\mu} \ln R + B_2 \qquad \text{Eq. 6.138}$$

The constants of integration B_1 and B_2 may be evaluated from the boundary conditions

$$U = \frac{\omega R_1}{\ln \frac{R_1}{R_2}} \ln \frac{R}{R_2} \qquad \text{Eq. 6.139}$$

Differentiating Equation 6.139 and evaluating at R_1,

$$\left.\frac{du}{dR}\right|_{R_1} = \frac{\omega}{\ln\left(\frac{R_1}{R_2}\right)} \qquad \text{Eq. 6.140}$$

Substituting Equation 6.140 into 6.136, the unit shear force at R_1 is,

$$\nu_{R_1} = \frac{\mu \omega}{\ln\left(\frac{R_1}{R_2}\right)} \qquad \text{Eq. 6.141}$$

The torque on the ring is

$$T_{rf} = \nu_{R_1} b_r \; 2\pi R_1^2 \qquad \text{Eq. 6.142}$$

and the power absorbed by the ring is

$$q_{rf} = T_{rf}\,\omega = \frac{\mu (R_1 \omega)^2 \, 2\pi b_r}{\ln\left(\frac{R_1}{R_2}\right)} \qquad \text{Eq. 6.143}$$

The head coefficient is

$$q_{rf} = \frac{Hg}{U_2^2} = \frac{P_{rf} g}{\gamma Q U_2^2} = \frac{8\mu b_r g}{\ln\left(\frac{R_1}{R_2}\right) \gamma d^2 U_2 \phi \, (1 - \tau^2)} \qquad \text{Eq. 6.144}$$

Letting

$$K_2 = \frac{b}{d} = \frac{b}{2R_1} \qquad \text{Eq. 6.145}$$

then

$$q_{rf} = \frac{4\mu l e_2 g}{\ln\left(\frac{R_1}{R_2}\right)\gamma R_1 U_2 \phi (1-\tau^2)} \qquad \text{Eq. 6.146}$$

If k_1 is defined by the equation

$$\frac{2\Lambda}{d} \qquad \text{Eq. 6.147}$$

then

$$\frac{R_1}{R_2} = \frac{1}{1+k_1} \qquad \text{Eq. 6.148}$$

and

$$q = \frac{2\mu l e_2 g}{\ln\left(\frac{1}{1+k_1}\right)\gamma R_1 U_2 \phi} \qquad \text{Eq. 6.149}$$

The pump Reynolds number may be introduced into Equation 1.155 from the fact that

$$\frac{\mu g}{\gamma R_1 U_2} = \frac{2\mu g}{\gamma D_2 U_2} = \frac{2}{R_e} \qquad \text{Eq. 6.150}$$

resulting in,

$$q_{rf} = \frac{8k_2}{\ln\left(\frac{1}{1+k_1}\right) R_e^* \phi \beta (1-\tau^2)} \qquad \text{Eq. 6.151}$$

Recommended values for k_1 and k_2 are discussed in Section 5.2.

6.1.9 Mixing Loss

Since the tangential and meridional velocity vectors of the flow at the exit of the impeller are not constant but vary over the width of the impeller because of the so-called slip, there exists an additional loss as the result of the mixing of these respective flow streams. Ref. 24 gives an expression for the mixing loss as,

Eq. 6.152

$$q_m = .125(1-\frac{1}{m})^2$$

6.2 Derivation of Suction Specific Speed Relationships

From the derivation of Equation 4.10 it is seen that

$$S \frac{N_s}{\left(\frac{H_{sv}}{H}\right)^{3/4}} = \frac{N_s}{\left(\frac{q_{sv}}{q_{out}}\right)^{3/4}} \qquad \text{Eq. 6.153}$$

Introducing N_s from Equation 5.25,

$$S = \frac{228.5\ \psi}{q_{sv}^{3/4}} \qquad \text{Eq. 6.154}$$

In order to evaluate q_{sv}, it is necessary to first analyze the net positive suction head at pump inlet H_{sv}. The total head at the pump inlet h_t is

$$h_t = h_a \pm h \qquad \text{Eq. 6.155}$$

where h_a is the head due to atmospheric pressure on the free surface of the liquid being pumped and h is the head due to elevation of the free surface of the liquid above or below the pump inlet, the negative sign indicating a free surface below the pump inlet.

The static head at the entrance to the impeller h_s is less than the total head at the pump inlet because of the loss of head h_f,

due to friction occurring between pump inlet and impeller entrance and because of the velocity head that exists as a result of the absolute velocity of the flow ahead of the impeller and the relative velocity of the fluid over the impeller vanes. Thus,

$$h_s = h_t - h_f - B_2 \frac{C_1^2}{2g} - B_3 \frac{W_1^2}{2g} \qquad \text{Eq. 6.156}$$

If it is assumed that cavitation inception occurs when the static head h_s equals the head due to vapor pressure h_v, then,

$$h_v = h_t - h_f - B_2 \frac{C_1^2}{2g} - B_3 \frac{W_1^2}{2g} \qquad \text{Eq. 6.157}$$

It is desired to relate the cavitation characteristics to conditions at the pump inlet and to eliminate the characteristics of the fluid from consideration. Thus, the net positive suction head, H_{sv}, available at the pump inlet is the total head minus the head due to vapor pressure, since this latter is not available to suppress cavitation and is a characteristic of the fluid, not the pump

$$H_{sv} = h_t - h_v \qquad \text{Eq. 6.158}$$

Solving Equation 6.158 for h_t, and substituting this into Equation 6.157,

$$H_{sv} = h_f - B_2 \frac{C_1^2}{2g} - B_3 \frac{W_1^2}{2g} \qquad \text{Eq. 6.159}$$

Using the Darcy and Blasius relationships, the friction head loss may be evaluated as,

$$h_f = B_1 \frac{(C_{m1}^2 + C_{u1}^2)}{2g} \qquad \text{Eq. 6.160}$$

Introducing this and equivalent expression for C, and W, into Equation 6.159,

$$H_{sv} = B_1 \frac{(C_{m1}^2 + C_{u1}^2)}{2g} + B_2 \frac{(C_{m1}^2 + C_{u1}^2)}{2g} + B_3 \frac{C_{m1}^2 + (\delta U_2 - C_{u1})^2}{2g} \qquad \text{Eq. 6.161}$$

Rearranging and dividing by the reference head U_2^2/g,

$$q_{sv} = \frac{1}{2}\left[\frac{\phi^2}{\sin^2\alpha_1}(B_1 + B_2 + B_3) + B_3\delta(\delta - 2\phi\cot\alpha_1)\right] = \frac{1}{2}\left[\frac{\phi^2}{\sin^2\alpha_1} B_4 + B_3\delta(\delta - 2\phi\cot\alpha_1)\right] \qquad \text{Eq. 6.162}$$

Substitution of this final equation into Equation 6.164 yields an expression for S. For a given value of ψ_1, S will be a maximum when q_{sv} is a minimum; q_{sv} will be a minimum when the general equation

$$\frac{\partial q_{sv}}{\partial \chi_1} + \lambda \frac{\partial \psi}{\partial \chi_1} = 0 \qquad \text{Eq. 6.163}$$

is satisfied. Partial differentiation with respect to δ, ϕ, and cot α, yields respectively,

$$B_3 (\delta - \phi \cot\alpha_1) + \lambda \phi^{1/2} = 0$$

$$\phi B_4 (1 + \cot^2\alpha_1) - B_3 \delta \cot\alpha_1 + \lambda \frac{1}{2} \frac{\delta}{\phi^{1/2}} = 0 \qquad \text{Eq. 6.164}$$

$$\phi^2 B_4 \cot\alpha_1 - B_3 \delta\phi = 0$$

In order to obtain a simultaneous solution, an additional equation is necessary. From Equation 5.27, assuming τ to be zero,

$$\psi = \delta \phi^{1/2} \qquad \text{Eq. 6.165}$$

provides the necessary restriction.

Solution of these four equations yields

$$\phi = \left[\frac{\psi^2}{2}\ \frac{B_3}{B_4}\left(1-\frac{B_3}{B_4}\right)\right]^{1/3} \qquad \text{Eq. 6.166}$$

$$\delta = \frac{\psi}{\phi^{1/2}} \qquad \text{Eq. 6.167}$$

$$\cot\alpha = \frac{B_3}{B_4}\ \frac{\psi}{\phi^{3/2}} \qquad \text{Eq. 6.168}$$

References 8 and 19 infer that accurate values of the empirical coefficients are not available at present, and it is possible that these are not constant over the entire N_s, D_s range. However, other authors do give values which yield results that are reasonably in line with test data from literature. Reference 20 gives

$$K_1 = B_1 + B_2 = 1.4 \qquad \text{Eq. 6.169}$$

and

$$K_2 = B_3 \quad B_3 = .085 \qquad \text{Eq. 6.170}$$

and gives for safe operating limits

$$B_1 + B_2 = 1.8 \qquad \text{Eq. 6.171}$$

and

$$B_2 = .23 \qquad \text{Eq. 6.172}$$

However, this is for complete breakdown, not for cavitation inception. The only other source giving values for these coefficients is Wislicenus (Reference 7), who confines B_3 from .1 to .4. References 18 and 21 indicate that some tension is supported in a fluid, so that vapor pressure alone does not completely define cavitation inception. Thus, a value of $B_1 + B_2 = 1.1$ was selected in Reference 18 and is used in this study. The same reference indicates that $B_3 = .3$ would be reasonable from purely analytical considerations, but this is too high for an empirically determined coefficient. Therefore, $B_3 = .2$ has been selected as the value of the coefficient.

In addition to attaining configurations which will yield the maximum suction specific speed, it is desirable also to calculate the suction specific speed for the maximum efficiency optimization previously run. It was also assumed that $\alpha_1 = 90^o$

at the best efficiency point if no preswirl guide vanes are provided. Introducing this value into Equation 6.162

$$q_{sv} = \frac{1}{2}(\phi^2 B_4 + \delta^2 B_5)$$

$$= \frac{1}{2}(1.1\phi^2 + .2\delta^2) \qquad \text{Eq. 6.173}$$

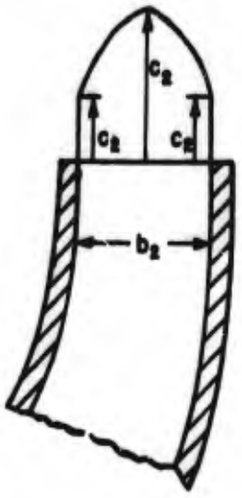

FIGURE 19 - SINUSOIDAL VELOCITY AT IMPELLER EXIT

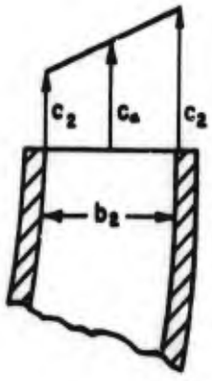

FIGURE 20- LINEAR VELOCITY AT IMPELLER EXIT

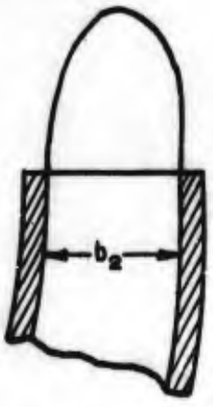

FIGURE 21. LINEAR PLUS A SINUSOIDAL ABSOLUTE VELOCITY AT IMPELLER EXIT.

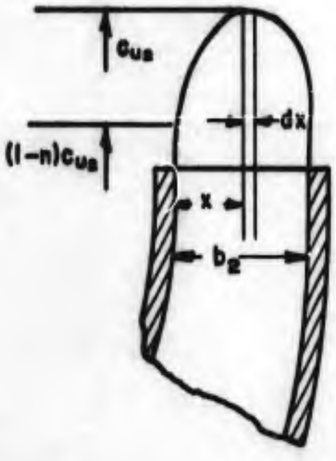

FIGURE 22. ELEMENT OF FLOW FROM THE IMPELLER

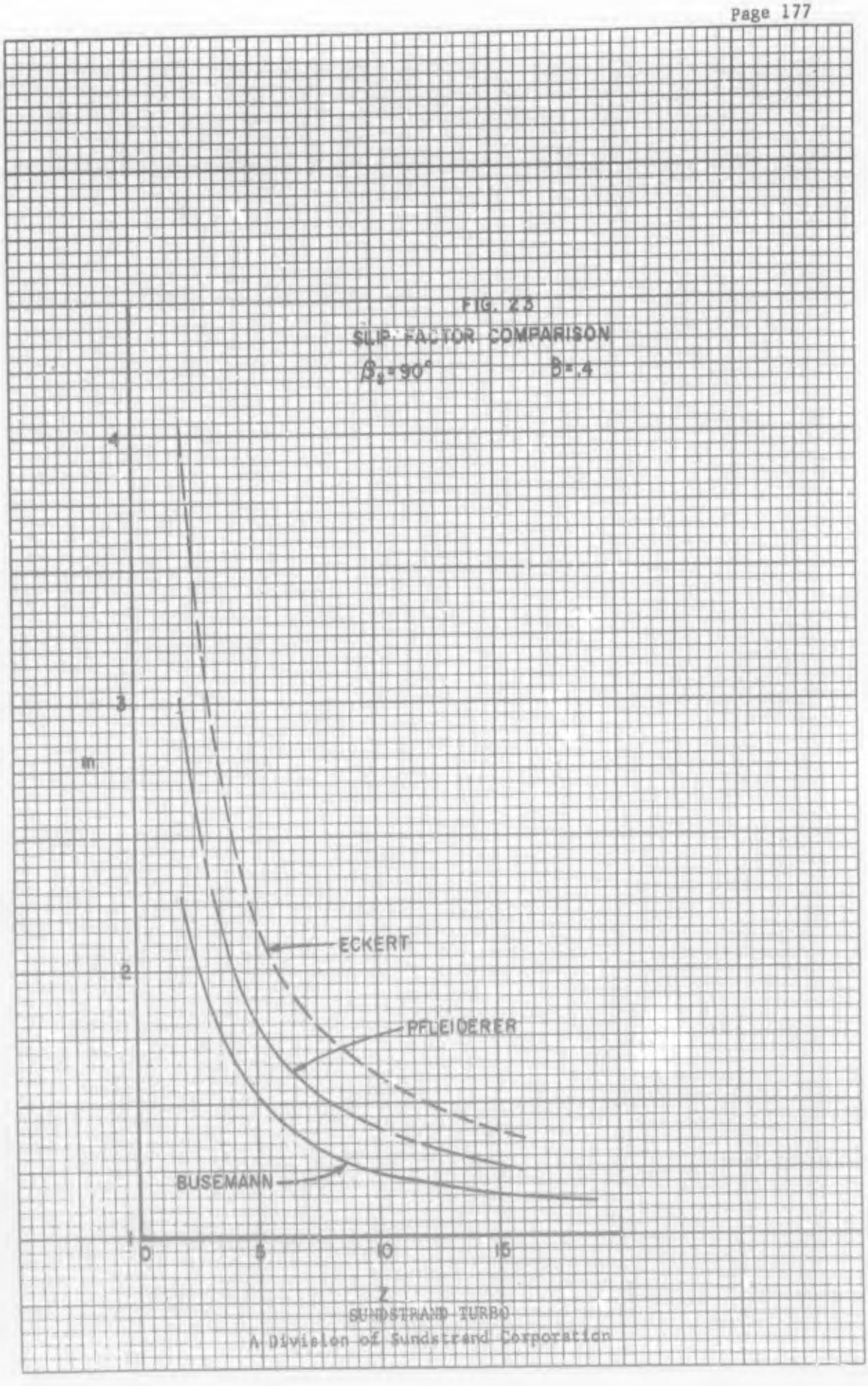
FIG. 23
SLIP FACTOR COMPARISON
$\beta_2 = 90°$ B=.4
4
3
m
2
1
ECKERT
PFLEIDERER
BUSEMANN
0
5
10
15
Z
SUNDSTRAND TURBO
A Division of Sundstrand Corporation

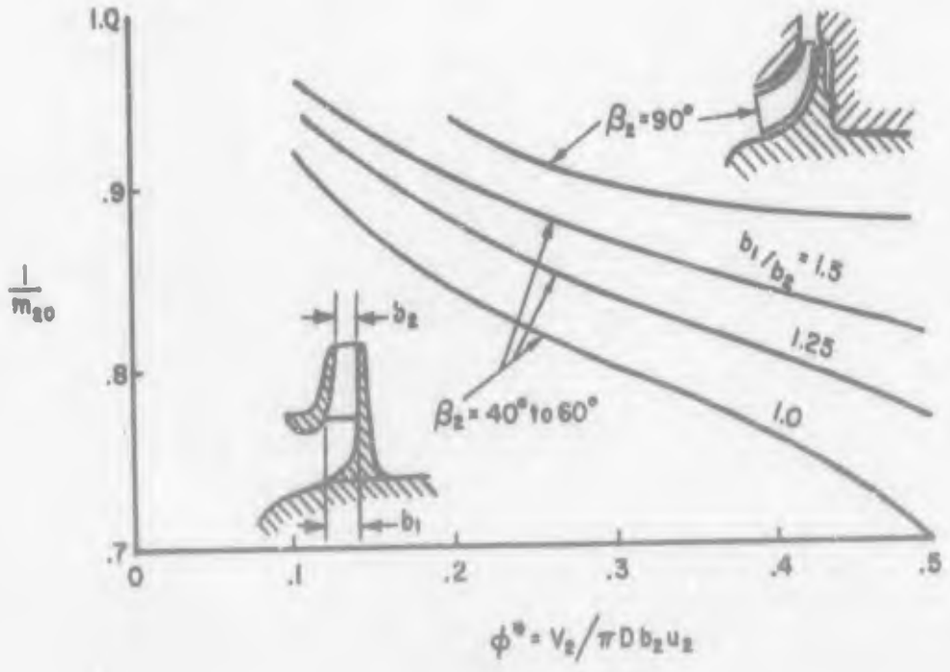

FIGURE 24 — SLIP FACTOR AS A FUNCTION OF ϕ

FIGURE 25

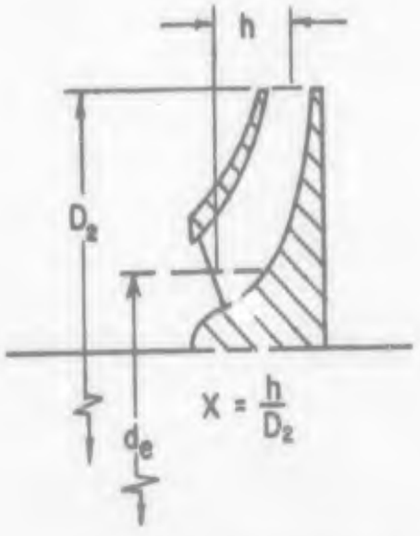

GEOMETRIC PARAMETER "X" OF THE IMPELLER

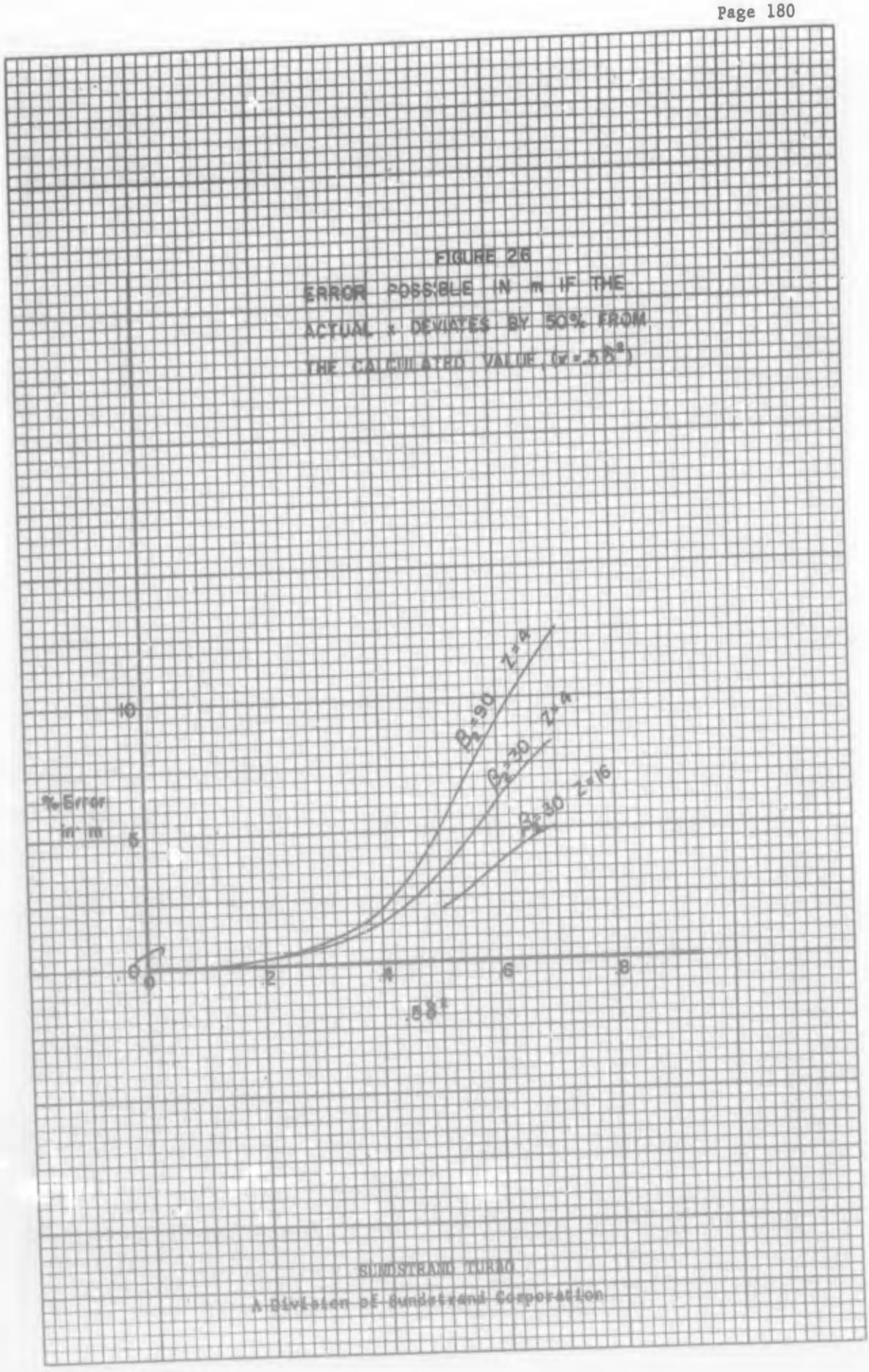
FIGURE 2.6
ERROR POSSIBLE IN m IF THE
ACTUAL s DEVIATES BY 50% FROM
THE CALCULATED VALUE (V = .5δ²)
% Error
in m
10
5
0
0
.2
.4
.6
.8
.8δ²
β=3.0
Z=4
β=2.0
Z=4
β=3.0
Z=16

FIGURE 27
THE ACTUAL FUNCTION AND THE LINEARIZED FUNCTION OF δ IN THE SLIP EQUATION

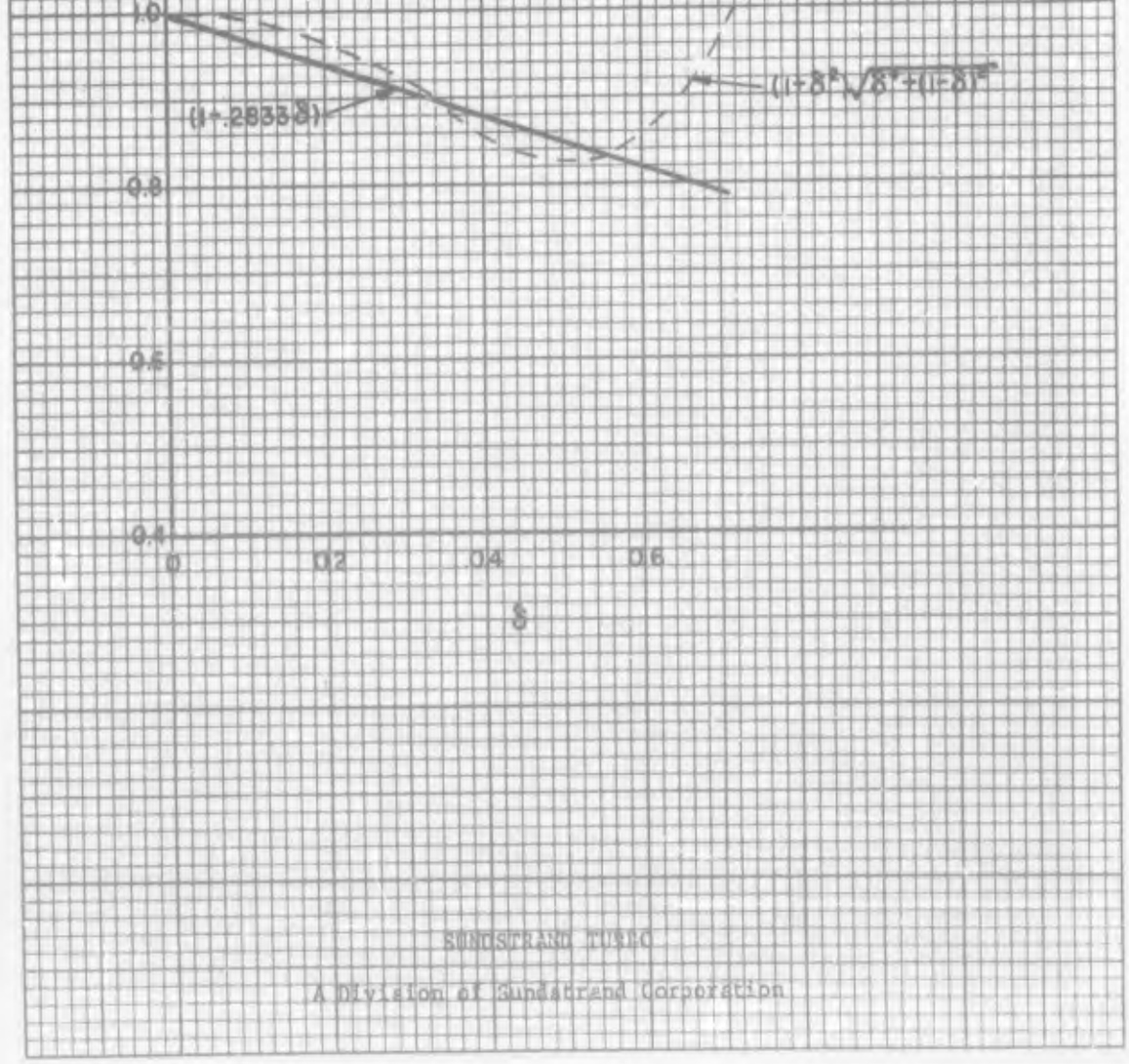

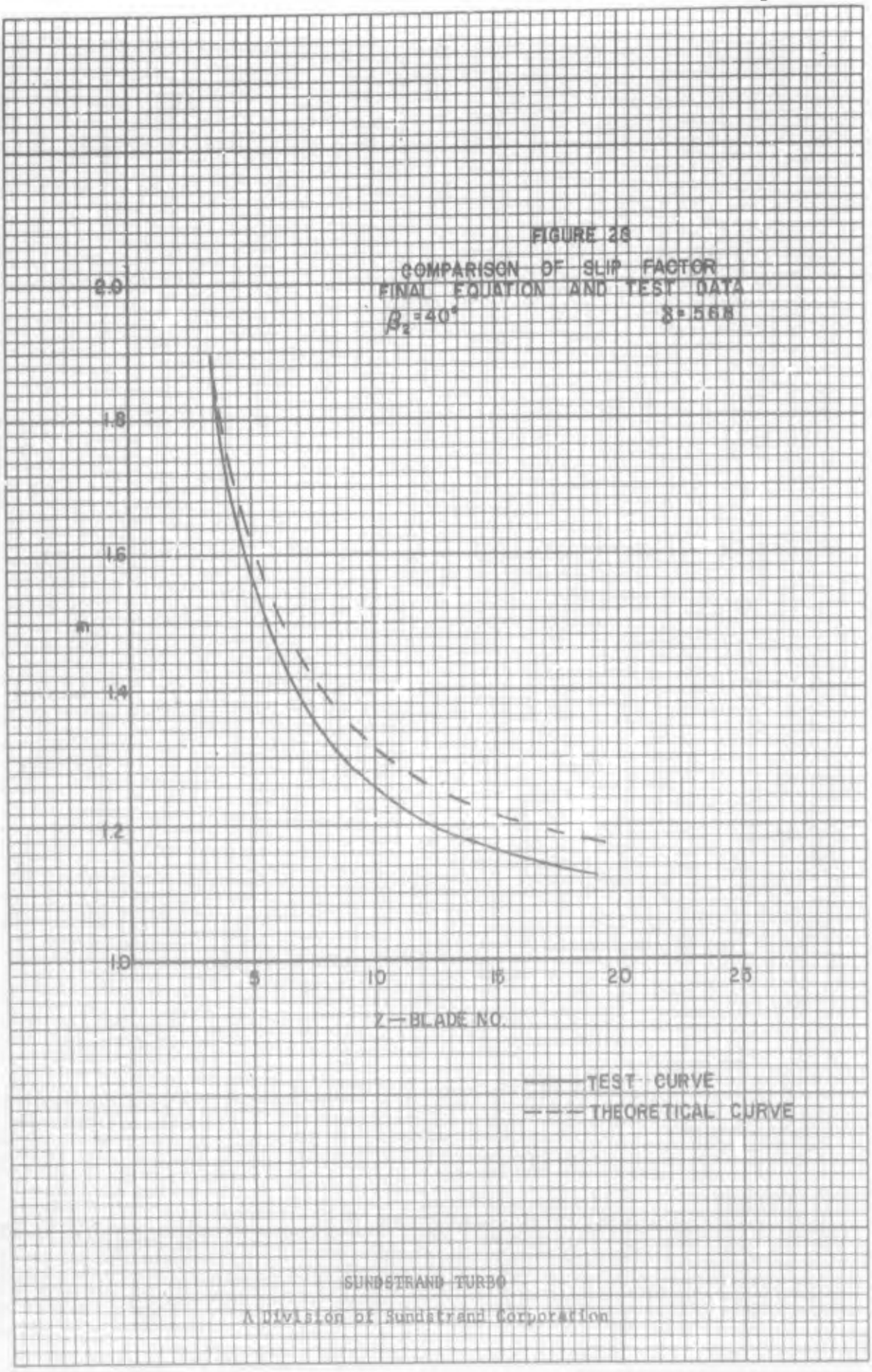
FIGURE 26
COMPARISON OF SLIP FACTOR
FINAL EQUATION AND TEST DATA
$\beta_2 = 40°$
$\delta = .566$
2.0
1.8
1.6
1.4
1.2
1.0
σ
5
10
15
20
25
Z — BLADE NO.
——— TEST CURVE
– – – THEORETICAL CURVE

FIGURE 29
NOTATION OF THE SCROLL

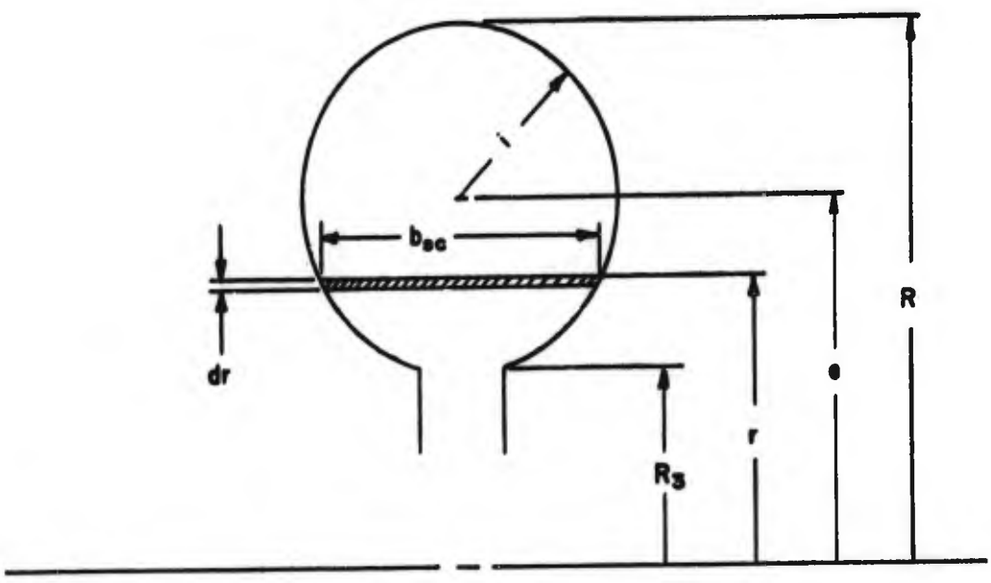

FIGURE 30
ELEMENT OF FLUID BETWEEN WEAR RINGS

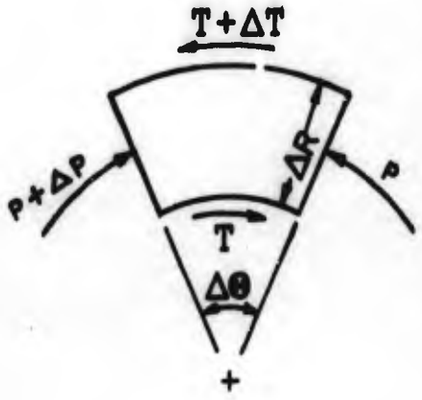

7. PRELIMINARY ANALYSIS ON PERFORMANCE CRITERIA OF PITOT PUMP

7.1 Description of Pitot Pump

Pitot pumps are known under various other names such as "skim pump", "spoon pump" or "scoop pump". The pitot pump analyzed in this report will be described and the major factors that distinguish this pump type from the more conventional centrifugal pump will be discussed. A pitot pump is shown schematically in Figure 31, and consists essentially of a pressure vessel or hollow impeller with internal vanes that tend to cause the fluid to rotate with the impeller. If it is assumed for the moment that the fluid rotates with the impeller as a solid body forming a forced vortex and that the inner diameter is very small, then the total pressure at any point will be equally divided between static pressure and velocity pressure. If now, a pitot probe is inserted inside the impeller, this high pressure fluid can be extracted from the pump. At shut-off conditions, the output pressure will be very nearly equal to the total head imparted to the fluid since the pitot pick-up will see the static pressure plus a high percentage of the

velocity pressure. As flow through the pump is increased the output pressure will fall off due to flow losses as the pitot tube conducts the fluid from the pump.

It should be noted that with this pump configuration the disc friction between the fluid pumped and the impeller housing (as occurs in conventional centrifugal pumps) is practically non-existent since the fluid is rotating with the housing. However, a new loss, probe drag, is introduced.

7.2 Theoretical Analysis.

By applying some fundamental relationships, it appears possible to obtain a preliminary estimate of the performance criteria for this type of pump. It has to be emphasized that an exact analysis of the flow mechanism taking place in the pitot pump is comparatively difficult. Some of the phenomena can only be estimated in a very approximate fashion. The prime emphasis of this analysis is directed toward the recognition of the essential design parameters and to the recognition of predominant trends. No exact numerical values should be expected from this analysis.

Figure 31 shows a schematic cross section through the essential parts of pitot pumps. The following notations are used:

D - the diameter at which the pitot pick-up is located

d - the inlet diameter of the housing

δ - the diameter of the pitot pick-up

Δ - the diameter of the pitot body

B - the axial extension of the rotating drum

b - The axial extension of the radial vanes

a - the spacing between the vanes

The governing philosophy for this analysis is (1) to determine the performance in cases that no losses have to be considered; (2) to determine the difference loss sources and appraise their approximate magnitude and tendencies, and (3) to combine all these relations in order to determine the efficiency as function of the similarity parameters, specific speed and specific diameter.

7.2.1 Theoretical Head

In order to determine the head theoretically developed, it appears admissible to use the Euler equation which

is derived by considering the change of moment of momentum of a flow entering the vanes at the diameter d, and being expelled from the vanes at the diameter D, whereby for simplicity reasons it is assumed that the pitot pick-up is located at the same diameter D (as shown in Figure 31). This relation reads

$$H = \frac{U_2 C_{u-2}}{g} \pm \frac{U_1 C_{u-1}}{g} \qquad \text{Eq. 7.1}$$

when U denotes the wheel speeds, C_u denotes the peripheral component of the flow in direction of rotation, and when subscript 1 refers to the diameter d and subscript 2 to the diameter D. Assuming, now, that no pre-swirl is present at the inlet of the pump, then the inlet peripheral component C_{u-1} becomes zero. Assuming, additionally that the vanes are strictly radial, then the exit component of the flow in direction of rotation becomes

$$C_{u-2} = \frac{U_2}{m_e} \qquad \text{Eq. 7.2}$$

when m_e denotes a slip factor which depends mainly on the number of blades Z and the diameter ratio D/d and m_e is

used to differentiate from the slip factor m, used in the analysis of centrifugal pumps. The slip can be expressed by the approximate relation

$$m_e = 1 + \frac{\pi}{2Z(1-\frac{d}{D})} \qquad \text{Eq. 7.3}$$

This is the Eckert expression discussed in Section 6.1.1. The Pfleiderer expression was chosen as most suitable for the centrifugal pump analysis, since the Eckert expression departed from experimental results at small blade angles. However, the Eckert expression shows good accuracy for straight radial vanes. Since vane angles are being restricted to 90° for the pitot pump analysis, the Eckert expression is used here because of its advantageour mathematical form. Equation 7.3 does neglect the influence of the vane width b which, for the half-open impeller type employed in Pitot pumps, must be expected to be of significant influence. This effect would be to increase the average apparent slip with decreasing b/D values. Due tc the lack of sufficient information regarding the magnitude of this influence, no b/D correction is introduced into Equation 7.3. Additional comments on this aspect are presented in section 7.3.2. Thus, the head theoretically developed in the pump is

$$H_{th} = \frac{U_2^2}{m_e g} \qquad \text{Eq. 7.4}$$

In order to simplify the analysis, it is advantageous to work with dimensionless coefficients. Simple and meaningful relations result when the head theoretically

developed is referred to a fictitious head which, for simplicity reasons, might be defined as

$$H_{ref} = \frac{U_2^2}{g} \qquad \text{Eq. 7.5}$$

The ratio of these two heads may be denoted the theoretical head coefficient which is defined as

$$q_{th} = \frac{H_{th}}{H_{ref}} \qquad \text{Eq. 7.6}$$

Introducing equation 7.4 into equation 7.6, the relation for the theoretical head coefficient becomes

$$q_{th} = \frac{1}{m_e} \qquad \text{Eq. 7.7}$$

when no preswirl is assumed and when strictly radial blades are incorporated into the design.

7.2.2 Head Losses

Several losses have to be considered. Different viewpoints can be taken as to the analysis of these losses. As a first approximation, the following considerations are presented.

The flow going through the vanes suffers a certain loss due to wall friction. Following the reasoning used for the centrifugal pump analysis, it is to be expected that this loss is proportional to the square of the radial velocity C_m, proportional to the channel lengths L, and inversely proportional to the hydraulic diameter d* of the channel. Hence, the basic equation for this loss reads

$$H_l = \left(\frac{C_m^2}{2g}\right)\left(\frac{L}{d^*}\right)\xi_l \qquad \text{Eq. 7.8}$$

when ξ_l denotes a loss factor which depends only on the Reynolds number. In order to account for the fact that the channels have a rectangular cross section rather than a round cross section, the hydraulic diameter will have to be defined as the ratio of cross section F to wetted perimeter p; i.e.,

$$d^* = \frac{F}{p} \qquad \text{Eq. 7.9}$$

Considering, now, that the channel geometry is defined by the diameter ratio and the number of blades, an approximate relation for this loss can be presented in the form

$$H_l = \xi_l \frac{C_m}{2g}\left(\frac{1-\frac{d}{D}}{2}\right)\left(\frac{D}{b}+\frac{Z}{\pi}\right) \qquad \text{Eq. 7.10}$$

The head H_p available at the inlet of the pitot pick-up is

$$H_p = H_{th} - H_l \qquad \text{Eq. 7.11}$$

This head denotes the total energy which has been imparted on the flow after entering the impeller and, consequently, denotes the rise in total pressure available at the pitot pick-up. Not all of the pressure at the pitot pick-up is available as static pressure rise across the pump. As a result of the velocity of the fluid in the pitot probe, the total pressure will contain a velocity head term, a substantial portion of which will be lost due to the poor diffusion characteristics possible in the pitot pick-up. This kinetic or velocity head loss is denoted by

$$H_k = \xi_k \frac{C^2}{2g} \qquad \text{Eq. 7.12}$$

where ξ_k denotes a loss coefficient.

There is a further head loss in the system resulting from the losses suffered within the ducting from the

pitot pick-up to the pump outlet. Since these losses are caused by wall friction, an equation in the form

$$H_D = \xi_D \frac{C^2}{2g} \qquad \text{Eq. 7.13}$$

can be used for calculating these losses when ξ_D denotes a loss coefficient. Hence, the static head H_{out} that is equivalent to the static pressure rise across the pump can be expressed by the relation

$$H_{out} = H_{th} - H_I - H_K - H_D \qquad \text{Eq. 7.14}$$

This equation can be simplified by introducing some dimensionless coefficients such as the head coefficient, which is defined by

$$q_{out} = \frac{H_{out}}{H_{ref}} \qquad \text{Eq. 7.15}$$

denoting the output head referred to the fictitious reference head, and by introducing a flow factor which denotes the ratio of the velocity within the pitot tube to the wheel tip speed; namely,

$$\phi = \frac{C}{U} = \frac{2C_m}{U} \qquad \text{Eq. 7.16}$$

With these notations the relation for the head coefficient reads

Eq. 7.17

$$q_{out} = \frac{1}{m_e} - \phi^2 \frac{\xi_1}{16}\left[\left(1-\frac{1}{e}\right)\left(\frac{D}{b}\ \frac{Z}{\pi}\right)\right] - \frac{y^2}{2}(\xi_K + \xi_D)$$

Other losses which have to be considered are the drag of the pitot pick-up and supporting strut on the flow, the energy losses occurring in the energy transfer from the fluid within the vanes to the fluid surrounding the probe and the wheel disc friction losses of the rotating drum caused by the difference in velocities between the walls and the surrounding gas. These three losses do not affect the pressure rise produced by the pump, but affect the power input into the pump required to generate the head.

There are several methods to account for the loss caused by the drag of the pitot pick-up. Resistance coefficients for pitot pick-ups can be found in literature, particularly Reference 23, indicating that the drag coefficient C_D depends on the body shape, attaining values of $C_D = 1.17$ for a flat disc and values of $C_D = .1$ for streamlined bodies. It is to be emphasized that these values are

valid only if it is assumed that the body is in a free stream. This assumption cannot be made for the pitot pump since the pitot body is located between the rotating vanes or slightly above them so that the distance between the vanes or walls and the pitot body becomes an influential value. It is to be expected that for close distance an interference drag exists which increases the apparent resistance of the body. Only little information on numerical values for the interference drag is found in the literature. Reference 23 deals with this aspect to some degree by presenting information on the interference drag of a pair of struts (one beside the other) indicating that the body drag coefficient about doubles when the distance between the struts is equal to the width of the strut, that the body drag quadruples when the distance is about one quarter of the strut width, and that no interference influence exists when the distance is about four times the strut widths (see Figure 32). Another interesting aspect is quoted in Reference 23 by quoting test data on the drag of a pair of struts, one behind the other, in tandem, so that the second strut operates in the wake of the first strut. The data (Figure 32) indicates that the drag coefficient of the rear strut doubles when the distance between the front of the struts is about 1.8 times

the strut length, and quadruples when the distance is about 1.2 times the strut length. No interference appears to exist when the distance is about 5 times the strut length. If this information is applied to the pitot pump, it would result that $\frac{a}{\Delta} \geq 9$ (see Figure 31 for notations) and $\frac{D}{\ell} = \frac{5}{\pi}$ in order to obtain a low body drag. It is unlikely that the numerical values are entirely valid -- it could, however, be expected that they are of the proper order of magnitude.

By using the drag concept, the resistance R , which the pitot body offers to the flow, can be expressed by the relation

$$R = \frac{U_2^2 \pi \Delta^2 \gamma C_w}{m_e^2 8 g} \qquad \text{Eq. 7.18}$$

and, therefore, the power required to overcome this resistance is

$$P = \frac{R U_2}{m_e} \quad \left[\frac{\text{ft-lb}}{\text{sec}} \right] \qquad \text{Eq. 7.19}$$

so that the corresponding head loss becomes

$$H_p = \frac{P}{w} = \frac{U_2^2 \Delta^2 C_w}{m_e^3 g \phi \delta^2 2} \qquad \text{Eq. 7.20}$$

since the weight flow W is

$$W = \phi U \frac{\pi}{4} \delta^2 \gamma \qquad \text{Eq. 7.21}$$

with ϕ denoting a flow factor defined by Equation 7.16 when c represents the velocity in the inlet of the pitot tube. The head loss can now be represented in a dimensionless form by dividing Equation 7.20 by the reference head, yielding

$$q_p = \frac{x^2 C_w}{2 m_e^3 \phi} \qquad \text{Eq. 7.22}$$

when the ratio X denotes the ratio of outer diameter to bore diameter of the pitot body; i.e.,

$$x = \frac{\Delta}{\delta} \qquad \text{Eq. 7.23}$$

If the pitot pick-up were removed from the pump and if the impeller filled with liquid were rotated as in normal

operation, the whole body of fluid within the impeller could be assumed to rotate as a forced vortex. However, with the introduction of the probe, the central ring of fluid not contained within the vanes would have a drag exerted upon it, slowing its rotation and converting some of its kinetic energy into temperature rise in the fluid. With this slower rotation, a lower static head would be developed at the periphery of the central fluid ring than is developed in the fluid ring within the vanes, which are still rotating as forced vortices, thereby inducing a circulating flow outward through the impeller vane spaces and inward through the central fluid ring. This would effect an energy exchange between the fluid issuing from the impeller and the fluid within the central ring; and, assuming steady state conditions to have been reached, the energy imparted to the central fluid ring would have to be exactly equal to the energy loss due to the pitot pick-up and strut drag. However, the energy input at the shaft required to offset the probe drag losses must be greater than the probe drag losses because of the energy losses occurring in the transmission of energy through the fluid coupling described above. Assuming that the efficiency η_B of this transmission is essentially constant,

the loss due to probe drag and energy transmission through the fluid coupling may be expressed by

$$q_b = \frac{q_p}{\eta_B} = \frac{x^2 C_w}{2 m_e^3 \phi \eta_B} \qquad \text{Eq. 7.24}$$

In addition to the drag of the pitot body, the drag of the supporting strut has to be accounted for. The resistance for the strut can again be expressed by a drag coefficient so that for the strut losses, a relation similar to Equation 7.24 results. For simplicity reasons, both losses -- pitot body drag as well as strut drag -- may be combined into one expression by using Equation 7.24 and interpreting C_w as the combined drag coefficient.

The wheel disc friction loss at the outer part of the rotating drum is comparatively easily determined by using the relation derived in Reference 13.

$$P_w = U_2^3 D(D + 5B)\, \beta_w\, \gamma_g \frac{1}{g} \qquad \text{Eq. 7.25}$$

which gives the power loss, whereby γ_g denotes the density of the gas surrounding the rotating drum. Converting this power loss again to a head loss and referring this

head loss to the reference head, a dimensionless expression for this loss results which reads

$$q_w = \frac{4(1+5\frac{\beta}{b})\beta_w}{\phi\,\pi}\left(\frac{D}{\delta}\right)^2\frac{\gamma_l}{\gamma} \qquad \text{Eq. 7.26}$$

With these relations the efficiency of the pitot pump can be expressed since the power input required is now the sum of the theoretical head, plus the head loss due to the transmission of energy to the central liquid ring plus the drag caused by the wheel disc friction. The required input head can be expressed in a dimensionless form by writing

$$q_{in} = q_{th} + q_B + q_w \qquad \text{Eq. 7.27}$$

then the efficiency relation becomes

$$\eta = \frac{q_{out}}{q_{in}} \qquad \text{Eq. 7.28}$$

Before introducing the individual quantities into Equation 7.28, it appears advisable to define some proportionality factors for the internal geometry of the pitot pump by defining, for example

$$\chi = \frac{\Delta}{\delta} \qquad \text{Eq. 7.23}$$

$$y = \frac{a}{\delta} \qquad \text{Eq. 7.29}$$

$$n = \frac{B}{\delta} \qquad \text{Eq. 7.30}$$

and

$$k = \frac{d}{\Delta} \qquad \text{Eq. 7.31}$$

when the notations of Figure 31 are used.

Introducing these relations into the individual equations, the relations for the different loss coefficients read

$$q_l = \phi^2 \frac{\xi_1}{16}\left[\left(1-\frac{k\chi}{D/\delta}\right)\left(\frac{2D/\delta}{n-y}+\frac{z}{\pi}\right)\right] \qquad \text{Eq. 7.32}$$

$$q_b = \frac{C_w \chi^2}{2 m_e^3 \phi \eta_B} \qquad \text{Eq. 7.33}$$

$$q_w = \frac{4\beta_w\left(1+\frac{5n}{D/\delta}\right)}{\phi \pi}\left(\frac{D}{\delta}\right)^2 \frac{\chi_1}{\gamma} \qquad \text{Eq. 7.34}$$

$$m_e = 1 + \frac{\pi}{2Z\left(1-\frac{kx}{D/\delta}\right)} \qquad \text{Eq. 7.35}$$

Introducing these relations into Equation 7.28 gives, as a final relation for the efficiency

$$\eta = \frac{\frac{1}{m_e} - \frac{\phi^2}{2}\left\{\frac{\xi_I}{8}\left[\left(1-\frac{kx}{D/\delta}\right)\left(\frac{2D/\delta}{n-y}+\frac{Z}{\pi}\right)\right]+\xi_k+\xi_D\right\}}{\frac{1}{m_e}+\frac{C_w x^2}{2m_e^3\phi\,\eta_B}+\frac{4\beta_w}{\phi\,\pi}\left(1+\frac{5n}{D/\delta}\right)\left(\frac{D}{\delta}\right)^2\frac{\gamma_g}{\gamma}} \qquad \text{Eq. 7.36}$$

Assuming constant values for the parameters x, y, z, n, and K, and the coefficients η_B, β_w, $\frac{\gamma_g}{\gamma}$, ξ_k, ξ_D, ξ_I, and C_w, the N_s-D_s diagram can be conveniently calculated by holding q_{out} constant through a range of $\frac{D}{\delta}$ values, calculating ϕ from the equation

$$\phi = \left[\frac{2\left(\frac{1}{m_e}-q_{out}\right)}{.125\,\xi_I\left(1-\frac{kx}{D/\delta}\right)\left(\frac{2D/\delta}{n-y}+\frac{z}{\pi}\right)+\xi_D+\xi_k}\right]^{\frac{1}{2}} \qquad \text{Eq. 7.37}$$

This is repeated for various q_{out} values. The efficiency may then be calculated using the selected values of q_{out} and $\frac{D}{\delta}$ and the calculated values of ϕ into the following equation:

$$\eta = \frac{q_{out}}{\frac{1}{m_e} + \frac{C_w \chi^2}{2 m_e^3 \phi \eta_B} + \frac{4 \beta_w}{\phi \pi}\left(1 + \frac{5n}{D/\delta}\right)\left(\frac{D}{\delta}\right)^2 \frac{\gamma_0}{\gamma}} \qquad \text{Eq. 7.38}$$

Plotting lines of constant q_{out} against η and ψ as was done for centrifugal pumps permits the reading of points of efficiency and the corresponding values of specific speed and specific diameter, which may then be plotted on the N_s-D_s diagram, as shown in Figure 33.

It is evident from Equation 7.36 that the parameter $\frac{D}{\delta}$ is of critical importance for the efficiency and that a certain optimum value for $\frac{D}{\delta}$ exists which must be expected to be a function of the specific speed. This is demonstrated in the calculated N_s-D_s diagram by showing lines of constant $\frac{D}{\delta}$ values, indicating that the optimum $\frac{D}{\delta}$ value increases with decreasing specific speeds; i.e., increasing specific diameter. This tendency is caused by the comparatively large pitot body drag which demands the smallest

possible frontal area, just large enough to pass the required volume flow through the pitot tube.

It is to be noted that Figure 33 has been calculated with assumed values for the resistance coefficients; however, an effort has been made to select realistic values. The most difficult choice was the selection of the C_w and η_B coefficients meaning that a high degree of uncertainty remains, since the flow conditions that determine C_w and η_B are not too well known. An effort was therefore made to determine the approximate magnitude of those values -- more explicitly the ratio C_w/η_B, experimentally. This is discussed in more detail in Section 7.3.

In using the calculated N_s-D_s diagram for pitot pumps presented in Figure 33, it must be recognized that the theoretical analysis for pitot pumps was performed with very little empirical data, as compared with the centrifugal pump analysis, and that the final equation for efficiency has been substantiated only with a relatively small amount of test data. Furthermore, there is no reason to assume that the pumps tested were optimum pumps, since no basis for optimization was available at the time

these pumps were designed. Therefore, the present analysis must be considered preliminary and not final.

The present preliminary analysis is, nevertheless, useful in that it presents qualitatively, if not quantitatively, the trends that can be expected in pitot pump performance. It does not appear unreasonable to assume that further development work may produce characteristics superior to those shown in Figure 33. Further, this preliminary analysis does provide an indication of future work which will permit optimization of pitot pump design.

7.3 Experimental Analysis of Pitot Pump Performance

The literature contains only very few references to the subject of pitot pumps. In particular, experimental data on pitot pumps is almost non-existent. Under a separate, company-sponsored experimental program, Sundstrand Turbo has been investigating the performance characteristics of pitot pumps. Although this experimental work was not included under the contract with the Office of Naval Research, its inclusion in this report should represent a significant contribution to the otherwise scanty literature on this subject.

7.3.1 Pitot Pump Test Vehicle

The pitot pump hardware that was used was not intended to be a variable geometry test vehicle. However, some changes in pump geometry were made which permitted the study of changes in some of the design parameters. The pitot pump is shown in an exploded view in Figure 34. Three different rotating housings or impellers were made, having different vane depths. This introduced changes in two variables simultaneously; namely, vane depth and clearance between vane and pitot probe. Although it would have been desirable to study these two variables separately, the construction of the test vehicle made this impractical. Two pitot probe configurations of substantially different design were used in combination with the three vane depths, giving six different configurations that could be studied. The two probes are shown in Figure 35.

7.3.2 Pitot Pump Tests

Each of the configurations was tested holding rotative speed constant at different values over the full flow range of the pump from shut-off to maximum flow. Output head was measured, and input head was obtained by

measuring the input driving torque. Figures 36 and 37 show the performance characterisitcs of the two probe configurations tested. These diagrams show the usual pump characteristic; i.e., decreasing output heads with increasing flow rates. The maximum efficiency of the test pumps was affected by the clearance between the vanes and the probe; however, the test data is not adequate for determining the optimum values of this parameter. This is because as the clearance between the probe and vanes was increased (in the test vehicle), thus lowering the probe drag coefficient, the vane depth had to decrease, resulting in a higher slip factor. This results in higher transmission losses; i.e., lower values of η_B.

7.3.3 Comparison of Theoretical and Experimental Results

It is now of interest to compare the test data with the analysis in an effort to determine some of the loss coefficients -- particularly, the ratio C_w/η_B. An examination of Equation 7.27 reveals that the ratio C_w/η_B

can be determined from the performance data, since q_{th} is known and q_w can be calculated from Equation 7.25. Analysis of the loss q_w reveals that the magnitude of β_w in equation 7.25 has very little influence on overall pump performance since this disc friction loss is comparatively small. By applying the Equation 7.27, q_B was calculated for the test pumps. Data from these test results were then corrected to a slip factor indicated by Equation 7.3 so that it could be compared to the theoretical analysis of probe drag coefficient. This comparison is shown in Figures 38 and 39 and indicates good agreement in the flow factor range where maximum pump efficiencies occur. This agreement further indicates that the magnitude of C_w/η_B used in calculating the N_s-D_s diagram is substantiated by the test data. The values used were

$$C_w = .50$$

$$\eta_B = .4$$

thus

$$\frac{C_w}{B} = 1.250$$

This value of C_w is considerably larger than the values indicated in Figure 32. It appears reasonable to assume

that the pump geometries tested to date are not optimum, and that smaller probe drag losses C_w/η_B values than those quoted are obtainable. Hence, the optimum spacing between probe and vane as well as the optimum vane widths are not yet established. Therefore, the calculated values of efficiency for Pitot pumps shown in Figure 33 should not be considered optimum.

Values of the coefficients ξ_r, ξ_k, and ξ_D, could be determined from the test data; however, the internal flow paths of the test probes and pumps were not considered optimum and values were established by considering more conventional flow loss factors. The values used in calculating the N_s-D_s efficiencies were:

$$\xi_r = 1.0$$

$$\xi_k = 0.50$$

$$\xi_D = 0.25$$

Figures 40 and 41 show pump efficiency versus q_{out} from the theoretical analysis and test data for two pumps with widely varying geometry. This comparison indicates that the theoretical analysis reasonably well indicates the trends found in the test vehicles. It is interesting to

note that Figure 40 and 41 show peak efficiencies at q_{out} values of .5 to .6. In contrast, the calculated N_s-D_s diagram for Pitot pumps shows η max values at q_{out} values of .5 to .4, whereby q_{out} decreases with increasing specific speeds. This difference stems from the fact that the optimum blade number, based on the theoretical analysis decreases with increasing specific speeds, thus causing q_{th} and, consequently, q_{out} to decrease with increasing N_s values; whereas, the test pumps have blade numbers which are somewhat higher than the optimum value.

7.4 Recommendations for Further Study of Pitot Pumps

Since one of the most significant and least explored losses occurring in pitot pumps is the probe drag loss, work needs to be done to establish more accurately the magnitude of this loss and how this loss is affected by changes in the geometric design parameters. This second part, how the geometric parameters influence the probe loss, is important if an accurate optimization of the design parameters is to be accomplished. Another factor affecting pump performance is the efficiency of the energy transfer between the fluid in the vanes and the inner fluid ring. Because little information is available in the literature on these subjects as applied to pitot pumps, it appears that a logical program would be to run a test vehicle in which the appropriate geometric design parameters may be varied sufficiently to provide the required factual analysis of the loss functions.

Another aspect of pitot pumps which is comparatively unexplored is the maximum obtainable suction specific speed. It is evident that cavitation is likely to occur in the wake of pitot body and strut; i.e., in a flow regime which is affected by the probe drag. Hence, the

design of the probe will affect the suction specific speed so that investigations dealing with the influence of the probe on the pump efficiency should be coupled with the investigations of the suction specific speed of pitot pumps.

FIGURE 31 — PITOT PUMP SCHEMATIC

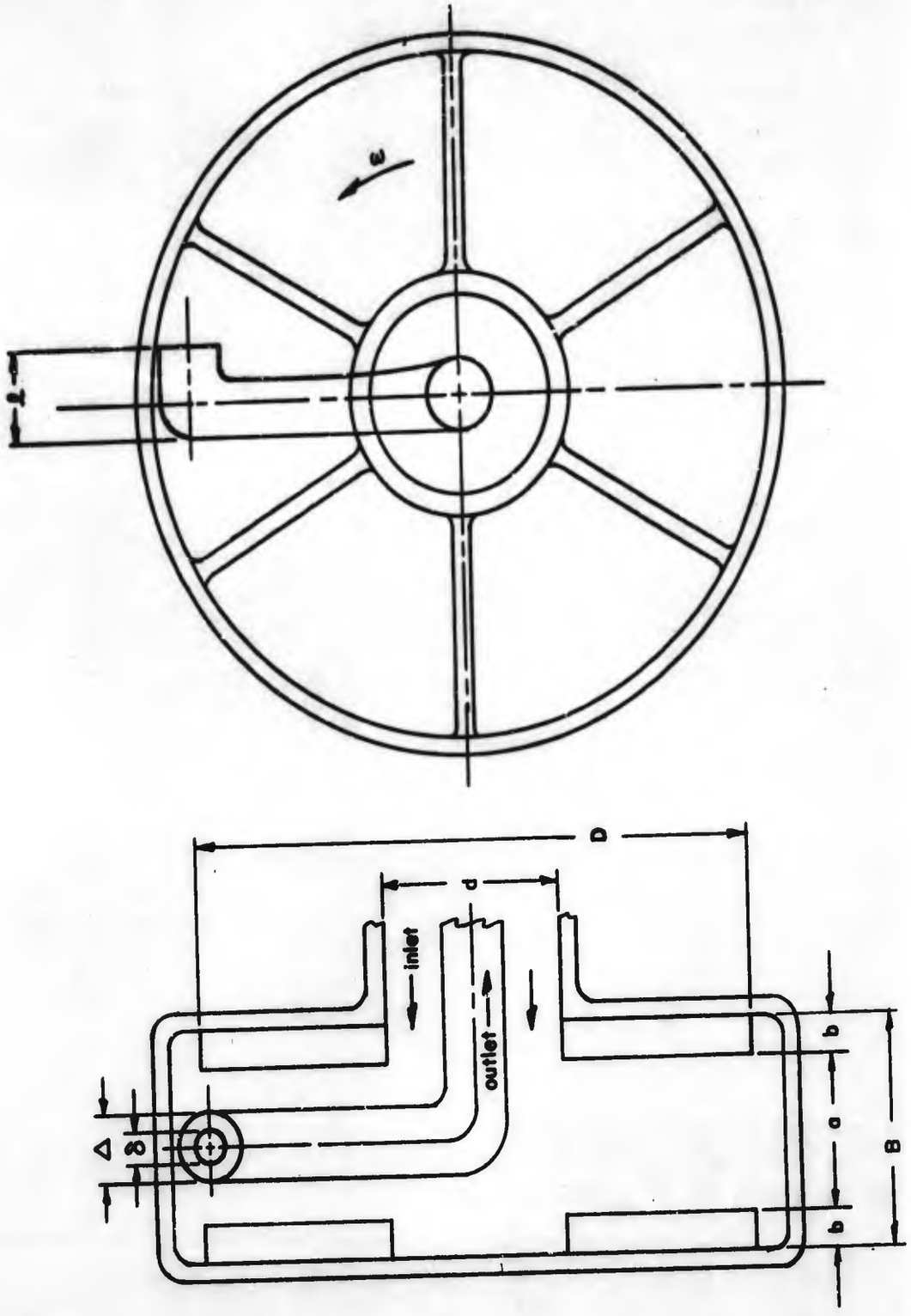

FIGURE 32a and 32b

DRAG COEFFICIENTS OF STREAMLINED STRUTS
AS A FUNCTION OF PROXIMITY (ref 23)

FIGURE 32a (C_D FOR ONE STRUT)

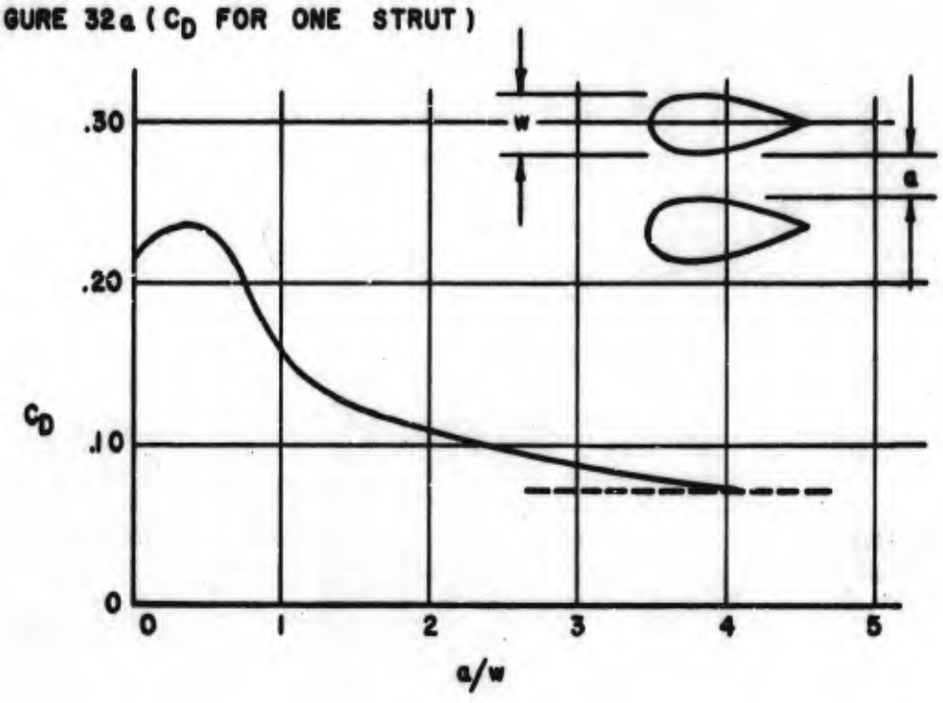

FIGURE 32b (C_D FOR REAR STRUT)

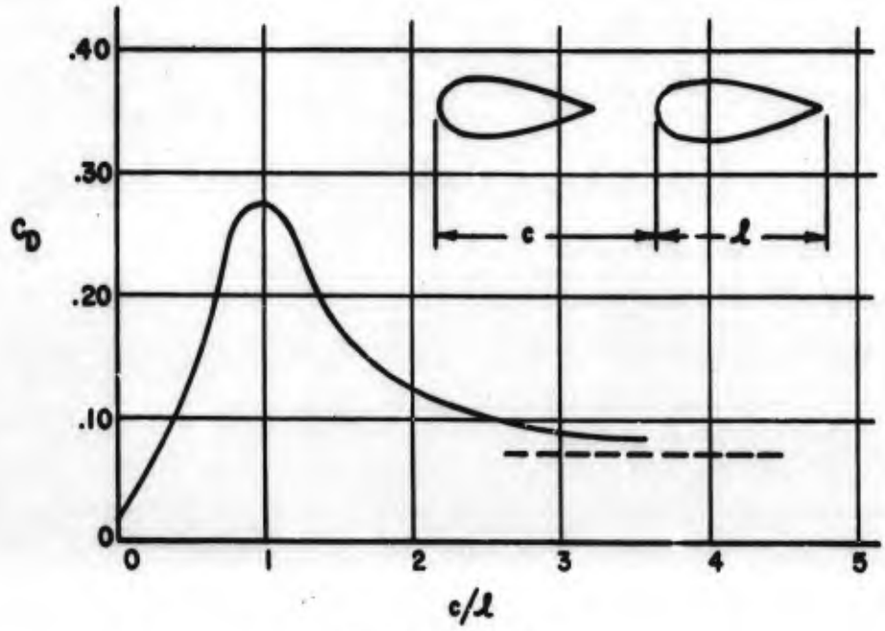

FIGURE 33
PITOT PUMP $N_s - D_s$ DIAGRAM
$R_s^* = 1 \times 10^7$

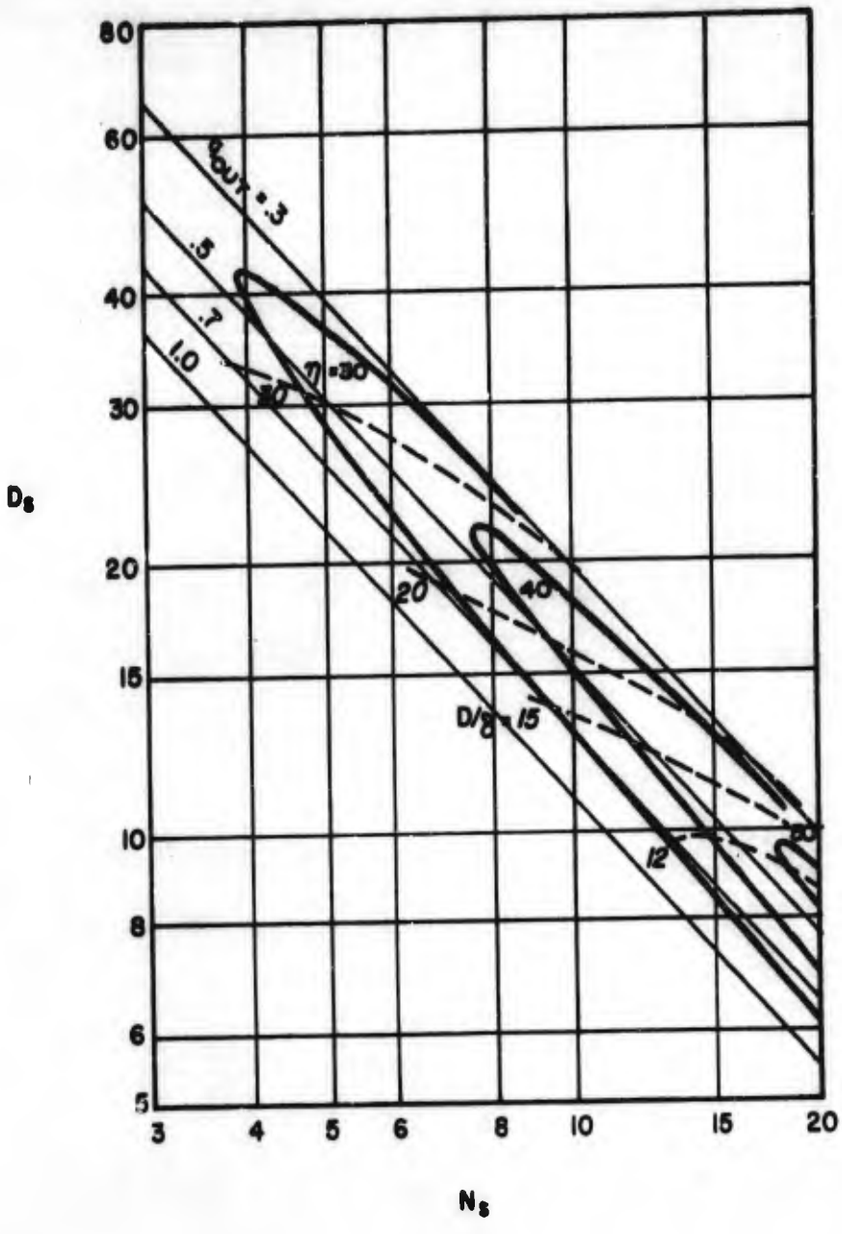

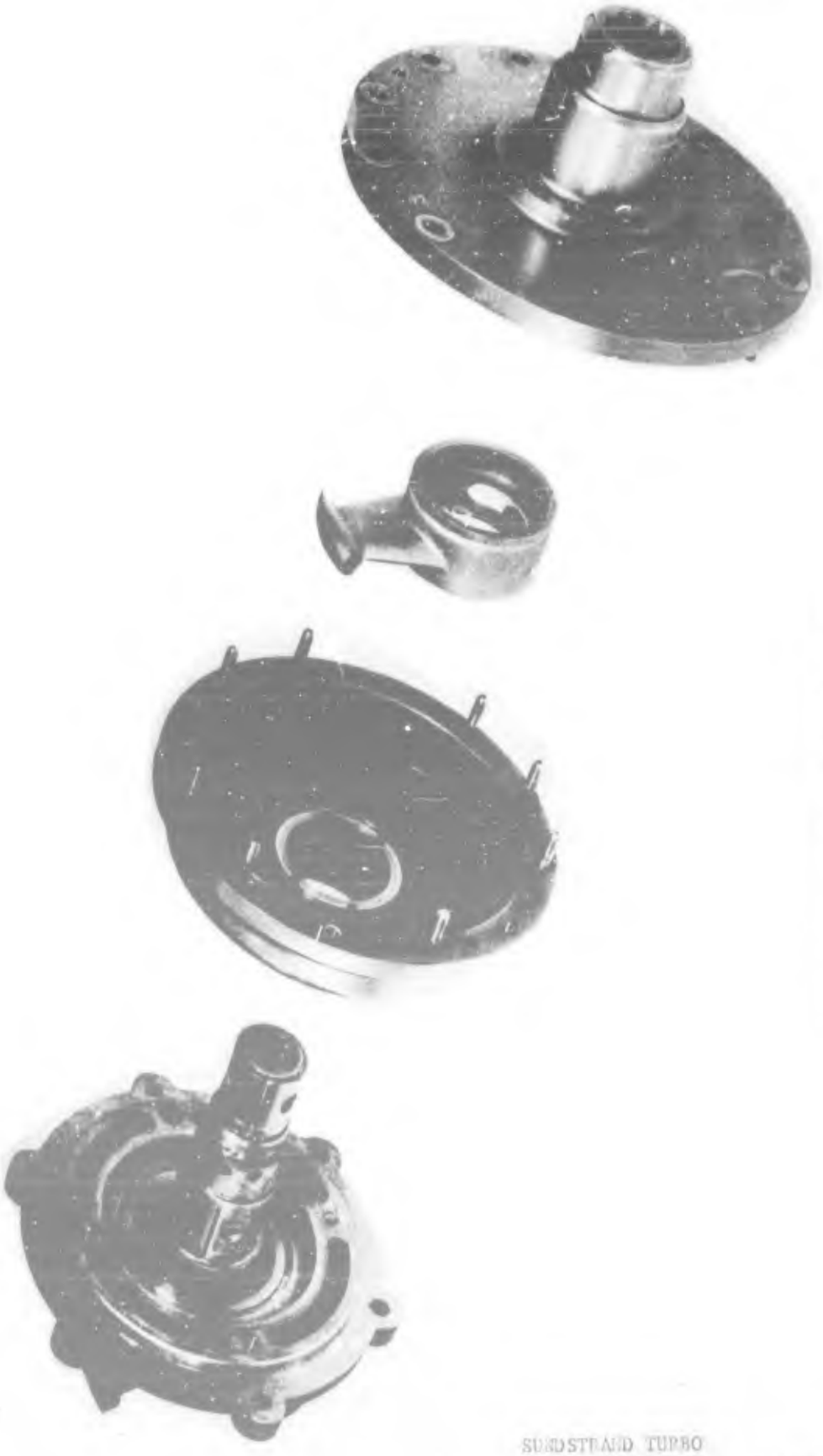

EXPLODED VIEW OF SUNDSTRAND TEST PITOT PUMP

FIGURE 35

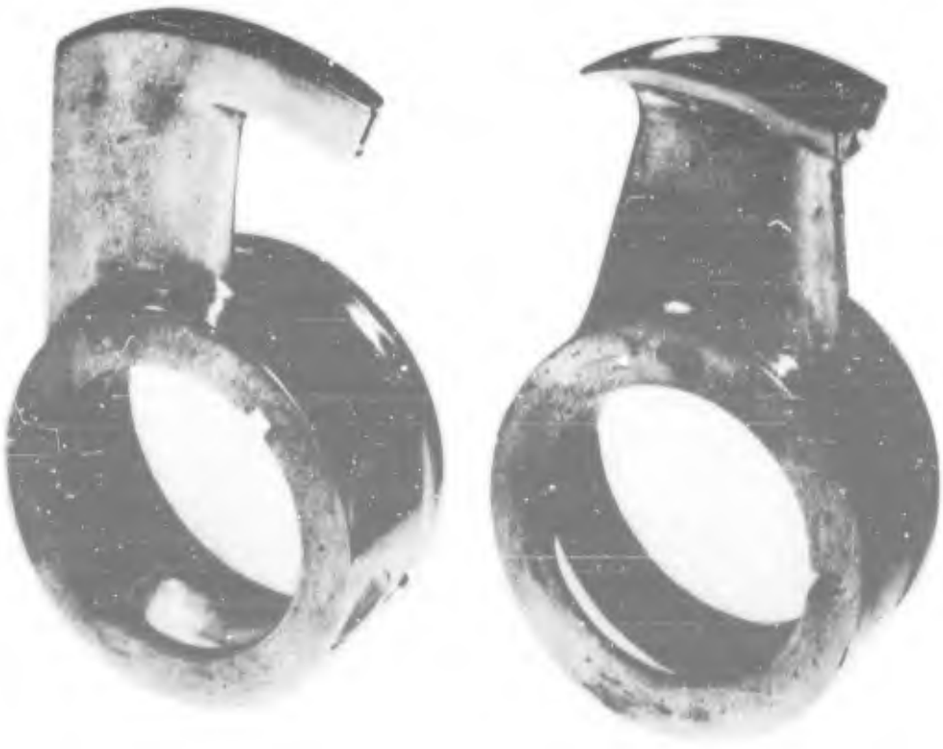

PROBE # 2

PROBE # 1

EXPERIMENTAL PROBES FROM
SUNDSTRAND TEST PITOT PUMP

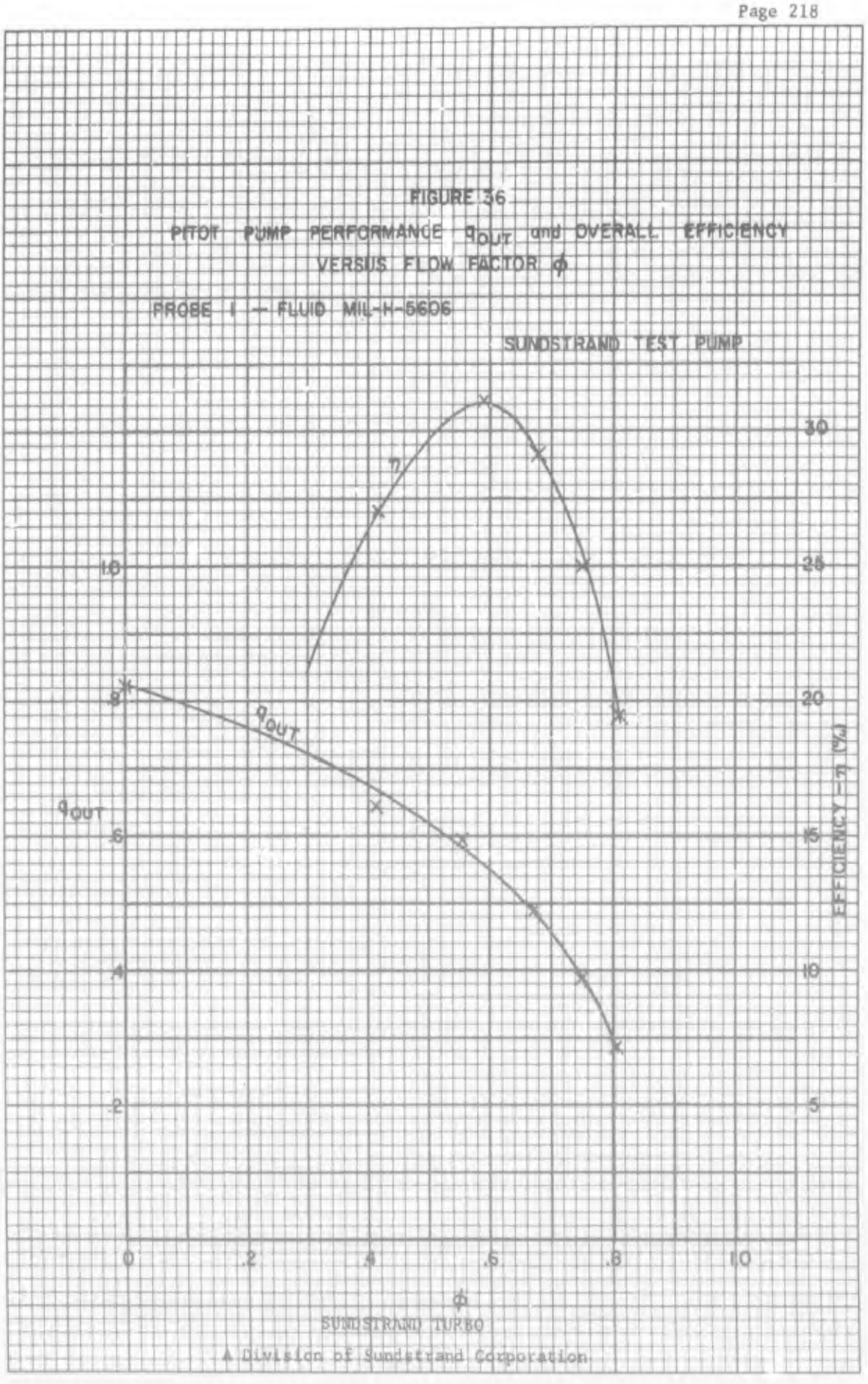

FIGURE 36

PITOT PUMP PERFORMANCE q_{OUT} and OVERALL EFFICIENCY VERSUS FLOW FACTOR ϕ

PROBE I -- FLUID MIL-H-5606

FIGURE 37

PITOT PUMP PERFORMANCE Q_{OUT} and OVERALL EFFICIENCY VERSUS FLOW FACTOR ϕ

PROBE 2 — FLUID MIL-H-5606

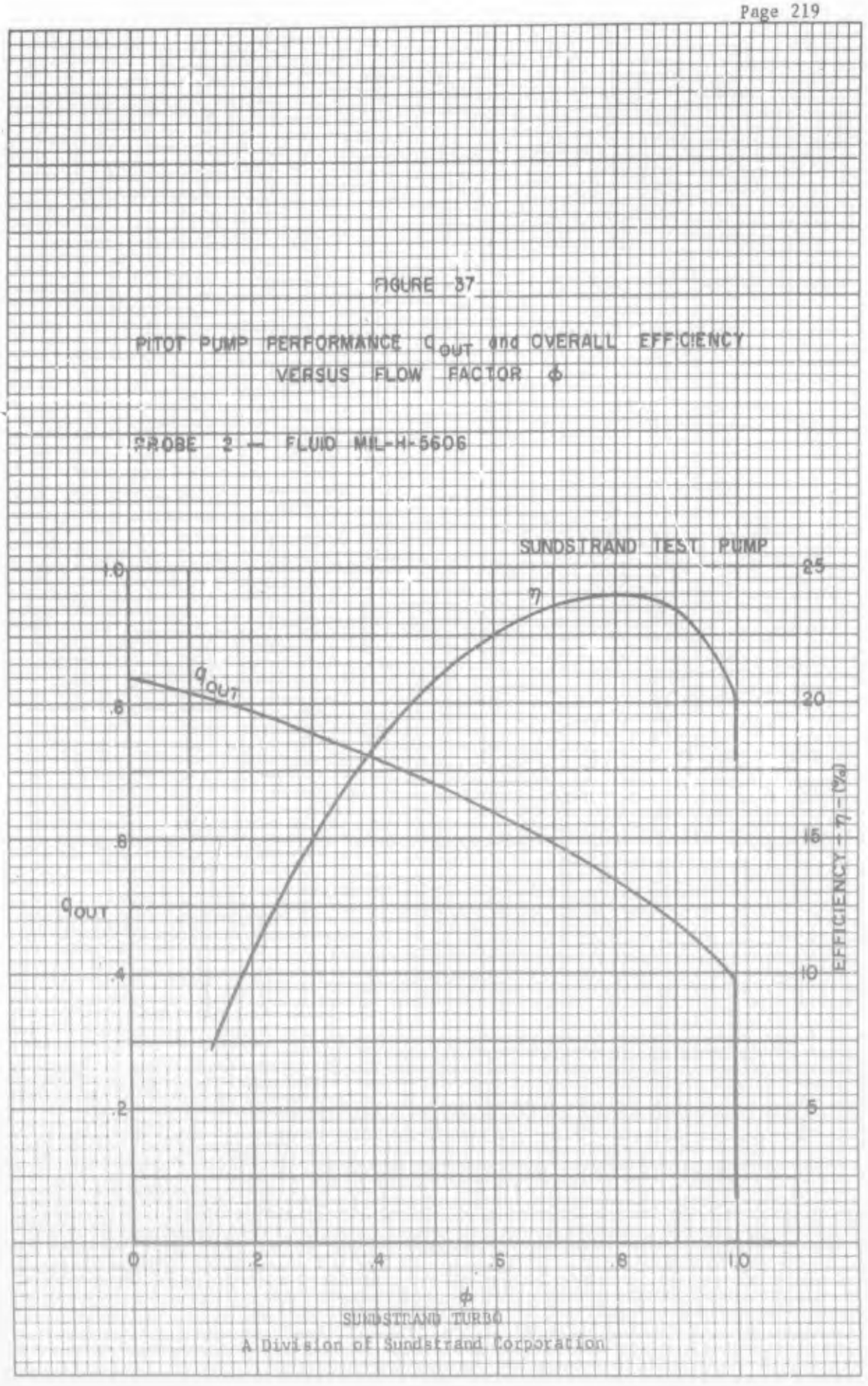

FIGURE 38

PROBE DRAG LOSS COEFFICIENT
FOR PITOT PUMPS

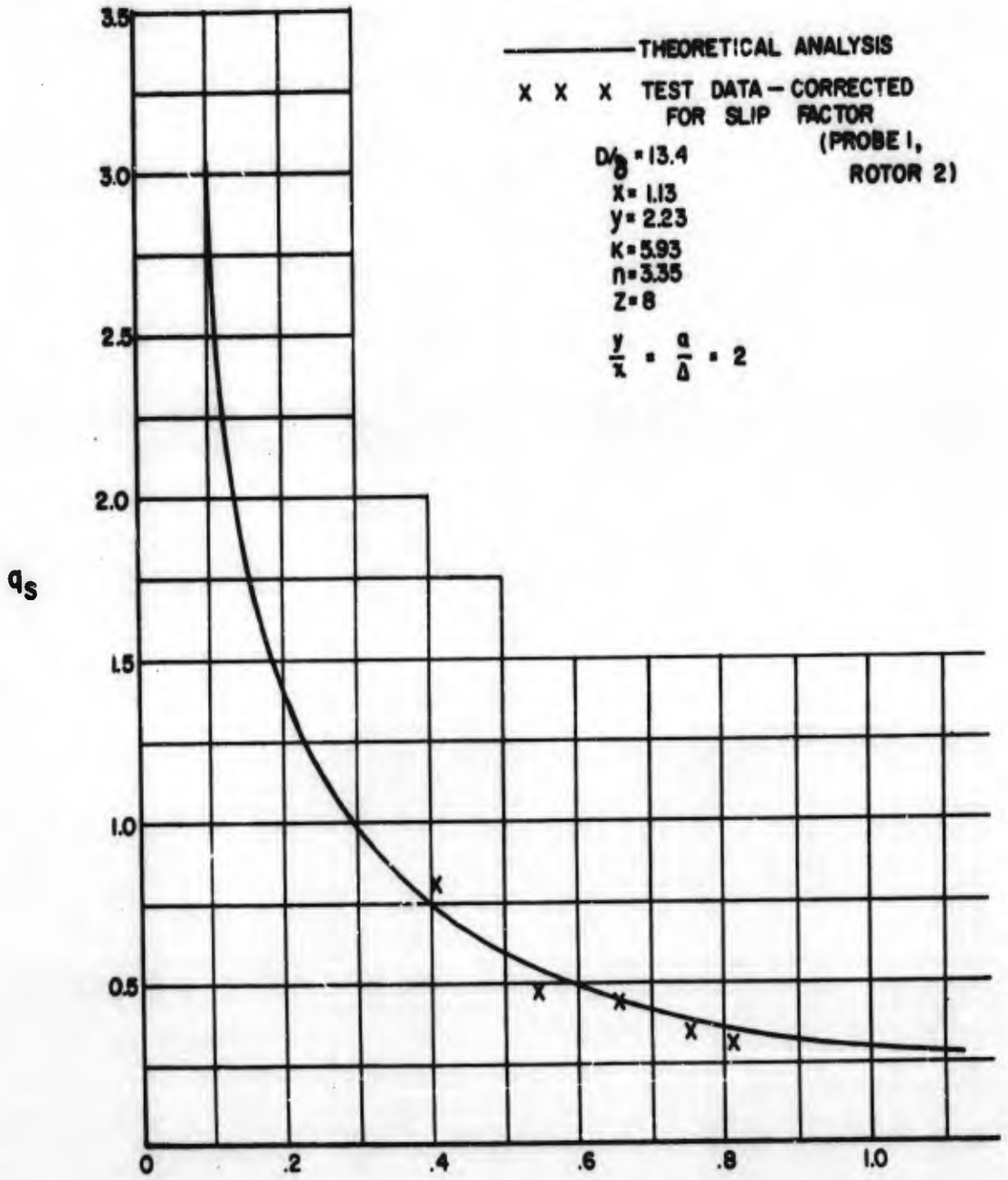

FIGURE 39

PROBE DRAG LOSS COEFFICIENT FOR PITOT PUMPS

———— THEORETICAL ANALYSIS

X X X TEST DATA - CORRECTED FOR SLIP FACTOR (PROBE 1, ROTOR 2)

$D_B = .27$

X = 1.13

Y = 3.38

K = 5.93

n = 6.75

Z = 8

$\frac{y}{x} = \frac{a}{\Delta} = 3$

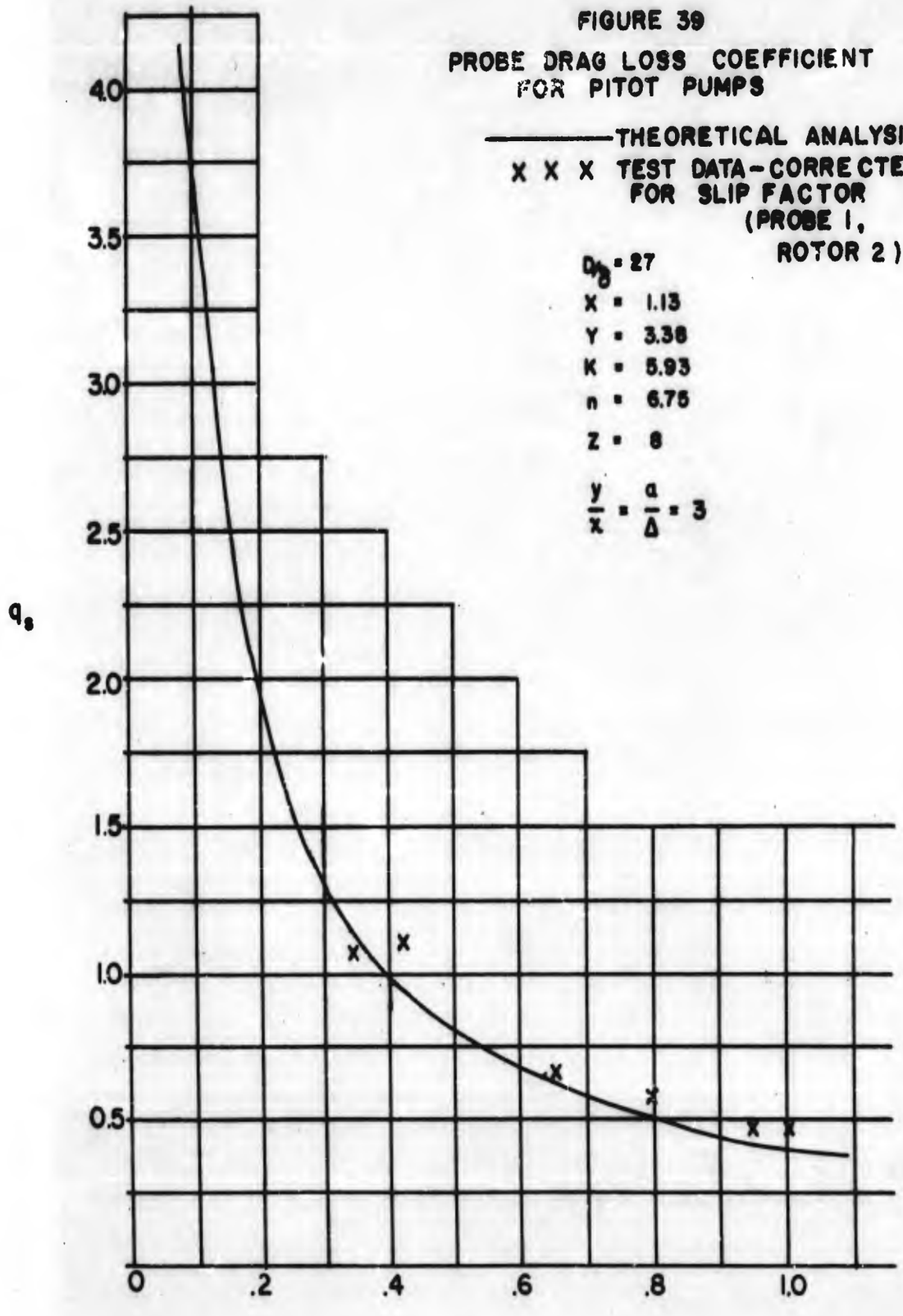

FIGURE 40

PITOT PUMP EFFICIENCY THEORETICAL AND TEST DATA

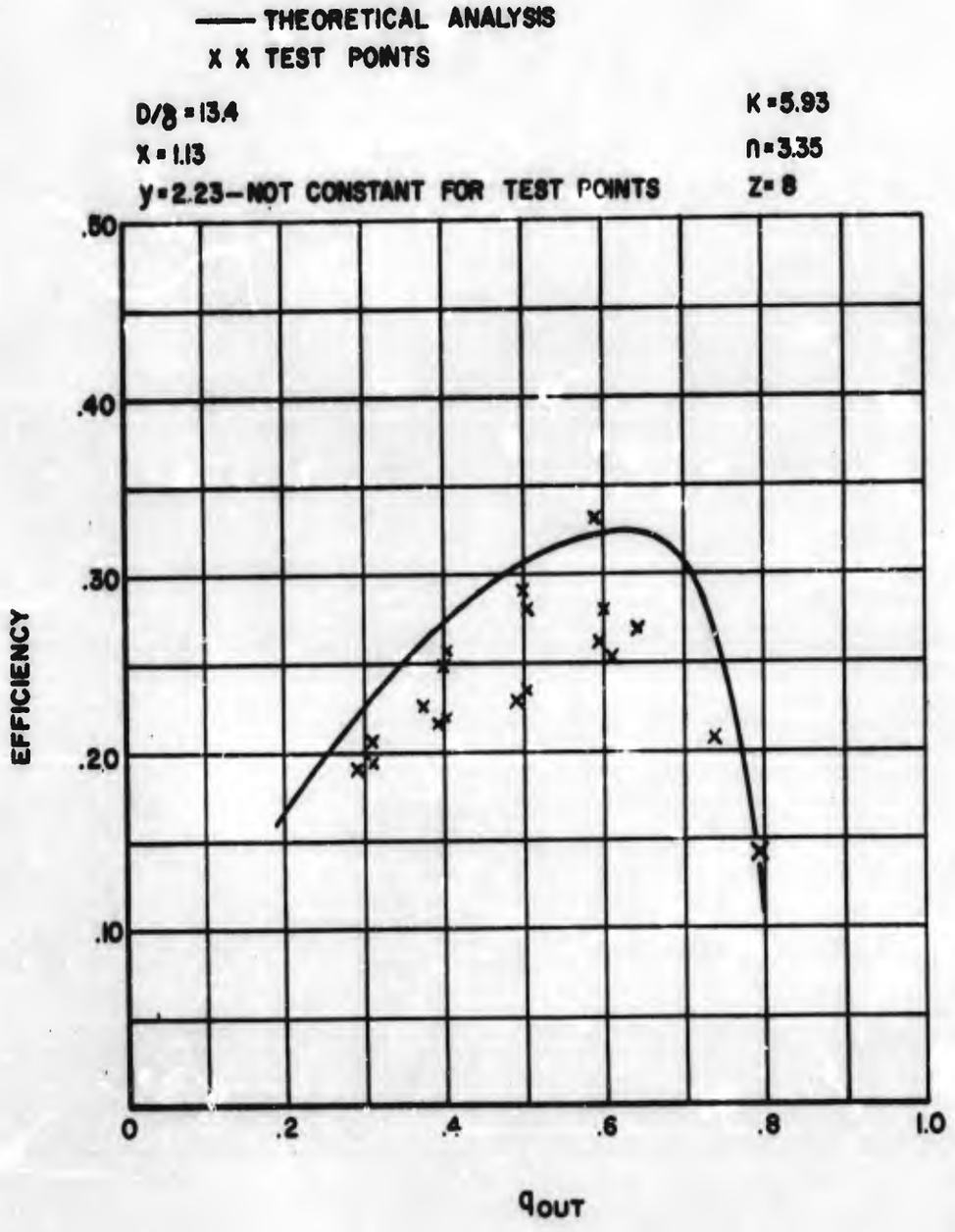

FIGURE 41

PITOT PUMP EFFICIENCY THEORETICAL AND TEST DATA

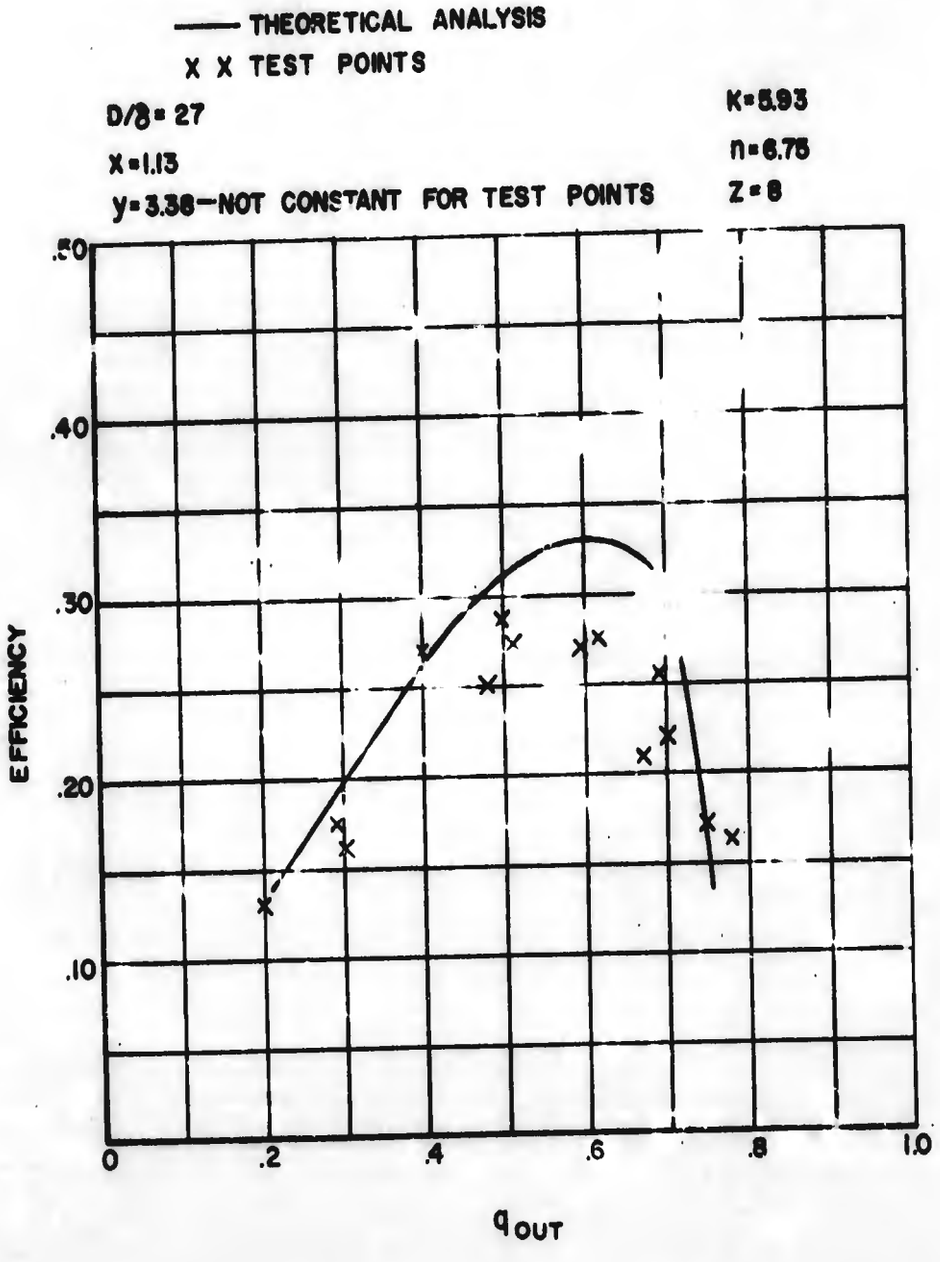

REFERENCES

Ref. No.	
1	Buckingham, E., "On Model Experiments and the Form of Empirical Equation", Trans. ASME, Vol. 37, p. 263, 1915
2	Davis, H., Kottas, H., and Moody, A.M.G., "The Influence of Reynolds Number on the Performance of Turbomachinery", Trans. ASME, Vol. 73, p. 499,
3	Rotzoll, R., "Untersuchungen an Einer Langsamlaufigen Kreiselpumpe bei Verschiedenen Reynoldszahlen", Konstruction, 10 (1958) 4.
4	Stepanoff, A. J., "Centrifugal and Axial Flow Pumps", 2nd Edition, 1957, John Wiley & Sons, Inc., N.Y.
5	"Mark's Mechanical Engineers Handbook", 1951, McGraw-Hill, N.Y.
6	Wislicenus, G. F, R. M. Waters and I. J. Karassik, "Cavitation Characteristics of Centrifugal Pumps Described by Similarity Considerations", Trans. ASME, 1939, p. 17.
7	Wislicenus, George F., "Fluid Mechanics of Turbomachinery", McGraw-Hill, N.Y., 1947.
8	Shepherd, D. G., "Principles of Turbomachinery", MacMillan Co., ist Edition, 1956.
9	Binder, R. C., and Knapp, R. T., "Experimental Determinations of the Flow Characteristics in the Volutes of Centrifugal Pumps", Trans. ASME, 1958, p. 649.
10	Stodola, "Steam and Gas Turbines", McGraw-Hill, N.Y., 1927.
11	Peck, F. J., "Investigations Concerning Flow Conditions in a Centrifugal Pump, and the Effect of Blade Loading on Head Slip", Proc. I, Mechanical Engineering, Vol. 164, No. 1, 1951, p. 1.
12	Eckert, B., "Axial Compressors and Radial Compressors", Springer-Verlag, Berlin, Germany, 1953.

Ref. No.

13 Pfleiderer, C., "Die Kreiselpumpen fur Flussigkeiten und Gase", Springer-Verlag, Berlin, Germany, 1955.

14 Kent's Mechanical Engineers Handbook, Power Volume, 12th Edition, John Wiley & Sons.

15 Brown and Bradshaw, " Design and Performance of a Family of Diffusing Scrolls", N.A.C.A.

16 Binder, R. C., "Advanced Fluid Dynamics and Fluid Machinery", Prentice-Hall, 1951.

17 Ippen, Arthur T., "The Influence of Viscosity on Centrifugal Pump Performance", Trans. ASME, Vol. 68, No. 8, 1946, p. 823.

18 Wislicenus, G. F., "Critical Considerations on Cavitation Limits of Centrifugal and Axial Flow Pumps", ASME Paper No. 55-A-144.

19 Church, Austin H., "Centrifugal Pumps and Blowers", John Wiley & Sons Inc., N.Y., 1955.

20 Gongwer, "A Theory of Cavitation Flow in Centrifugal Pump Impellers", ASME Trans., 1941, p. 29.

21 Kermeen, R. W., McGraw, J. T., and Parkin, B. R., "Mechanism of Cavitation Inception and the Related Scale Problems", ASME Trans., May 1955, P. 533.

22 Traupel, Walter, "Thermische Turbomachinen", Springer-Verlag, Berlin, Germany, 1958.

23 Hoener, S. F., "Fluid-Dynamic Drag", 1958

24 Balje, O. E., "A Contribution to the Problem of Designing Radial Turbomachines", ASME Trans, May 1952.

25 Iverson, H. W., "Performance of the Periphery Pump", ASME Trans., 1955.

26 McCulloch Corporation, Advance Development Division, 6101 W. Century Blvd., Los Angeles, California

27 Barske, U. M., "The Design of Open Impeller Centrifugal Pumps", RAE Technical Note 77, Farnsborough, Hants, Eng.

NOMENCLATURE

a -- constant relating w to l

A -- area, $ft.^2$

B -- empirical coefficient

b -- width, ft.

c -- absolute velocity, ft/sec

C -- absolute velocity, ft/sec

C_w -- probe drag coefficient

d -- diameter, ft.

D -- outer diameter, ft.

D* -- hydraulic diameter, ft.

D_s -- specific diameter (dimensionless)

e -- parameter used in scroll analysis

E -- power, ft-lb/sec.

f -- friction factor, dimensionless

F -- channel cross section in Pitot pump, $ft.^2$

g -- gravitational constant, $ft/sec.^2$

G -- weight rate of flow, lb/sec.

h -- head at pump inlet

H -- head, ft.

i -- parameter used in scroll analysis

J -- a function of geometry

k -- clearance or width ratio associated with wear-rings or empirical constant

K -- ratio of meridional flow velocities

l -- point along flow passage

L -- length of flow passage, ft.

m -- slip factor

n -- proportionality constant

N -- rotative speed, revolutions per minute

N_s -- specific speed, dimensionless

p -- wetted perimeter in Pitot pump

P -- power

q -- head coefficient

Q -- volume flow rate $ft.^3/sec.$

r -- radius, ft.

R -- radius or resistance in Pitot pump analysis

R_e -- local Reynolds number

Rg -- Reynolds number of turbomachine

S -- suction specific speed

t -- vane thickness, ft.

T -- torque, lb.-ft.

u -- impeller tangential velocity, ft./sec.

w -- relative velocity, ft./sec.

W -- relative velocity, ft./sec.

x -- geometric parameter of impeller

X -- ratio of straight diffuser length to impeller outer diameter

y -- geometric parameter in Pitot pump

z -- blade number in Pitot pump

Z -- vane number

α -- exponent in Reynolds number correction, or absolute flow angle

β -- blade or vane angle, degrees

β_w -- loss coefficient in Pitot pump disc friction

γ -- density, lb./ft.^{3}

δ -- ratio of impeller eye to outer diameter, or Pitot probe inlet diameter, ft.

Δ -- Pitot probe body diameter, ft.

ζ -- loss coefficient, dimensionless

η -- efficiency, percent

θ -- angle

Λ -- wear-ring clearance

λ -- ratio of annular diffuser outer to inner diameter

μ -- absolute viscosity, slug/ft.-sec.

ν -- shear force, lbs.

ξ -- loss coefficient, dimensionless

π -- constants

ρ -- fluid density, slugs/ft.^{3}

σ -- Thoma cavitation parameter

τ -- ratio of hub to eye diameter

ϕ -- flow factor

χ -- ratio of probe body diameter to probe inlet diameter

ψ -- dimensionless parameter

ω -- angular velocity, radians/sec.

Subscripts

A -- average condition or atmospheric

ad -- annular diffuser

B -- probe and transmission loss

D -- ducting loss in Pitot pump or drag

d_f -- disc friction

e -- effective or Eckert in Pitot pump analysis

f -- friction

g -- gas

i -- impeller

ic -- curved section of impeller

id -- diffusion in impeller

il -- impeller loss

is -- straight portion of impeller

k -- kinetic energy loss in Pitot pump

m -- mixing, or meridional flow velocities

p -- probe in Pitot pump

rf -- wear-ring friction

rl -- wear-ring leakage

s -- static

ss -- specific

sc -- scroll

sd -- straight diffuser

sv -- net positive suction

t -- total

th -- theoretical

u -- tangential component

v -- vapor

x -- annular diffuser discharge

1 -- impeller inlet

2 -- impeller outlet

3 -- inlet to scroll

4 -- straight diffuser inlet

5 -- straight diffuser discharge